Realistic numerical modelling of the yarn behaviour in the production of stitched sandwich panels

Lode Daelemans

Promotoren: prof. dr. ir. Wim Van Paepegem, prof. dr. ir. Lieva Van Langenhove
Begeleiders: ir. Jana Faes, dr. ir. Simon De Meulemeester

Masterproef ingediend tot het behalen van de academische graad van
Master in de ingenieurswetenschappen: materiaalkunde

Vakgroep Toegepaste Materiaalwetenschappen
Voorzitter: prof. dr. ir. Joris Degrieck

Vakgroep Textielkunde
Voorzitter: prof. dr. Paul Kiekens

Faculteit Ingenieurswetenschappen en Architectuur
Academiejaar 2012-2013

UNIVERSITEIT
GENT

Preface

When I chose this topic back in May 2012, I was not really sure what to expect, since my experience with finite element analysis was rather limited. The fact that we had to develop a finite element yarn model from scratch seemed challenging at first. Nevertheless, now that I am writing these last concluding words, I am glad I took on this challenge. Researching the stitching of sandwich panels was a very interesting experience, because it spans the domains of textile processing, composites and numerical modelling, and I learned so many new exciting things. Working on the problem was almost addictive. Every time a simulation yielded interesting results, it boosted the motivation for more simulations. There is still a lot of work to do concerning this topic, but I hope this thesis can offer useful information for further research.

I would like to thank my promoters professor Wim Van Paepegem and professor Lieva Van Langenhove for their time, dedication and for providing such an interesting subject to work on. I am also grateful to my supervisors Jana Faes and Simon De Meulemeester, who were always available when I struggled with a problem, explained the ins and outs of ABAQUS and helped me with my simulations. I would also like to thank Roel Callebaut and Roeland De Vriese from Acrosoma, who helped a lot by providing real life experience and data from the stitching process. Furthermore, I would like to express my gratitude to the people at the Department of Materials Science and the Department of Textile for their help.

Lode Daelemans,
June 2013

3 June, 2013

Realistic numerical modelling of the yarn behaviour in the production of stitched sandwich panels

by

Lode Daelemans

Masterproef ingediend tot het behalen van de academische graad van

Master in de ingenieurswetenschappen:

materiaalkunde

Promotoren: prof. dr. ir. W Van Paepegem, prof. dr. ir. L Van Langenhove
Begeleiders: ir. Jana Faes, dr. ir. Simon De Meulemeester

Vakgroep Toegepaste Materiaalwetenschappen
Voorzitter: prof. dr. ir. Joris Degrieck

Vakgroep Textielkunde
Voorzitter: prof. dr. Paul Kiekens

Faculteit Ingenieurswetenschappen en Architectuur, Universiteit Gent
Academiejaar 2012 – 2013

Summary

This study investigates the possibility of using the finite element package ABAQUS for simulating the stitching process, and, in particular, to develop a model capable of simulating the yarn behaviour during the production of stitched sandwich panels.

Keywords

3D reinforced sandwich panels, stitching process, finite element analysis (FEA), yarn behaviour, truss elements.

Realistic numerical modelling of the yarn behaviour in the production of stitched sandwich panels

Lode Daelemans

Supervisors: prof. dr. ir. Wim Van Paepegem, prof. dr. ir. Lieva Van Langenhove

Abstract—**Stitched sandwich panels provide high mechanical properties at low weight without being as susceptible to delamination as regular sandwich panels. Their properties offer great potential in times where fuel costs keep rising and the demand for new high-performance grows every year. However, the production of these reinforced panels proves to be difficult, often leading to stitch faults which can have a detrimental effect on the final properties.**

This study investigates the possibility of using the finite element package ABAQUS for simulating the stitching process, and in particular, the possibility to develop a model capable of simulating the yarn behaviour during production. Several modelling possibilities were tried in order to select the one that is most suited for modelling flexible yarns.

The yarn model was based on a chain of truss elements connected by frictionless pins. These chains are arranged in a bundle to describe the fibrous behaviour of yarns. Other models were constructed for the polymer foam core and the needle system. The formation of a Z-stitched sandwich panel was simulated using these models.

The yarn model proved to be useful for modelling fibrous materials. However, more research is necessary in order to develop a computationally efficient simulation of the whole stitching process.

Keywords— **3D reinforced sandwich panels, stitching process, finite element analysis (FEA), yarn behaviour, truss elements.**

I. Introduction

Sandwich panels are used because of their high stiffness and strength with minimal weight. Their use is, however, limited due to their sensitivity to failure by delamination between the core and the skins. Through-the-thickness reinforced sandwich panels are less prone to this kind of failure, because an extra link is created between the different parts [1]. A promising method to produce reinforced sandwich panels is to stitch them before resin injection [2], [3]. The stitching process, although common to the textile industry, is relatively new in the production of sandwich panels. Hence, a lot of research has to be done to optimise the production in order to obtain the full gain these panels can provide.

Most of the research is concerned with determining the mechanical properties of the panels after resin injection. These properties are, however, often related to the stitched dry preform structure, and simulating the stitching process can help identify the problems related to it. Nevertheless, research dedicated to the simulating of the process is very limited, probably due to the difficulties associated with modelling a yarn capable of large deformations with reasonable computation time in a finite element environment.

This study concerns the construction of a general yarn model that can be used for simulating the stitching of sandwich panels. This also required the construction of a model for the foam core of the panels. The simulated process was similar to the one used by Acrosoma, which uses a stretch-broken carbon yarn and a Rohacell 71 RIST foam core.

II. Yarn model

A yarn is made up from hundreds or thousands of aligned fibres, which can slide and realign themselves. This results in a flexible structure which has a high stiffness and strength in the fibre direction, contrary to those in the transversal direction.

Semi-discrete methods model approximate the yarn by a relatively small amount of fibres. This way, the fibrous behaviour of the yarn is taken into account without leading to too high computational costs. In most of the research, beam elements are used to model the fibres [4], [5], [6]. However, the bending stiffness of the fibres had to be decreased artificially in order to obtain a flexible yarn. A chain of truss elements offers the same possibility of representing a yarn as a bundle of fibres, but it has no inherent bending stiffness. Hence, it is more suited for modelling flexible yarns.

A. Simulations

Truss elements only transmit axial loads. When a chain of truss elements (T3D2) is defined in ABAQUS, their nodes act as frictionless pins. This makes the chain very flexible, especially when the elements are small. The explicit solver ABAQUS/Explicit was used in order to define contact on the truss elements.

Simple tests were performed to investigate the model's behaviour, e.g. contact with other elements, flexibility and transversal deformation of the fibre bundle. These simple tests had, however, no physical counterpart. In order to illustrate a more representative example, a bundle of 19 initially straight fibres modelled with truss elements was twisted. During the twisting of yarns, fibres on the outer surface will develop higher tensile stresses and migrate towards the centre.

A fully flexible yarn would behave as an ideal string. The yarn model was validated by comparing simulated frequencies of standing waves with those obtained from the theory of standing waves for a piece of string/yarn with a length of 100 mm. It showed that the yarn behaves as an ideal string for small truss element lengths.

B. Results

The results of the simple tests showed that using a bundle of truss elements chains allowed for fibre realignment and high flexibility. Contact with rigid bodies and deformable elements could be achieved by using the general contact algorithm in ABAQUS. Fibre realignment led to realistic cross-section deformation and flexible yarn behaviour.

The truss element's length was an important parameter for the usability of the model: elements which are to small led to high

computational costs due to a decrease in stable time increment, elements which are too large, however, decreased the flexibility of the chain and led to contact problems. An element length which is about 70 % of the element's diameter seemed to yield a good optimum. Furthermore, the dynamical effects had to be minimised in the explicit analysis, which also increased computational expenses.

The twisting simulation illustrates the fibre realignment and migration nicely, see Figure 1.

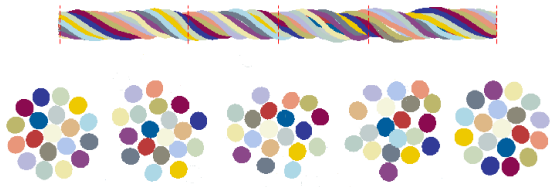

Fig. 1. Results for the twisting of a bundle of 19 initially straight fibres. It shows that outer fibres constantly migrate towards the center, leading to an entangled yarn. Notice, for example, the light blue fibre initially at the outer surface migrates towards the centre and back to the surface.

III. Foam model

A. Introduction

Polymer foams have a cellular structure, which progressively collapses when loaded in compression. This leads to a long zone of approximately constant stress in the compressive stress-strain diagram. Furthermore, during plastic deformation, the Poisson's ratio is approximately zero, leading to a change in volume during deformation. It is important to construct a good constitutive model that captures this specific behaviour in order to obtain realistic results from the stitching simulation.

B. Simulations

The crushable foam plasticity model of ABAQUS was used to model the Rohacell 71 RIST foam core. The model was validated by comparing the results from quasi-static compression simulations with those from experimental data. The model requires stress-strain data which can be obtained from a simple compression test. During stitching, needles penetrate the foam core. The forces on these needles are important because they influence the process. Although the plasticity model allows for strain-rate sensitive behaviour, this was not necessary for the Rohacell 71 RIST material model. Experiments showed that the needle penetration speed had a negligible effect on the force exerted on the needle. Failure of the foam material was modelled with the ductile damage criterion of ABAQUS, which is intented to model failure of ductile metals, because no failure models for crushable foam were available in ABAQUS. The parameters for the criterion were inversely determined from a needle penetration simulation.

A quasi-static needle penetration in foam was simulated with ABAQUS/Explicit. The needle was assumed to be axisymmetric with a radius of 1.5 mm and penetrated the foam vertically at a speed of 5 m/s. The foam was modelled as a disk with a radius of 15 mm and a height of 30 mm. The foam disk was constrained in all directions at its cylindrical surface. The needle was modelled as a rigid body and constrained in all directions except the vertical one. A tangential friction coefficient of 0.3 was assumed. Similar experiments were performed by Acrosoma. However, they used a realistic stitch needle, of which the needle tip was not axisymmetric.

C. Results

The total vertical force exerted on the needle showed good agreement with those experimentally determined, see Figure 2. The force increases to a maximum when the foam is fully penetrated by the needle and falls to a constant value after the needle tip has left the foam. This residual force is due to friction between the needle and the foam. The crushing of the foam occurred only locally around the needle tip. Hence, stresses and strains were confined to a small region around the needle.

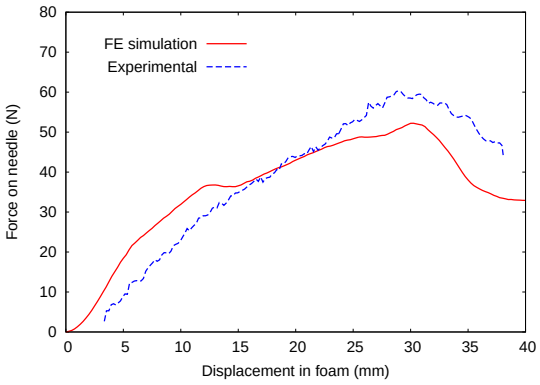

Fig. 2. Force-displacement diagram for a needle penetrating Rohacell 71 RIST foam (30 mm heigth).

After investigating the energy outputs of the simulation could be concluded that the exerted force on the needle was mainly due to friction and due to crushing in a lesser extent, see Figure 3. Crushing only occurs at the needle tip, hence, the crushing force stayed constant when the needle tip had fully entered the foam. Friction increases to a maximum, because there is a part due to friction with the needle tip and a part due to friction with the needle body.

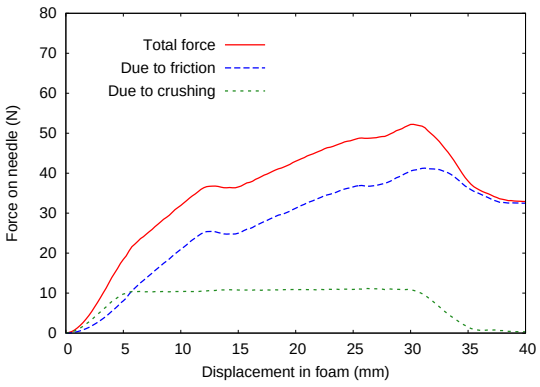

Fig. 3. Force-displacement diagram for a needle penetrating Rohacell 71 RIST foam with its components due to friction and due to crushing of the foam.

IV. Simulating the stitching process

A. The Z-stitch

The production of Z-stitched panels was simulated. The steps in the formation of a Z-stitch are illustrated in Figure 4. The average needle speed in the production process of Acrosoma is around 30 mm/s. Hence, the formation of one stitch happens in several seconds. This natural time scale is rather large for an explicit simulation, which influences the computational costs negatively.

B. Factors influencing computational costs

In explicit methods, the stable time increment Δt_{stable} determines the progression of the simulation. If it is small compared to the simulation's time scale, many time increments are needed, and hence, the computational costs increase. The stable time increment is automatically calculated by ABAQUS and is dependent on the smallest element (shortest length L), its Young's modulus E and its density ρ:

$$\Delta t_{stable} \propto L\sqrt{\frac{\rho}{E}} \tag{1}$$

The stitching simulation's Δt_{stable} is rather small compared to its natural time scale, due to the small elements and relatively low E and ρ for the yarn and the foam. This increased the computational costs significantly. Furthermore, it was found that complex contact interactions also had a negative effect on the computational costs. This made it difficult to obtain a computationally feasible simulation of the process.

C. Simulations

The Z-stitching was simulated by using the constructed yarn and foam model. The needle and looping hook were modelled as rigid bodies, and were displacement controlled in a series of steps to produce a Z-stitch. A predrilled foam was also modelled, because this reduced the computational costs significantly. Furthermore, Acrosoma uses predrilled foams on some occasions to facilitate the stitching process with carbon yarns.

Several simulations were done with a difference in yarn properties, foam mesh density and simulation speed, in order to select the most efficient models. Mass scaling was used in every simulation on the foam. The yarn was modelled with one truss element chain for the preliminary testing. A tangential friction coefficient of 0.3 was used between all parts in the simulation.

D. Results

The results indicated that most of the models were just not computationally feasible. Furthermore, contact problems between the yarn and needle system occurred. These problems led to faulty stresses in the yarn or a loss of contact between the yarn and the needle. The base for this problem was the simplification of the needle that was used. The real stitching needle is smoothly curved in order to reduce friction with the yarn. However, meshing such a complex geometry proved to be difficult. Therefore, the geometry was simplified to one with more straight edges. It was noticed that truss elements get stuck behind these straight sharp edges. This problem could partly be overcome by decreasing the yarn's Young's modulus (by a factor of 10) or by using frictionless contact. A fine meshed needle geometry with smoothly curved surfaces is recommended though.

The results of the stitching simulation for a predrilled foam with frictionless contact and a low yarn's Young's modulus is shown in Figure 4. It shows that the constructed yarn, foam and needle models are capable of simulating the production of these panels. However, the models still requires more investigation and optimization of the parts and parameters, in order to reduce the contact problems and the computational costs.

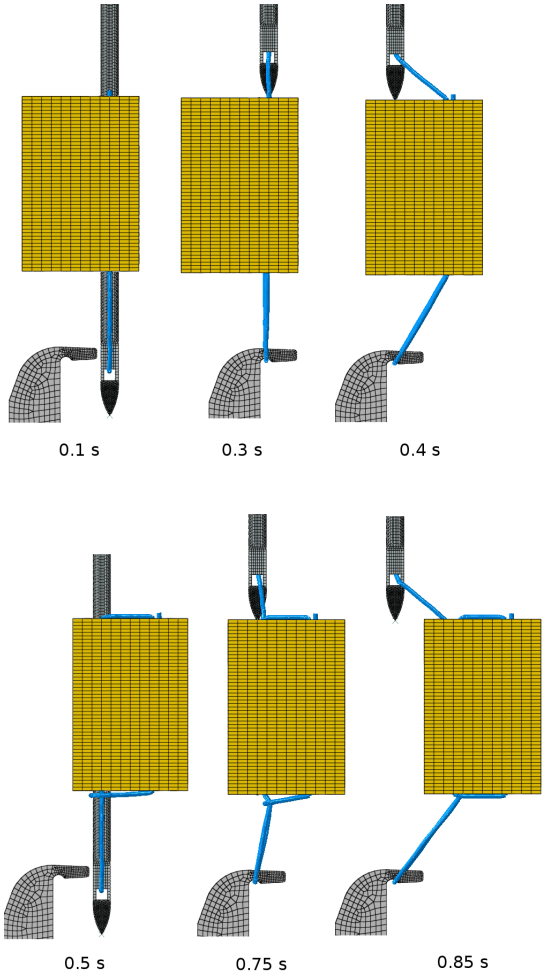

Fig. 4. Formation of a Z-stitch through a foam core.

V. Conclusion

The models constructed in this thesis can be used to model a stitching process and to study the yarn behaviour. However, their use is still limited due to the high computational costs of the stitching simulation. A possible solution laid in the use of predrilled foams which could reduce these costs. The yarn model and the foam model already showed great potential, but a realistic needle geometry should be used for further simulations in order to reduce the locking of truss elements with sharp needle edges.

The yarn model offers a versatile way of modelling fibrous

materials and can be used both in the specific case of a stitching process as well as in other research areas.

REFERENCES

[1] Anamaría Henao, Marco Carrera, Antonio Miravete, and Luis Castejón, "Mechanical performance of through-thickness tufted sandwich structures," *Composite Structures*, vol. 92, no. 9, pp. 2052–2059, 2010.

[2] P Potluri, E Kusak, and T.Y Reddy, "Novel stitch-bonded sandwich composite structures," *Composite Structures*, vol. 59, no. 2, pp. 251 – 259, 2003.

[3] C Sickinger and A Herrmann, "Structural stitching as a method to design high-performance composites in future," in *Proceedings TechTextil Symposium*, 2001.

[4] Damien Durville, "Finite element simulation of textile materials at mesoscopic scale," *Finite element modelling of textiles and textile composites*, 2007.

[5] Y Mahadik and SR Hallett, "Finite element modelling of tow geometry in 3d woven fabrics," *Composites Part A: Applied Science and Manufacturing*, vol. 41, no. 9, pp. 1192–1200, 2010.

[6] Steve Green, Andrew Long, and Stephen Hallet, "Numerical modelling of 3d woven composite preform deformations," 2012, Presented at the ACCIS annual conference in 2012, Bristol, United Kingdom.

Realistische numerieke modellering van het gedrag van garens in de productie van gestikte sandwichpanelen

Lode Daelemans

Promotoren: prof. dr. ir. Wim Van Paepegem, prof. dr. ir. Lieva Van Langenhove

Abstract—**De vraag naar nieuwe lichte structurele materialen blijft stijgen, bijvoorbeeld om te besparen op brandstofkosten. Gestikte sandwichpanelen bieden goede mechanische eigenschappen, gecombineerd met laag gewicht en zijn, in tegenstelling tot gewone sandwichpanelen, beter bestand tegen falen door delaminatie. De productie van deze panelen is echter niet vanzelfsprekend. Er worden bijvoorbeeld nog vaak stikfouten teruggevonden die nefast zijn voor de mechanische eigenschappen.**

Deze studie onderzoekt het gebruik van het eindige elementen pakket ABAQUS voor de simulatie van het stikproces in de productie van gestikte sandwichpanelen. De nadruk ligt op het ontwikkelen van een model dat geschikt is om het gedrag van een garen te simuleren. Verschillende modellen werden getest om te komen tot het model dat het meest geschikt is voor de modellering van flexibele garens.

Het garenmodel is gebaseerd op een keten van *truss* elementen die aan elkaar hangen met wrijvingsloze pennen. Verschillende ketens werden gebundeld om zo het vezelachtige karakter van een garen te bekomen. Tevens werden er modellen opgesteld om de schuimkern van het sandwichpaneel en het naaldensysteem te kunnen simuleren. Deze werden uiteindelijk gebruikt om de productie van een Z-gestikt paneel te simuleren.

Het garenmodel bleek uitermate geschikt om textielmaterialen te modelleren. De simulatie van het volledige stikproces vereist echter nog verder onderzoek om de berekeningstijd te kunnen verkorten.

Keywords—**3D versterkte sandwichpanelen, stikproces, eindige elementen analyse, gedrag van garens, truss elementen.**

I. Inleiding

Sandwichpanelen worden gebruikt omwille van hun hoge stijfheid en sterkte, gecombineerd met een laag gewicht. Hun gebruik is echter beperkt vanwege de gevoeligheid aan falen door delaminatie van de kern en de huiden. Doorheen de dikte versterkte sandwichpanelen zijn hier minder gevoelig aan, omdat er een extra verbinding wordt gecreëerd tussen de verschillende lagen [1]. Een veelbelovende methode om deze versterkte panelen te produceren is door ze te stikken voor de harsinjectie [2], [3]. Het stikproces, dat goed gekend is in de textielindustrie, is echter nog relatief nieuw voor de productie van versterkte panelen. Uitvoerig onderzoek is daarom nodig zodat het proces geoptimaliseerd kan worden, en zodat de panelen optimaal kunnen worden gebruikt.

Het meeste onderzoek hierrond is gewijd aan de determinatie van de mechanische eigenschappen van de uiteindelijke panelen. Deze eigenschappen zijn echter vaak gerelateerd aan de structuur van de gestikte droge voorvorm. Een simulatie van het stikproces kan de problemen die een vermindering van eigenschappen tot gevolg hebben identificeren. Het onderzoek naar de simulatie van het stikproces is echter zeer beperkt. Dit is wellicht te wijten aan de moeilijkheden die met het modelleren van een garen in een eindige elementen omgeving gepaard gaan.

Deze studie beoogt het ontwerpen van een algemeen garenmodel dat gebruikt kan worden voor de simulatie van het stikproces van sandwichpanelen. Daarom werden er ook modellen opgesteld om (1) de schuimkern en (2) het naaldensysteem te simuleren. Het stikproces gebruikt door Acrosoma diende als voorbeeld. Hierin wordt gebruikgemaakt van een *stretch-broken* koolstofgaren en van een Rohacell RIST 71 schuimkern.

II. Garenmodel

A. Inleiding

Een garen bestaat uit honderden of duizenden gealigneerde vezels die over elkaar kunnen glijden en zich kunnen herpositioneren. Hierdoor vertoont een garen een hoge flexibiliteit, gecombineerd met een hoge stijfheid en sterkte in de vezelrichting.

Semi-discrete methodes benaderen een garen als een bundel met een relatief klein aantal vezels. Op deze manier wordt rekening gehouden met het vezelachtige karakter zonder dat de computationele kosten te hoog oplopen. De meeste onderzoekers gebruiken *beam* elementen om de vezels te modelleren [4], [5], [6]. De buigstijfheid van de elementen wordt echter artificieel verlaagd om een flexibel garen te bekomen. Een keten van truss elementen geeft dezelfde mogelijkheid om een garen als een bundel vezels te modelleren, maar heeft daarentegen geen inherente buigstijfheid. Dergelijke ketens van truss elementen zijn daardoor zeer geschikt om flexibele garens te modelleren.

B. Simulaties

Truss elementen geven enkel axiale krachten door. Wanneer een keten van truss elementen (T3D2) wordt gedefinieerd in ABAQUS, reageren de knopen in die elementen als wrijvingsloze pennen. Dit zorgt voor de flexibiliteit van de keten, zeker wanneer de elementen klein zijn. De expliciete *solver* ABAQUS/Explicit werd gebruikt om contact met de truss elementen te definiëren.

Eenvoudige tests werden uitgevoerd om een duidelijk beeld te krijgen van het model, onder andere van het contact met andere elementen en de flexibiliteit en transversale vervorming van de vezelbundel. Deze eenvoudige tests hadden echter geen experimentele tegenhanger. Voor een meer representatief voorbeeld werd nog een test uitgevoerd, waarbij een bundel met 19 initieel rechte vezels gemodelleerd met truss elementen werd getwist. Tijdens het twisten van garens zullen de vezels aan het oppervlak hogere trekkrachten ontwikkelen en daardoor migreren naar het midden van het garen.

Een volledig flexibel garen zou zich gedragen als een ideale snaar. Het garenmodel werd gevalideerd door de frequenties van staande golven te vergelijken met degene bekomen uit de

theorie van staande golven voor een stuk garen met een lengte van 100 mm. Hieruit bleek dat het garen zich gedraagt als een ideale snaar voor kleine truss elementen.

C. Resultaten

De resultaten van de eenvoudige tests toonden aan dat het gebruik van een bundel ketens van truss elementen ervoor zorgt dat vezelherpositionering en hoge flexibiliteit mogelijk zijn. Contact met vaste lichamen en vervormbare elementen was mogelijk door het *general contact* algoritme in ABAQUS te gebruiken. De vezelherpositionering zorgde tevens voor realistische doorsnedeveranderingen.

De lengte van de truss elementen is een belangrijke parameter voor de bruikbaarheid van het model: te kleine elementen leiden tot hoge computationale kosten vanwege een verlaging van het stabiele tijd increment. Te grote elementen zorgen dan weer voor een afname van de flexibiliteit van de ketens, en veroorzaken contactproblemen. Een verhouding van de elementlengte op de elementdiameter van ongeveer 70 % bleek optimaal. Verder diende de dynamische effecten in de expliciete analyse te worden beperkt, wat leidde tot hogere computationele kosten.

De twistsimulatie toont duidelijk de vezelherpositionering en -migratie, zie Figuur 1.

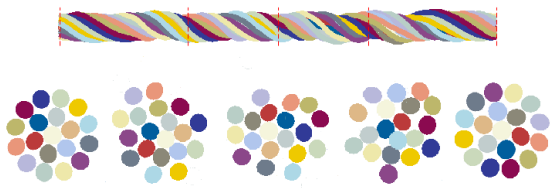

Fig. 1. Resultaat na het twisten van een bundel van 19 oorspronkelijk rechte vezels. Dit resultaat toont aan dat de vezels aan het oppervlak continu migreren richting het midden van het garen. Dit leidt tot een verstrengeld garen.

III. Schuimmodel

A. Inleiding

Polymeerschuim vertoont een cellulaire structuur, die progressief ineenklapt wanneer deze belast wordt in druk. Dit leidt tot een lange zone van relatief constante spanning in het compressieve spanning-rek diagram. Tijdens de plastische vervorming bedraagt de Poisson-factor ongeveer nul. Dit leidt tot een verandering in volume tijdens de vervorming. Hierdoor is het belangrijk om een goed constitutief model te ontwikkelen dat dit specifieke gedrag kan simuleren, om zo tot realistische resultaten te komen.

B. Simulaties

Het plasticiteitsmodel voor *crushable* schuimen in ABAQUS werd gebruikt om de Rohacell 71 RIST schuimkern te modelleren. Het model werd geëvalueerd op basis van een vergelijking van de resultaten van quasi-statische drukproeven bekomen uit simulaties met die van experimentele data. Het model vereist spanning-rek data die kunnen worden bekomen uit een eenvoudige drukproef. Tijdens het stikken penetreren de naalden de schuimkern. De krachten op deze naalden zijn zeer belangrijk voor het goede verloop van het proces. Hoewel het plasticiteitsmodel snelheidsafhankelijk gedrag toelaat, was dit niet vereist voor het Rohacell 71 RIST materiaalmodel. Verschillende experimenten toonden immers aan dat de naaldenpenetratie-snelheid een verwaarloosbaar effect had op de krachten uitgeoefend op de naalden. Het *ductile damage* criterium van ABAQUS (bestemd voor ductiele metalen) werd gebruikt voor het modelleren van het falen van het schuim omdat er geen faalmodel specifiek voor schuimen beschikbaar is. De parameters voor het gebruikte criterium werden invers bepaald aan de hand van een naaldenpenetratie-simulatie.

Een quasi-statische naaldenpenetratie in schuim werd gesimuleerd in ABAQUS/Explicit. De naald werd verondersteld axisymmetrisch te zijn met een straal van 1.5 mm, en penetreerde het schuim verticaal aan een snelheid van 5 m/s. Het schuim werd gemodelleerd in de vorm van een schijf met een straal van 15 mm en een hoogte van 30 mm. De schuimschijf werd vastgehouden in alle richtingen aan zijn cilindrisch buitenoppervlak. De naald werd gemodelleerd als een vast lichaam en beperkt in alle richtingen, behalve de verticale richting. Een tangentiële frictiecoëfficiënt van 0.3 werd verondersteld. Gelijkaardige experimenten werden uitgevoerd door Acrosoma. Hierbij werd echter gebruiktgemaakt van een realistische stiknaald waarvan de punt niet axisymmetrisch was.

C. Resultaten

De totale verticale kracht uitgeoefend op de naald vertoonde een goede overeenkomst met de kracht die experimenteel werd bepaald, zie Figuur 2. De kracht bereikt een maximale waarde daar waar de naald volledig in het schuim zit, en valt daarna terug tot een constante waarde wanneer de punt uit het schuim komt. De overgebleven kracht op de naald is afkomstig van de wrijving tussen de naald en het schuim. Het verbrijzelen van het schuim gebeurt enkel lokaal, rond de naaldpunt. Hierdoor blijft de spanning en de rek beperkt tot vlak rond de naald.

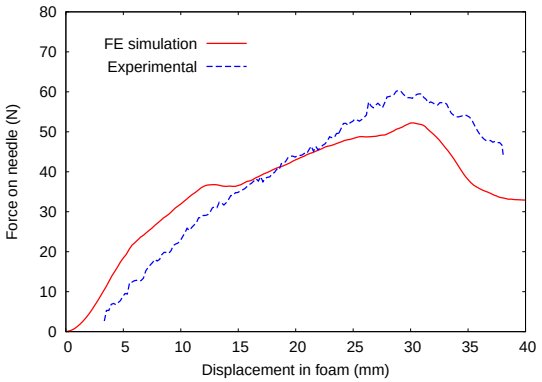

Fig. 2. Kracht-verplaatsing diagram voor de penetratie van een Rohacell 71 RIST schuim (dikte 30 mm) door een naald.

Na onderzoek van de energie-output gegenereerd door ABAQUS, kon worden geconcludeerd dat de uitgeoefende kracht op de naald voornamelijk te wijten was aan de wrijving en in mindere mate aan de verbrijzeling van het schuim, zie Figuur 3. Verbrijzeling vindt enkel plaats aan de naaldpunt, waardoor de verbrijzelkracht constant blijft wanneer de naaldpunt

zich volledig in het schuim bevindt. De wrijvingskracht neemt toe tot een maximale waarde daar waar de naald zich volledig in het schuim bevindt.

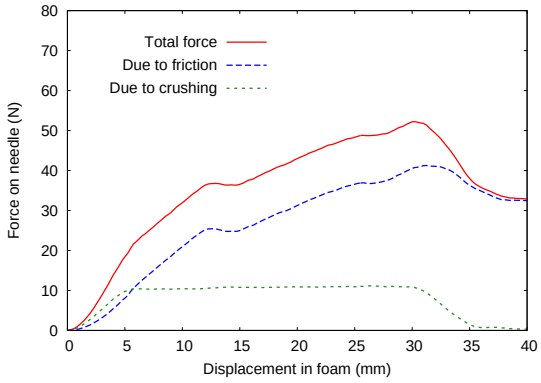

Fig. 3. Kracht-verplaatsing diagram voor de penetratie van een Rohacell 71 RIST schuim (dikte 30 mm) door een naald, en de compenten vanwege frictie en verbrijzeling.

IV. Simulatie van het stikproces

A. De Z-steek

De productie van Z-gestikte sandwichpanelen werd gesimuleerd met behulp van het garen- en het schuimmodel. De verschillende stappen in de vorming van een Z-steek zijn geïllustreerd in Figuur 4. De gemiddelde naaldsnelheid in het productieproces van Acrosoma bedraagt ongeveer 30 mm/s. Daardoor beslaat de vorming van één Z-steek enkele seconden. Deze natuurlijke tijdschaal is eerder groot voor een expliciete simulatie, wat negatieve effecten heeft op de computationele kosten.

B. Factoren die de computationele kosten beïnvloeden

In expliciete analyses bepaalt het stabiele tijdsincrement Δt_{stable} de voortgang van de simulatie. Wanneer Δt_{stable} klein is in vergelijking met de tijdschaal van de simulatie, zijn er zeer veel tijdsincrementen nodig. Hierdoor nemen de computationele kosten toe. Het stabiele tijdsincrement wordt automatisch berekend door ABAQUS, en wordt bepaald door het element met de kortste lengte L, de Young's modulus E en de densiteit ρ van dat element:

$$\Delta t_{stable} \propto L \sqrt{\frac{\rho}{E}} \tag{1}$$

Het stabiele tijdsincrement van de stiksimulatie is eerder klein in vergelijking met de natuurlijke tijdschaal van het stikproces. Hierdoor namen de computationele kosten sterk toe. Verder hadden ook de complexe contact interacties een nadelige invloed op de computationele kosten. Deze factoren beperkten de bruikbaarheid van het model.

C. Simulaties

De naald en de haak werden gemodelleerd als vaste lichamen en werden verplaatsingsgestuurd bewogen in verschillende stappen vergelijkbaar met die in Figuur 4. Er werd gekozen om ook een voorgeboord schuim te modelleren omdat dit de computationele kosten aanzienlijk vermindert. Ook Acrosoma maakt af en toe gebruik van voorgeboorde schuimen om het stikproces met koolstofgaren te vergemakkelijken.

Verschillende simulaties werden uitgevoerd, waarbij de gareneigenschappen, de schuimmaasgrootte en de penetratiesnelheid gevarieerd werden. Dit om tot een efficiënt model te kunnen komen. Er werd *mass scaling* toegepast op het schuim in elke simulatie. Het garenmodel voor een eerste test werd gemodelleerd met één keten van truss elementen. Een tangentiële frictiecoëfficiënt van 0.3 werd gebruikt voor alle onderdelen van de simulatie.

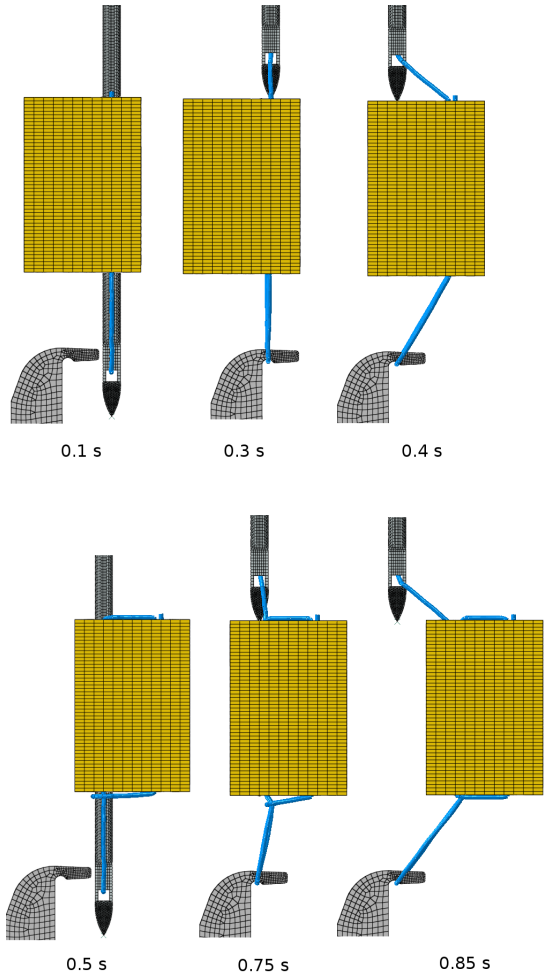

Fig. 4. Vorming van een Z-steek doorheen een schuimkern.

D. Resultaten

De resultaten gaven aan dat de meeste modellen niet haalbaar waren vanwege hun hoge computationele kosten. Verder werden ook contactproblemen tussen het garen en de naald waargenomen. Deze problemen leidden tot foute spanningen in het garen of tot contactverlies tussen het garen en de naald. Aan de basis van dit probleem lag de vereenvoudiging van de gebruikte naaldgeometrie. De eigenlijke stiknaald heeft een complexere geometrie, zodat de wrijving met het garen verminderd wordt.

Een maas toekennen aan dergelijke geometrie bleek moeilijk. De geometrie werd daarom vereenvoudigd naar een geometrie met meer rechte hoeken. Hierbij werd waargenomen dat de truss elementen vast kwamen te zitten achter deze scherpe rechte hoeken. Dit probleem kon gedeeltelijk worden opgelost door de Young's modulus van het garen te verlagen (met een factor 10), of door wrijvingsloos contact te gebruiken. Toch is een fijnmazige naaldgeometrie met afgeronde hoeken aangewezen.

De resultaten van de stiksimulatie voor een voorgeboord schuim gekenmerkt door wrijvingsloos contact en een lage Young's modulus voor het garen worden getoond in Figuur 4. Hierop is te zien dat deze modellen geschikt zijn voor de simulatie van het stikproces van sandwichpanelen. Er is echter nood aan verder onderzoek en aan een optimalisatie van de onderdelen en de parameters van de stiksimulatie om de contactproblemen te vermijden en de computationele kosten te verminderen.

V. Conclusie

De modellen die in deze thesis werden ontwikkeld kunnen worden gebruikt om een stikproces te modelleren en om het gedrag van garens te onderzoeken. Hun gebruik voor de stiksimulatie is echter nog beperkt vanwege de te hoge computationele kosten. Een mogelijke oplossing hiervoor ligt in het gebruik van voorgeboorde schuimen. Het garenmodel en het schuimmodel leveren reeds goede resultaten op, maar een realistische naaldgeometrie moet worden gebruikt in verdere testen om zo het vasthaken van de truss elementen aan scherpe hoeken te voorkomen.

Het garenmodel laat toe om verschillende vezelmaterialen te simuleren en kan zowel worden gebruikt voor het stikproces als voor andere toepassingen.

Referenties

[1] Anamaría Henao, Marco Carrera, Antonio Miravete, and Luis Castejón, "Mechanical performance of through-thickness tufted sandwich structures," *Composite Structures*, vol. 92, no. 9, pp. 2052–2059, 2010.

[2] P Potluri, E Kusak, and T.Y Reddy, "Novel stitch-bonded sandwich composite structures," *Composite Structures*, vol. 59, no. 2, pp. 251 – 259, 2003.

[3] C Sickinger and A Herrmann, "Structural stitching as a method to design high-performance composites in future," in *Proceedings TechTextil Symposium*, 2001.

[4] Damien Durville, "Finite element simulation of textile materials at mesoscopic scale," *Finite element modelling of textiles and textile composites*, 2007.

[5] Y Mahadik and SR Hallett, "Finite element modelling of tow geometry in 3d woven fabrics," *Composites Part A: Applied Science and Manufacturing*, vol. 41, no. 9, pp. 1192–1200, 2010.

[6] Steve Green, Andrew Long, and Stephen Hallet, "Numerical modelling of 3d woven composite preform deformations," 2012, Presented at the ACCIS annual conference in 2012, Bristol, United Kingdom.

Contents

Chapter 1

Introduction

Sandwich composite structures have been used since World War II, where they were utilised as a lightweight structural material in planes [2]. The next decades, they were mainly used for marine and aerospace applications [3, 4]. However, in times where fuel costs keep rising and the demand for new high-performance materials grows every year, sandwich structures are now used in all sorts of applications because of their high structural capacities with minimal weight [5, 6]. For example, replacing conventional steel parts in trailer trucks with light-weight sandwich structures, reduces the weight of the vehicle significantly, which decreases fuel costs and emissions [7]. However, in spite of the many benefits, sandwich structures are very sensitive to failure, especially failure due to delamination of the core and skins. This led to the development of relatively new through-the-thickness reinforced sandwich structures [8]. One of the most promising methods to obtain this reinforcement, is by using the well known textile process of stitching [4, 9, 10, 11]. The research focused on stitched sandwich structures is, however, still rather limited [11]. Before these new materials can replace today's common materials and have a profound presence in our society, for example in the fuselage of new Boeing aeroplanes, their production and behaviour have to be fully understood. Simulating the stitching process is a great way to increase the understanding of these new materials, as this production step determines to great extent the final mechanical properties.

This thesis aims to assess the feasibility of using the commercial finite element analysis software package *ABAQUS* to simulate the stitching process of sandwich structures, and in particular, to construct a model that is able to simulate the yarn behaviour during this process. Due to the fact that the the constituting materials show a variety in properties (stiff needles, crushable foams or flexible yarns), a realistic simulation requires precise modelling of each component in the stitching process. The different steps required for

the modelling of the stitching process are therefore treated in different chapters. Chapter 2 gives more information on the mechanics and properties of stitched sandwich panels, the production process of Acrosoma and the finite element package ABAQUS. Chapter 3, Chapter 4 and Chapter 5 treat the development of a yarn model. The key to modelling the stitching process is a good yarn model. The published literature concerning the numerical modelling of fibrous materials is treated in Chapter 3. Several yarn models are constructed and tested with a simple benchmark in order to choose the most suited model for the stitching simulation in Chapter 4. The most suited yarn model is then developed in depth in Chapter 5. The two other main components in the process are the foam core and the needle system, which are treated in Chapter 6 and Chapter 7 respectively. The constructed models are used in Chapter 8 to simulate the stitching of a sandwich panel.

A collaboration between the Department of Materials Science and Engineering and the Department of Textiles at Ghent University made it possible to use the knowledge of both departments in their specific area of research to its fullest extent. Furthermore, industrial partner Acrosoma has much experience with stitching sandwich structures, and made it possible to work on a real-life application: simulating their stitching process.

Chapter 2

Technical introduction

2.1 Properties and production of 3D reinforced sandwich panels

The term *sandwich panels* designates the class of structural composite materials, also known as sandwich-structured composites. Sandwich panels consist of two relatively thin outer skins which are separated by a low-density core, see Figure 2.1. The skins are made of stiff and strong materials, like metal sheets, fibre-reinforced polymer (FRP) composites or even wood. These are bonded to a thick low-density core usually made from a low-strength material. Typical core materials are: rigid polymeric foams, metal foams, balsa wood or honeycomb structures. Sandwich panels have a wide range of applications, e.g. wings and fuselage in aircraft, walls in buildings etc. They are used because of their high strength- and stiffness-to-weight ratio, good thermal insulation properties and damping abilities.

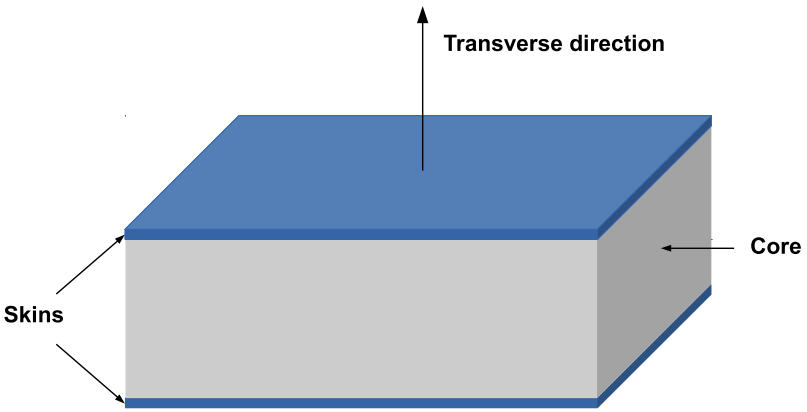

Figure 2.1: Schematic diagram of a sandwich panel.

The main idea behind sandwich panels is to increase the bending stiffness without a significant increase in weight. The core provides support for the skins and prevents them from buckling. The core's thickness provides high bending stiffness to the panel. This is illustrated in Figure 2.2.

Bending Stiffness	1.0	7.0	37.0
Weight	1.0	~ 1.0	~ 1.0

Figure 2.2: Relative increase in bending stiffness and weight by thickening the core.

2.1.1 Failure in sandwich panels and reinforcement techniques

Sandwich panels are often loaded transversally during application. During loading, one skin experiences compression and the other experiences tension, while the core will be stressed mainly in shear. It must have sufficient shear strength and stiffness to withstand these stresses. A common type of failure encountered in sandwich panels is failure of the core due to shear stress, directly followed by delamination between core and skins [12]. Failure due to delamination is also common in other composites, such as laminates. Transversally reinforcing sandwich panels by stitching can improve the delamination resistance [13, 14, 15]. This method is in particular applicable to sandwich panels consisting of a foam core and FRP composite skins, but can also be used in other composite structures, such as laminates. The core and skins are sewed together by a high tensile strength yarn, mostly carbon, glass or aramid yarn, see Figure 2.3. After resin injection, the yarn acts as a rigid column under compression and provides a solid link between the layers. The stitches will delay and stop the growth of delaminations. Furthermore, the yarns in the transversal direction also improve the out-of-plane strength and stiffness. These panels are usually called trough-thickness reinforced composites, stitched composites or 3D reinforced composites. Similar ways of reinforcing often used include Z-pinning, whereby stiff metallic or FRP pins are inserted in the panel [16, 17, 18], column or tube reinforcing [14], or 3D weaving. Stitching, which is a process common to the textile industry, has several benefits over the other reinforcement methods, making it useful for fast and relatively easy production of sandwich panels [4]. 3D woven composites require in-situ core formation, making it difficult to obtain a high quality core material. The Z-pinning process is only used for aerospace

applications because it is expensive and slow.

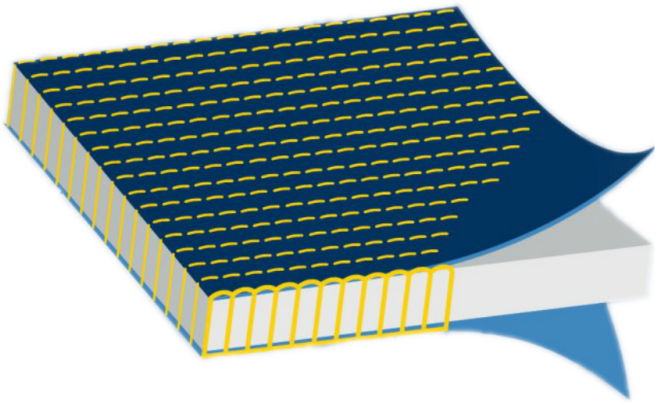

Figure 2.3: Illustration of a stitched composite panel. The stitch yarn sews the skins to the core.[19]

Reinforced sandwich panels are less prone to failure by delamination or failure due to compressive stresses acting on the core. However, the damage introduced by the reinforcement can decrease the strength of the material [20, 21, 18]. During stitching, steel needles are punched trough skin and core material. This introduces damage in both materials which can act as a crack initiation site under loading. When FRP composite skins are used, the needles can create lenticular openings in the fibrous materials which leads to resin rich zones, so-called *resin eyes*. This is shown in Figure 2.4. In their review articles on the effect of stitching on the mechanical properties of FRP composites, Mouritz et al. [22, 23] conclude that stitching could have a profound effect on the in-plane mechanical properties, with reductions up to 20 %. However, the reduction of in-plane properties could be less severe in sandwich panels, because the foam core is probably less sensitive to this kind of damage.

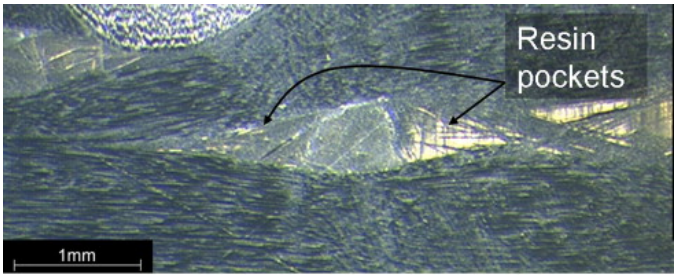

Figure 2.4: Resin rich zones formed by a stitching thread.[11]

2.2 Stitching sandwich panels

The previous section showed that stitching the sandwich panels increases the delamination resistance. This section deals with the stitching process. The mechanical properties of the panels are influenced by the used process parameters and materials, e.g. stitch density, needle thickness, yarn thickness, yarn material, etc. Most research treats the stitching of laminated composites, but the conclusions are still applicable to sandwich panels due to their similarity and the fact that the skins are usually made from laminates.

2.2.1 General overview of the stitching process

The stitching of sandwich panels basically involves sewing a high strength yarn through a dry preform, i.e. a foam core and dry fibrous skins, with an industrial sewing machine. The process is very similar to tufting, which is a common process in the textile industry, e.g. in the production of carpets. A row of needles penetrates the sandwich assembly and the stitch yarns are inserted trough the structure. Depending on the type of process and type of stitch being used, the yarns can form loops, be cut or lock with other yarns (bobbin yarns) on the other side of the sandwich panel. When the needles retract, the yarns are tensioned and loops can be tightened. The sandwich assembly is then pulled forward a certain distance and the next set of stitches is produced. The process described here is just the basic idea behind the process of stitching sandwich panels. There are many possibilities to obtain a more complex final result, e.g. stitching the panel from both bottom and top layer, varying the angle of the needles, etc. An illustration of a possible tufting process is shown in Figure 2.5. This process combines weaving and tufting techniques: a locking yarn is inserted in the same manner weft yarns are inserted in woven fabrics.

2.2.2 Parameters influencing the properties of a stitched sandwich panel

The final mechanical properties depend on a whole range of factors. They can be divided roughly as process parameters, e.g. needle spacing and yarn tension, and material parameters, e.g. properties of core and skin and yarn tensile strength. An overview of possible influences is given in Figure 2.6. This section explains some of the basic parameters and their possible effects, but is not intended as a thorough parametric study. These parameters are suggested here mainly because they could be studied by simulating the stitching process.

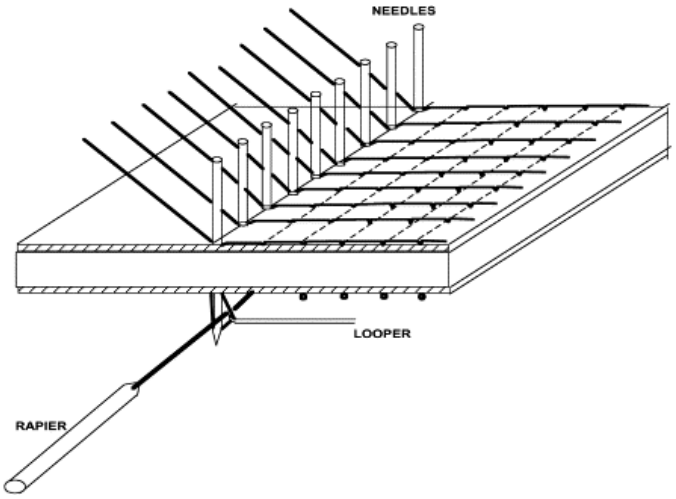

Figure 2.5: Illustration of a tufting process for sandwich structures.[4]

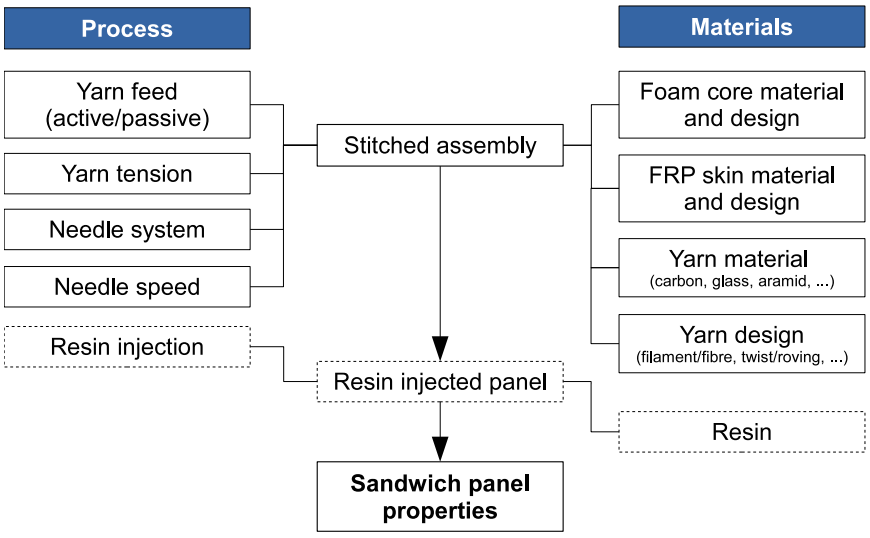

Figure 2.6: Schematic overview of the elements influencing the properties of a stitched sandwich panel. (Elements in dashed lines are not part of the simulation considered in this thesis)

Yarn feed

The yarn is fed from bobbins to the stitching needles. These bobbins can have an active or passive control system. The tension in the yarn is determined by the yarn feed if no other tensioning devices are used.

In a passive system, the tension in the yarn is solely responsible for the unwinding of the bobbin. As the needle punches trough the sandwich panel, the yarn is pulled along this distance creating tension in the yarn. This tension acts as an unwinding force, resulting in the extra length of yarn being reeled off. The yarn is usually reeled off transversely from the bobbins, so only a small force is necessary for unwinding. The amount of tension in the yarn is mainly determined by the weight of the length of yarn between the needles and the bobbin. This makes the process less controllable, because inhomogeneities in yarn tension can lead to faults in the stitching process.

Actively driven feeding systems avoid these problems by giving full control over the unwinding of the bobbins and the yarn tension. Although more expensive, these systems have the potential to obtain higher quality sandwich panels by assuring a uniform controllable tension in the yarn during stitching.

Yarn tension

A certain amount of tension is always needed for the stitching process. It assures that the yarns remain straight after insertion, which is necessary to obtain good reinforcement properties after resin injection. Furthermore, it is also necessary when loops formed by the stitching process need to be tightened. However, when the yarn tension is too high, the foam could be severely damaged by the yarn, which leads to panels of inferior quality.

Needle system

The term needle system designates all parameters concerning the row of needles, e.g. stitch density, needle diameter, needle shape, etc. The needle speed could also be included here, but this is treated separately below.

Stitch density

The stitch density is defined as the amount of stitches per square meter. This density depends on the spacing of the needles in the needle row and the pultrusion distance of the sandwich assembly after each stitch. Increasing the stitch density increases the fibre fraction in the material. This should lead to an improvement in out-of-plane stiffness and strength, but could also lead

to a significant decrease in in-plane properties. Furthermore, it also leads to an increase of the mass, which is unwanted as these panels are often used for their low weight. Wang et al. [14] found that increasing the stitching density improves the bending failure strength while decreasing the flexural rigidity. Lascoup et al. [12] found similar results for the bending failure stress and also found improvements in compressive and shear strength. Furthermore, they take change in density into account by comparing the specific properties of stitched specimens. Henao et al. [8] show that a higher stitch density also increases the edge-wise compression strength.

Stitch angle

The stitch angle can be varied anywhere from 0°, i.e. vertical stitches, up to 50° - 60°. Most commonly found stitching angles are 0° and 45°. Vertical stitches improve the out-of-plane properties, but are more susceptible to buckling, whilst 45°-angle stitches should result in better shear properties [12]. An illustration of a possible stitch with stitch angle different from 0° is given in Figure 2.7.

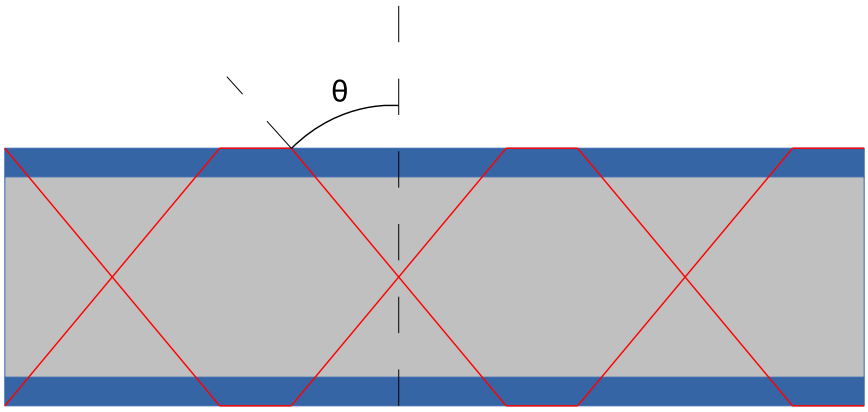

Figure 2.7: Illustration of a θ stitch angle in a sandwich panel.

Needle diameter

For a fixed yarn diameter, increasing the needle diameter results in thicker resin columns after resin injection. This increases the weight of the sandwich panel without improving its strength, as the strength of the FRP columns is coming from the high strength yarn.

Needle shape

The needles that are used to produce stitched composites are similar to those used in textile tufting processes. Due to the higher density and thickness of the foam cores compared to most textile materials, the needles are stiffer

and stronger to withstand the higher stresses during stitching. Since the sandwich assembly can be several centimetres thick, the needles are also somewhat longer than those commonly used in other textile processes. The shape of the needle tip will affect the forces exerted on the needle, see Section 6.3 in Chapter 6. Furthermore, an optimised shape could potentially decrease the friction between the yarn and the foam or decrease the effect of damage.

Needle speed

Low stitching speed could result in less damage induced by the needle, which leads to better quality materials, but is not economically viable. Too high stitching speeds, however, could result in more damage induced by the needle as well as more stitching faults, which leads to lesser quality materials and more costs.

Foam core materials and design

Rigid polymer foams suitable for structural cores are made by many manufacturers and vary in a wide range of properties. Their material properties determine to a great extent those of the final sandwich panel. Foam core materials should thus be carefully chosen, keeping in mind the intended application of the sandwich panel, e.g. low cost, low weight, high strength, etc.

The most important factors concerning foam cores in stitching is their density, cellular homogeneity and thickness. Dense foams result in higher forces acting on the needles which could lead to breakage or blunting of the needles. A homogeneous cellular structure of the foam is necessary, because differences in local density could lead to small misalignments of the needles resulting stitching faults. The thickness is important because it poses practical limitations on the stitching process. It cannot be increased extensively because this would require very stiff, strong and long needles.

FRP skin materials and design

Just like the foam cores, the skin materials can also vary widely in material and structure, e.g. woven plies, laminated preforms, UD fibre layers, non crimp fabrics, etc. All these structures have their own advantages and disadvantages as skin materials. However, it is important that all these structures could be damaged by stitching. The stitching needle and yarn distort the geometry of the fibre materials locally, forming resin rich zones, see Figure 2.4,

or deflecting the in-plane fibres in the transversal direction, i.e. crimping, see Figure 2.9. Local breakage of fibre material is also observed, see Figure 2.8. These defects could lead to the deterioration of in-plane mechanical properties [22, 23].

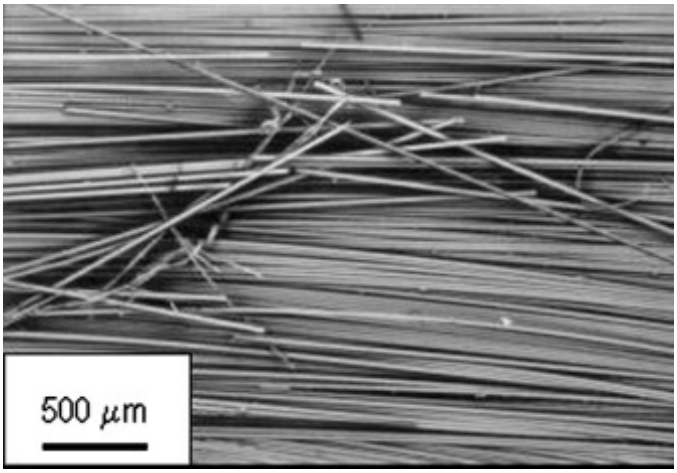

Figure 2.8: Fracture of the in-plane fibres due to interaction with a stitching needle.[24]

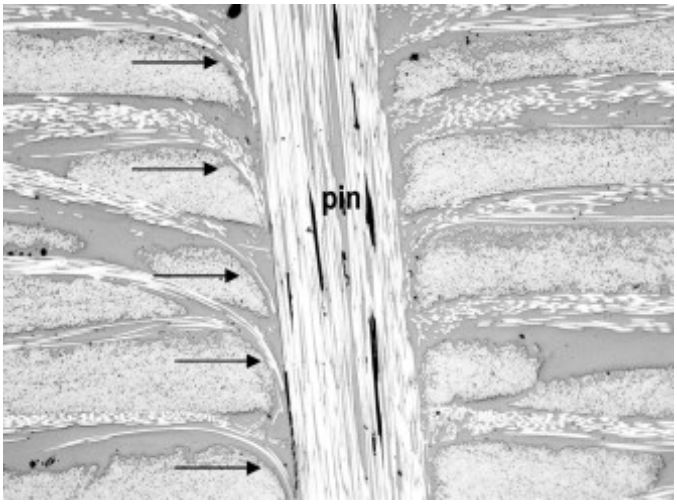

Figure 2.9: Crimping of the in-plane fibres due to stitching.[25]

Yarn material

Most scientific research focusses on carbon, glass or aramid yarns, although some studies also mention other materials [12]. Commercially available stitched sandwich panels are found with glass, aramid, nylon or steel yarn

stitching. Carbon yarns are less common. The aerospace industry is not too keen on using aramid reinforced sandwich panels as aramid fibres are susceptible to moisture absorption.

The most important properties of the yarn are its flexibility, tensile stiffness and tensile strength. A high flexibility is needed in order for the yarn to be suitable for the stitching. process. High tensile stiffness and strength assure good reinforcement properties. The reason why carbon yarns are less commonly found in stitched sandwich panels is probably due to the low flexibility of carbon fibres. Therefore, stretch-broken carbon yarns are used for stitching, see also Section 4.1 in Chapter 4.

Yarn design

Yarns made from long continuous filaments or from short staple fibres are called filament yarns and staple yarns respectively. Staple yarns require a certain amount of twist to hold the fibres together, whilst in filament yarns this is not necessary due to the length of the filaments (although a small amount of twist is usually applied for easier handling of the yarn). In composites, untwisted filament yarns are called rovings. Rovings provide better features for reinforcing, as the lack of twist results in straight yarns, which can take up more of the load. Furthermore, there are no protruding fibres at the yarn surface which could act as crack initiation points.

Different yarn diameters can also be used for stitching. Mouritz and Cox [24] report that changing the yarn diameter has little influence, but suggest that thinner reinforcements offer the possibility of minimizing damage, especially with Z-pinning. This is an interesting finding as thinner yarns also require less resin take-up and thus lighter structures can be obtained.

2.3 Acrosoma stitched sandwich panels

2.3.1 Production process

Acrosoma is a company specialised in the design, development and manufacturing of structural composite structures. It is based in Lokeren, Belgium. They started as a spin-off from a trailer building company in 1993 and developed a patented technology to produce 3D stitched sandwich panels. The main aspect of their method is the continuous production of stitched sandwich panels. The different stages in this process are illustrated in Figure 2.10. From left to right, one can see the foam core and skins entering the stitching stage, resin infusion and curing of the preform, and a pultrusion system that pulls the final sandwich panel forwards. The machine is able

to produce up to 150 m^2 per hour. Only the first stage is of interest to this study. Subsequent resin injection and curing will not be simulated.

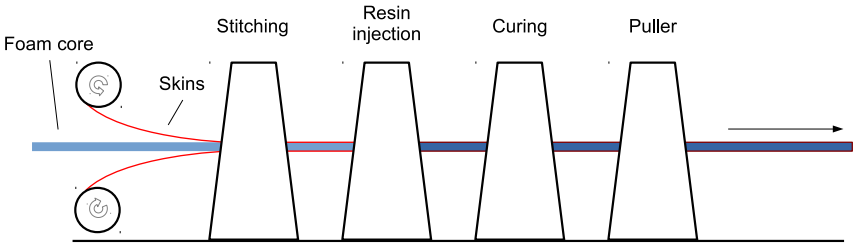

Figure 2.10: Schematic overview of the continuous production process for Acrosoma sandwich panels.

Acrosoma produces panels with 0° and 45° stitch angles. The simulated process produces stitch angles of 0°, which are called Z-stitches. The different steps in the stitching process are illustrated in Figure 2.11. Needles push through the foam in vertical direction and take the yarn to the other side of the panel. The yarn is transferred to a looping hook and the needle is retracted, forming a loop at the bottom of the panel. The panel moves one step forward and the process is repeated. The needle goes through the formed loop, before the yarn is transferred to the holder, and a second loop is formed. As the process continues, a series of entangled loops are formed.

2.3.2 Materials

An overview of the used materials in the studied panel is given in Figure 2.12. The top layer is a non crimp fabric, which provides the skins with high strength and stiffness after resin injection. Furthermore, it somewhat protects the underlying glass fibre mat and the yarn loops from outside influences. Rohacell 71 RIST structural foam is used for the core material. This material is optimised for core applications with resin infusion techniques. The foam core and glass fibre mat are stitched with a carbon fibre yarn from Schappe Techniques. While the fabric layers and the resin are extremely important for the behaviour of the final structure, these are not essential to the stitching process. Therefore, only the foam core and the yarn are further investigated and modelled. More information about the yarn and foam material can be found in Chapters 3 to 6.

2.4 ABAQUS: finite element analysis software

The concept of a FE-analysis is demonstrated in Figure 2.13 with an example from the ABAQUS manual [1]. During pre-processing, the initial geometry

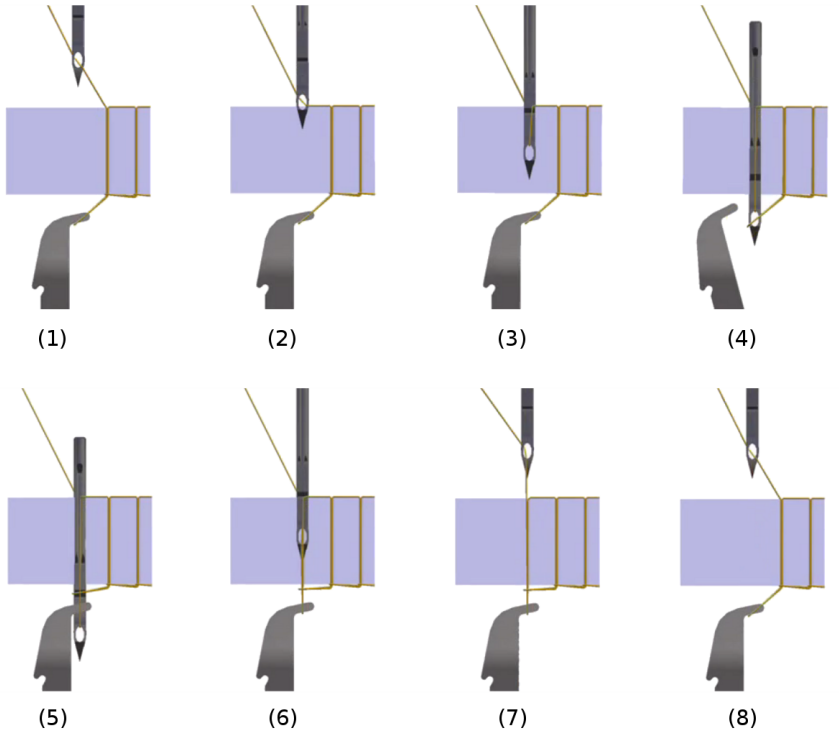

Figure 2.11: Overview of the steps in the forming of a Z-stitch.

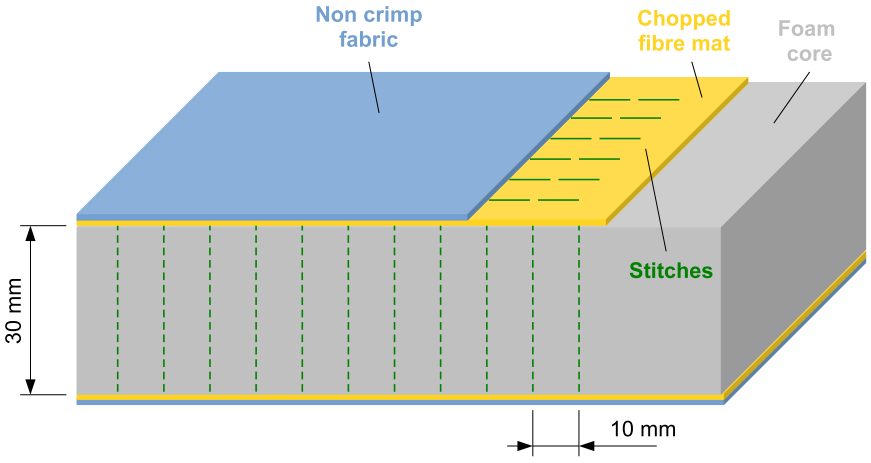

Figure 2.12: Overview of the different parts in the sandwich panel.

of the model is constructed and appropriate material properties, mesh elements and boundary conditions are applied to the model. The deformed state is calculated during processing and the results can be visualised in the post-processing step.

ABAQUS (or Abaqus unified FEA) is a commercially available software suite from Dassault Systems to perform finite element analysis. It can be used to simulate all sorts of engineering problems, e.g. linear and nonlinear material behaviour, thermal and electrical problems, crash and impact events, etc. The software consists out of a pre-processing (ABAQUS/CAE), a processing (e.g. ABAQUS/Standard or ABAQUS/Explicit) and a post-processing (ABAQUS/CAE) unit, making it possible to do a whole FE-analysis of a problem with only one software suite. ABAQUS version 6.12 was chosen to simulate the stitching process since the Department of Materials Science and Engineering has extensive experience with the software package. Furthermore, it has a well established reputation in academic and research institutions and is also used by Acrosoma.

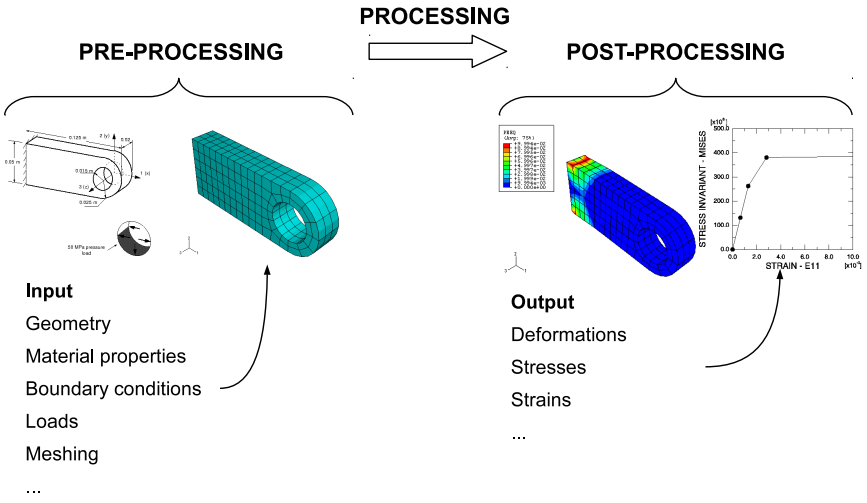

Figure 2.13: FE-analysis of the stresses in a connection lug (images taken from the ABAQUS manual [1]).

Chapter 3

Modelling the yarn: overview

Fibrous materials constitute a class of materials which are used in a wide range of applications, such as composites, technical textiles or clothing. In composites, these materials offer an efficient reinforcing method and are used in various forms, e.g. as individual fibres, yarns, structured fabrics or non-structured fabrics. The properties and geometry of the fibrous preforms determine to a great extent the mechanical properties of the final composite part. Other applications also depend heavily on the properties and structure of the fibrous materials, e.g. filtration applications or bullet-proof garments. The development of new and optimized materials would benefit considerably from modelling techniques, making it possible to assess the properties of the final structure without expensive and time-consuming experimental prototyping. Hence, at the beginning of the 20th century, modelling began in order to predict the behaviour of these complex materials when subjected to various loadings. This led to a better understanding of their behaviour, but it did not result in many quantitative predictions, especially not when compared to the extensive research conducted on other materials [26]. Furthermore, the textile industry has been around for many centuries and relied to a great extent on intuition and practical knowledge. Apart from this, fibrous materials are rather complex and it is difficult to capture their behaviour in analytical models. Therefore, modelling these materials was for a long time restricted by computing power. Since computational capabilities have grown substantially in the past decade and fibrous materials are being used more and more in high-end composite applications, e.g. the aerospace industry, the amount of research on modelling these materials has increased very recently. A great part of the research is concerned with the prediction of composite part behaviour, but it is mainly focused on the final composite structure, where the resin injected fibrous material behaves completely different from its dry preform structure (e.g. [27]). Models of dry fibrous materials are still not numerous, but progress is made and several

approaches are yielding good results.

3.1 Fibrous materials

Fibrous materials differ substantially from other, more common materials, e.g. metals, ceramics or plastics, due to their intrinsic complexity. Several characteristics contribute to this complexity, making it difficult to construct a fully realistic model.

A first feature is the multi-scaled nature: depending on the scale, these materials are made up of fibres or yarns. At the *macroscopic scale* the material is considered as continuous. It denotes the whole component scale and has dimensions ranging from a few centimetres to several meters. Yarns make up the *mesoscopic scale* with dimensions from one to several millimetres. Meso-scale modelling often treats the yarns as continuous materials, whereby the fibrous nature is taken into account by using appropriate constitutive laws. Usually materials are modelled by means of a representative unit cell (RUC) in the case of periodic materials, e.g. woven, knitted or braided fabrics, or a representative elementary volume (REV) in the case of non-woven fabrics. By using periodic boundary conditions, a RUC can be extended to represent the whole scale component. The most realistic results are obtained by modelling at the *microscopic scale* where the individual fibres are modelled. Dimensions range from one to several micrometres and the material is effectively continuous at this scale. Although yielding the best results, micro-scale modelling is limited by computing power. The amount of fibres in a yarn could easily be as high as a few thousand, which would result in enormous computational costs. The fibres form the building blocks of these materials. Hence, macroscopic properties depend to great extent on the microscopic fibre properties and their arrangement. This hierarchy makes it possible to construct efficient models based on the results from simulations at the underlying scales by using a homogenisation approach. A small segment of a yarn can be simulated using a high amount of fibres. The resulting properties are then used to define a model at meso-scale. The results from the meso-scale, in turn, are used for constructing a model at macro-scale. This approach makes it possible to model large amounts of material, while still including the fibrous behaviour at microscopic scale. However, when fibre properties are changed, all the steps should be redone. Furthermore, with each step a small amount of information is lost and a fully realistic model is only possible by modelling the whole material at microscopic scale. Nevertheless, it is possible to obtain much information from homogenised models. The hierarchy of fibrous materials is illustrated in Figure 3.1.

A second feature is the actual fibrous nature which results in geometrical

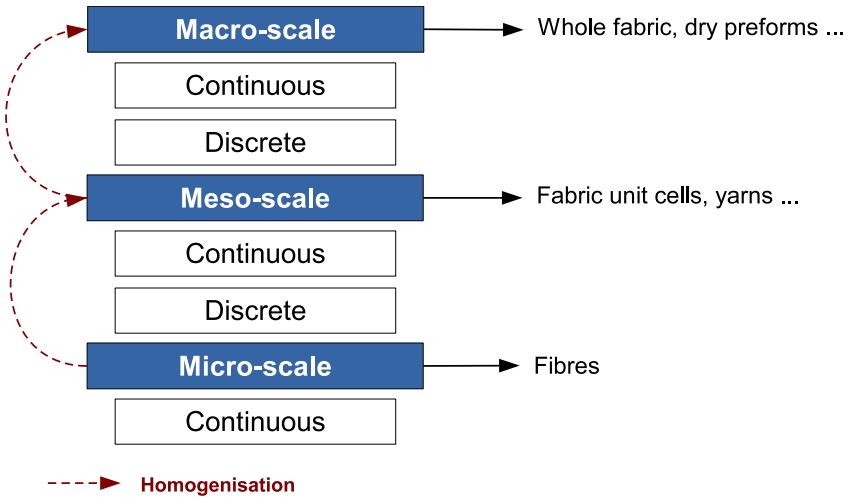

Figure 3.1: Hierarchy of the multi-scale modelling of fibrous materials.

heterogeneity, porosity, anisotropy, high compressibility, low in-plane shear stiffness and low bending stiffness of the material. Usually the fibres are aligned, leading to a high tensile stiffness and strength in this direction. Cohesion between fibres is governed by inter-fibre friction and is quite low. This makes relative displacements of fibres possible, which are the cause of the high anisotropy found in fibrous materials. The bending stiffness is very low, especially when compared to other materials. Therefore, it is often neglected. However, the value of bending stiffness is important when modelling draping behaviour, as it determines the shape and size of wrinkles, or modelling the stretching of knitted fabrics, which is determined by the bending of the loops.

3.2 Models of fibrous materials

In this section an overview is given of the published literature on the numerical modelling of fibrous materials. The focus of this thesis lies on the finite element (FE) analysis of a stitching process. Therefore, emphasis lies in particular on FE-analysis of yarns, but a broad overview is given to illustrate the widely available methods to fibrous materials modelling. The general approaches to model yarn behaviour will be illustrated and several models will be explained to give the reader an idea of the possibilities and difficulties of numerical modelling.

Models are classified according to the scale of interest, i.e. macro-, meso- or microscopic scale. A further classification for FE-models can be made into continuous, discrete and semi-discrete methods (e.g. [28, 29, 30]). Many

models are designed for applications under certain conditions (e.g. [29, 31]): specific loading cases, e.g. bending, torsion, tension, etc., and/or specific structures, e.g. yarns, woven fabric, knitted fabric etc. All these different models can thus be easily classified according to their scale of interest and modelling method.

3.2.1 Macro-scale modelling

Macro-scale modelling is often used for simulating the draping behaviour of fabrics, for example, to study the formability of fabric reinforcements in composite production processes such as the Liquid Composite Moulding (LCM) process. These simulations require large dimensions of fabric, and modelling each yarn/fibre would lead to high computational costs. Furthermore, the local behaviour of yarns is less important than the global fabric behaviour and wrinkling. Nevertheless, discrete methods do account for each yarn in a fabric, but many simplifications to their structure are made to obtain a computationally feasible model.

Continuous methods

At the macroscopic scale, a fabric can be approximated by a 2D structure. Therefore, conventional 2D finite elements such as shell or membrane elements are often used to simulate fabric behaviour (e.g. [32]). Homogenised material properties are used to take the fibrous behaviour of the underlying structure into account.

Lim et al. [33] studied the ballistic impact of fabric armor by representing the fabric as a 2D structure, see Figure 3.2. Suitable material properties accounting for the viscoelasticity of the fabric were obtained by a three-element spring-dashpot model. The fabric was modelled using membrane elements. This made it possible to describe global impact phenomena of fabrics, but no local information on the behaviour of the yarns constituting the fabric is possible.

Boisse et al. [30, 34] constructed their own finite elements to simulate composite forming behaviour. These elements are based on the simplification that the behaviour of the fabric is only governed by the stiffness in the fibre direction and the in-plane shear stiffness. Bending stiffness is not taken into account because it is low compared to the other stiffnesses. However, the exact shape of the wrinkles also depends on the bending stiffness. It is therefore questionable that these elements will simulate the draping behaviour, and wrinkling in particular, to great detail.

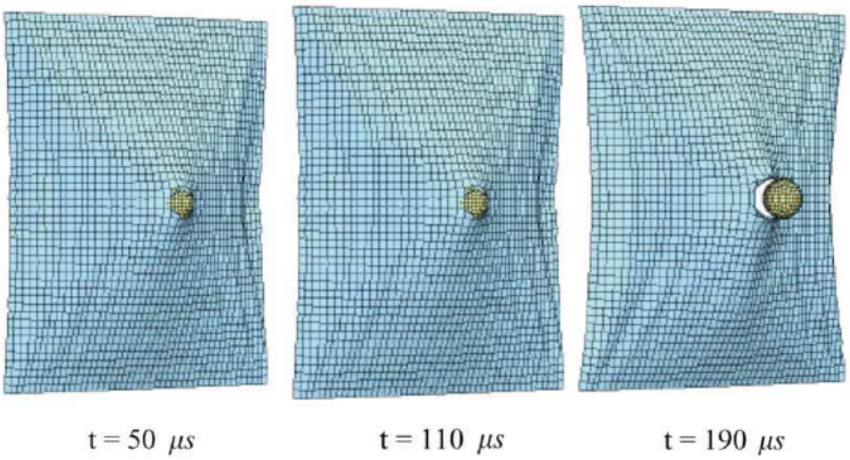

Figure 3.2: Ballistic impact against a fabric represented by continuous membrane elements.[33]

Discrete methods

Fishnet models (e.g. [35, 36]) treat the fabric as a pin-jointed net. This is a geometrical approach usually used for studying draping behaviour and it does not take material properties into account.

Similar to the fishnet approach are *pin-jointed networks* of 1D elements (e.g. [37, 38, 39, 40]), first proposed by Kawabata et al. [41, 42, 43], see Figure 3.3. In this method, cross-over points of the fabric are modelled as nodes with an associated mass. These nodes are then connected by 1D elements, e.g. truss elements, beam elements, spring elements etc., which leads to a pin-jointed net. The yarn interactions, such as crimp, locking or shearing, can be represented by using appropriate elements. Boubaker et al. [44] discretised a fabric into point masses connected by stretching, torsional, shear and extensional springs to account for the yarn behaviour. Cherouat and Billot [45] used a pin-jointed net of truss elements combined with membrane elements to model the forming behaviour of pre-impregnated woven fabrics, see Figure 3.4.

The results of pin-jointed models could also be used to define a material model for shell or membrane elements in continuous methods [46].

3.2.2 Meso-scale modelling

At the mesoscopic scale, yarn behaviour forms the main interest. Two very distinct methods of modelling can be found in literature: continuous methods, which treat the yarn as a continuous material and discrete methods, in

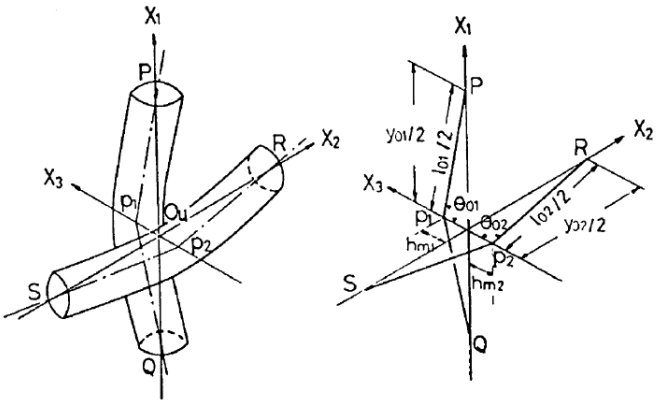

Figure 3.3: Pin-jointed netwerk proposed by Kawabata.[41]

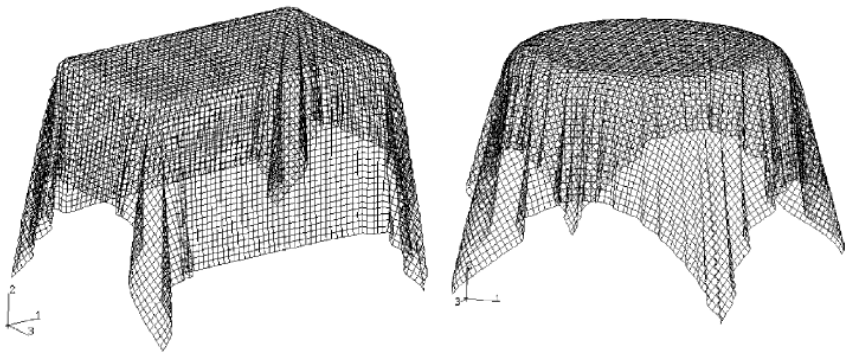

Figure 3.4: Deformed shapes for draping a rectangular (left) and circular (right) table.[45]

which the yarn is made up from a bundle of fibres. More research has been conducted on the first approach, probably because these models are easier to construct and computationally less expensive. Discrete modelling requires efficient handling of the numerous contacts between fibres. Nevertheless, the discrete approach captures the fibrous behaviour automatically without requiring complex constitutive laws.

Continuous methods

Continuous methods require proper constitutive laws and mechanical coefficients to describe the fibrous behaviour of yarns. The behaviour is usually taken orthotropic since the behaviour in the fibre direction is very distinct from the behaviour in the transversal directions. A further simplification of transversal isotropy is often used. An appropriate continuous model should take several specificities into account. These are described by Gasser et al. [47] for the study of woven fabric as: (1) flexible thread behaviour requires quasi-zero values for some stiffnesses, (2) the low value of these stiffnesses can lead to numerical instabilities, (3) the mechanical properties should be given in the material directions during computing, (4) yarn crushing should be taken into account, (5) the theory of large transformations should be used because of geometrical non-linearities (large strains), (6) contact and friction between yarns should be taken into account and (7) boundary conditions must ensure the periodicity of the unit cell. Flexible thread behaviour is obtained when the shear moduli and Poisson's ratios are zero and the transversal Young's moduli are small compared to the Young's modulus in the fibre direction [47, 48].

A first area where meso-scale modelling is of high interest, is the study of the mechanical behaviour of woven fabrics. Gasser et al. [47] simulated the biaxial tension behaviour for different types of weave (plain, twill), material (glass, carbon) and initial undulation. The transversal crushing of yarns is described by a transversal Young's modulus which increases when the transverse and longitudinal strain increases. Gasser et al. assumed a crushing law of the following form:

$$E_k = A|\varepsilon_{kk}^m|\varepsilon_{11}^n + E_{k,0} \tag{3.1}$$

where A, m and n are material parameters obtained by an inverse method from a biaxial tension test, $E_{k,0}$ is the initial transversal Young's modulus, which is small or equal to zero. Subscript k denotes a transversal direction perpendicular to the fibre direction, which is denoted by subscript 1. Hourglass control is used to overcome numerical instabilities due to the small or zero values of some moduli, see also Appendix A. These properties are then used in a FE-package and assigned to 3D continuous elements making up the initial geometry of the fabric. The FE-model is depicted in Figure 3.5.

They obtained results in good agreement with experiments. Boisse et al. [48] studied the behaviour of textile reinforcements for thin composites. Simulations of fabric unit cells provided local information on the fabric behaviour. Reinforcement bar (rebar) elements were used to link the finite elements in the fibre direction and ensuring that the orthotropic directions follow the material directions. Boisse et al. [49, 50, 34], Badel et al. [51, 52] and Nguyen et al. [53] used a similar FE-model to analyse the behaviour of woven unit cells in biaxial tension, in-plane shear and compaction respectively. These simulations are an effective alternative to difficult and costly experiments. Furthermore, the results can be used to define a finite element for analysing the forming behaviour at macroscopic scale [30, 34]. A refined approach to better follow the fibre direction was defined by Boisse et al. [50] and Badel et al. [52] and implemented in ABAQUS through a user subroutine. This approach was necessary to overcome converging problems which occurred when using the classical FE-codes approaches of following material direction, see Figure 3.6. The classical approaches are more suitable for isotropic materials, such as metals, and can lead to inaccurate results in some cases [52].

The compression behaviour of woven fabric is dependent on the fibrous behaviour of the yarns, see Figure 3.7. Potluri and Sager [54] used a linear elastic orthotropic material with transversal isotropy. They assumed a ratio of longitudinal Young's modulus on transversal Young's modulus equal to 100 (as suggested by Page and Wang [55]) and (quasi-)zero values for the shear moduli and Poisson's ratios (as suggested by Gasser et al. [47]). A RUC was modelled with 3D continuum elements and compressed by two rigid plates. The results did not entirely agree with those obtained from experiments, probably due to the assumption of a constant transverse modulus, while this modulus actually changes according to a crushing law. Lin et al. [56] also studied the compaction behaviour of one layer of woven fabric. They assumed a power law to describe the transversal Young's modulus and implemented their material model into an ABAQUS/Standard user subroutine.

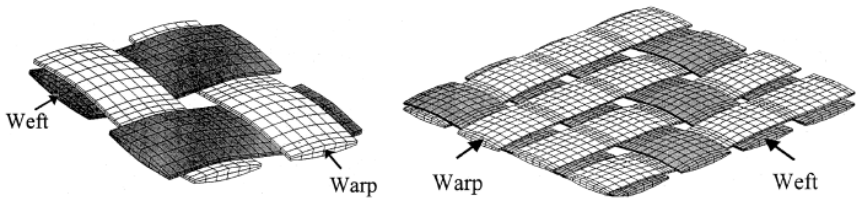

Figure 3.5: RUC of a plain weave (left) and a 3 x 1 twill weave (right).[47]

A second area where meso-scale modelling is of high interest, is the study of ballistic impact on woven fabrics made from high strength fibres, such

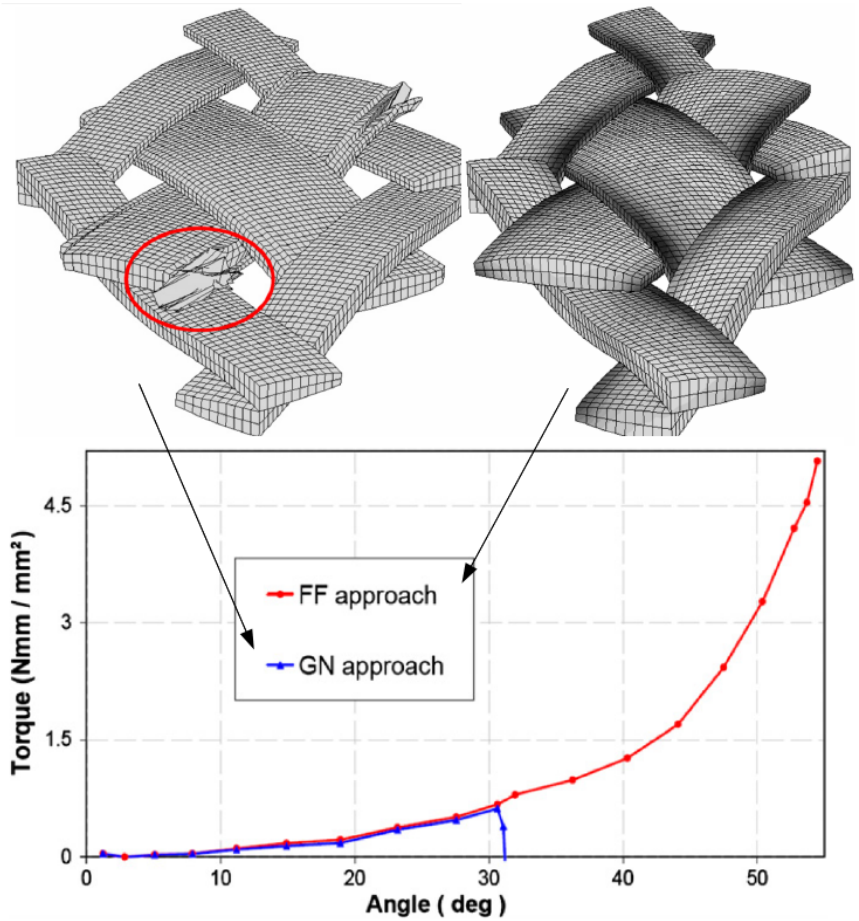

Figure 3.6: Convergence issues arise when shearing a woven fabric with the classical FE-code material orientation approach (GN) and disappear when an alternative approach based on fibre rotation (FF) is used.[52]

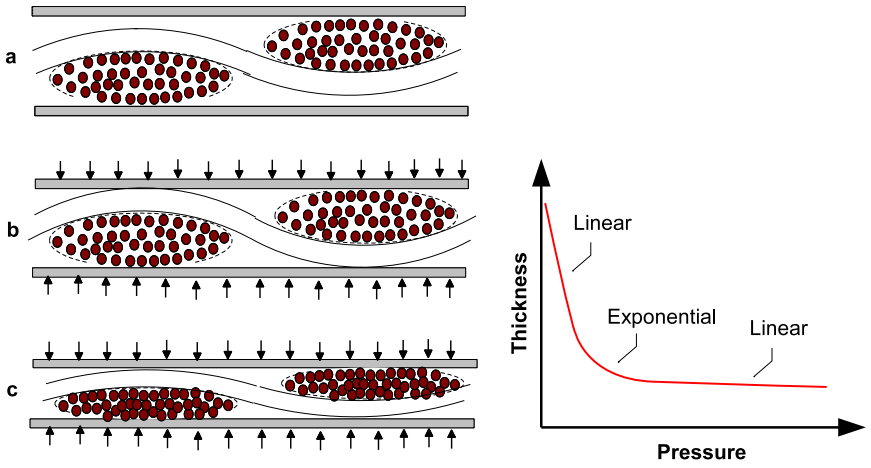

Figure 3.7: Stages of fabric compression (left) and the compression behaviour (right).[54]

as para-aramid or high density polyethylenes [57, 58, 59, 60, 61, 62]. The protection level of these fabrics is not only dependent on the yarn properties, e.g. number of filaments, stiffness, strength, etc., but also on the fabric properties, e.g. weave type, surface density, etc. [57]. By modelling the individual yarns, the effect of weave type and yarn-yarn friction on local impact phenomena can be investigated. Yarns are either modelled by 3D solid elements [59, 60, 61, 62], by shell elements [57, 58] or by a combination of both elements [63, 64]. Shell elements are used to reduce the calculation time of the simulations, however, they do not allow for a change in yarn cross-section during the simulation [57]. Four shell elements with different thicknesses were used to approach the lenticular shape of a yarn in a woven fabric. Several aspects of the model using shell elements are illustrated in Figure 3.8. It shows the rather coarse geometry of the yarns due to the small amount of shell elements. Solid elements allow for a fully orthotropic elastic definition of the material. Duan et al. [59, 60, 61, 62] used an orthotropic behaviour similar to the one suggested by Gasser et al. [47]. However, a constant transversal Young's modulus was assumed, with a ratio of longitudinal on transversal Young's modulus equal to 100. The mesh of the initial geometry and the results from a ballistic impact are given in Figure 3.9 and Figure 3.10 respectively.

The cross-sections of continuous yarns are defined as the envelope of the fibres. This geometry can be observed by tomography or optical microscopy [65, 66], see Figure 3.11. However, it is usually not mentioned whether the initial geometry of the cross-section is taken from experiments or if it is just a general lenticular shape. Furthermore, the initial geometry used in the simulation depends on the studied fabric and has to be defined beforehand.

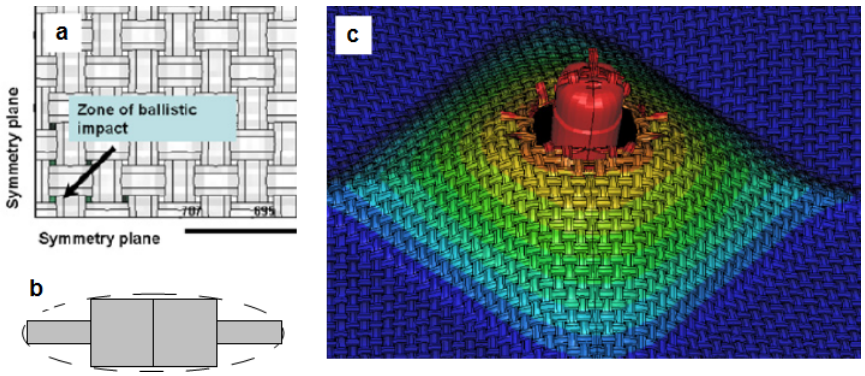

Figure 3.8: Initial geometry (a), cross section with 4 shell elements (b) and ballistic impact against fabric (c) for the shell model.[57]

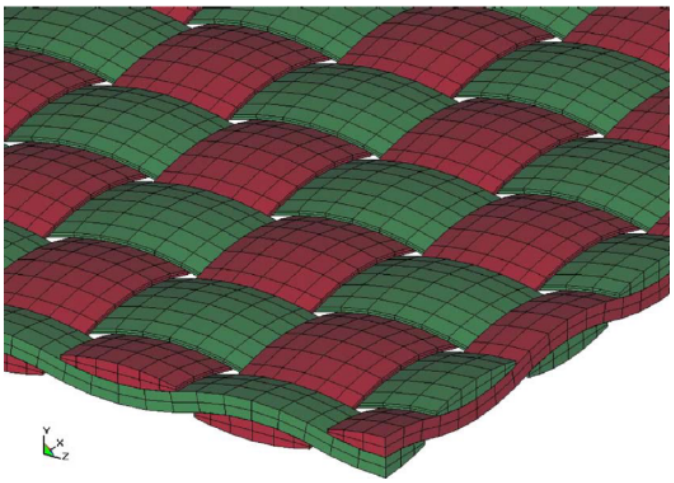

Figure 3.9: Finite element mesh of a plain weave.[61]

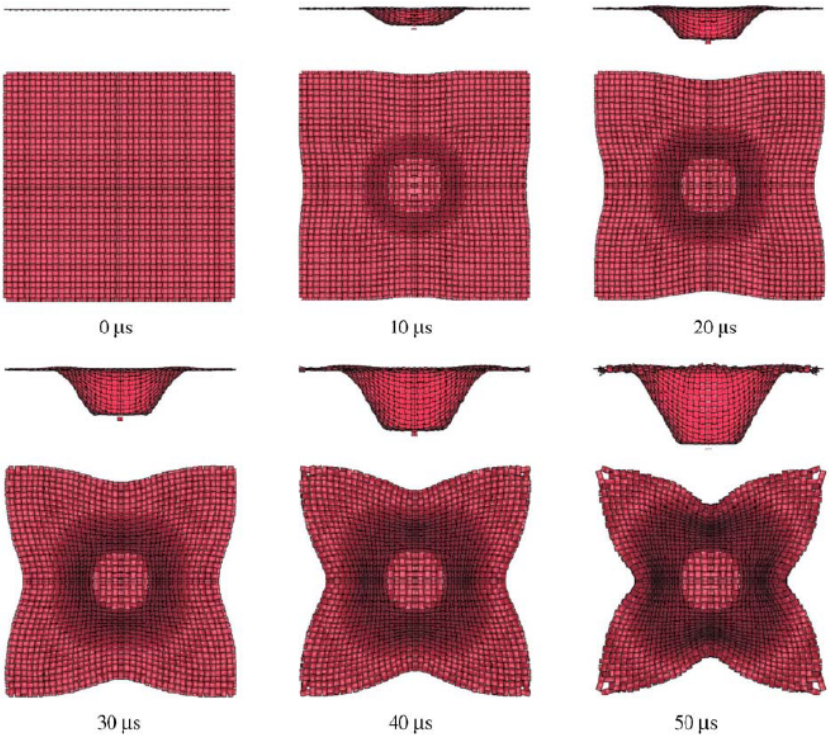

Figure 3.10: Simulation of ballistic impact against a plain woven fabric at various instants of time.[60]

This makes the method less useful for simulation stitching, where the geometry of the yarn can change significantly during the process. Several software packages are available for constructing fabric unit cells, namely WiseTex [67] and TexGen [68]. These geometries can be exported to conventional FE-software. Although it is difficult to obtain homogenised parameters for the continuous methods, treating the yarn as a continuum has several advantages, especially in the field of composites. Once the deformed geometry of the dry fabric has been obtained, this geometry can easily be used to study the final resin-injected composite. By changing the material properties to those of a resin-infused fabric and adding a matrix, the mechanical behaviour of the final composite can be simulated. Discrete methods would require the definition of an envelope surface to the fibres before they could be used to model resin-injected fibrous materials.

Figure 3.11: Experimental observation of the fibres in a yarn.[30]

A different approach to yarn modelling was taken by De Meulemeester et al. [69, 70, 71], who used a finite volume method to study the dynamic yarn behaviour on air-jet looms. A yarn was represented by a number of cylindrical segments along its length. The mass of these segments was assumed to be concentrated on a node in the center of each segment. These nodes were linked by springs to describe the elastic behaviour of yarns. Their model accounted for internal forces, i.e. tensile force, and external forces, i.e. aerodynamic, frictional and gravitational force. An explicit time integration method was used. The model was validated by comparing the shape of the yarn during weft insertion with that from high-speed recordings, see Figure 3.12. Very good agreement was found. The method developed by De Meulemeester et al. was a first inspiration for this thesis. While their model captures the yarn behaviour on air-jet looms accurately, it requires self-written code (as did many other researched methods). The goal of our study however, is to assess the possibility of simulating a similar textile process, i.e. stitching, with the commercially available FE-software ABAQUS.

Discrete methods

In discrete methods, yarns are made up of virtual fibres. The number of fibres in the cross-section of a real yarn is far greater than the number of

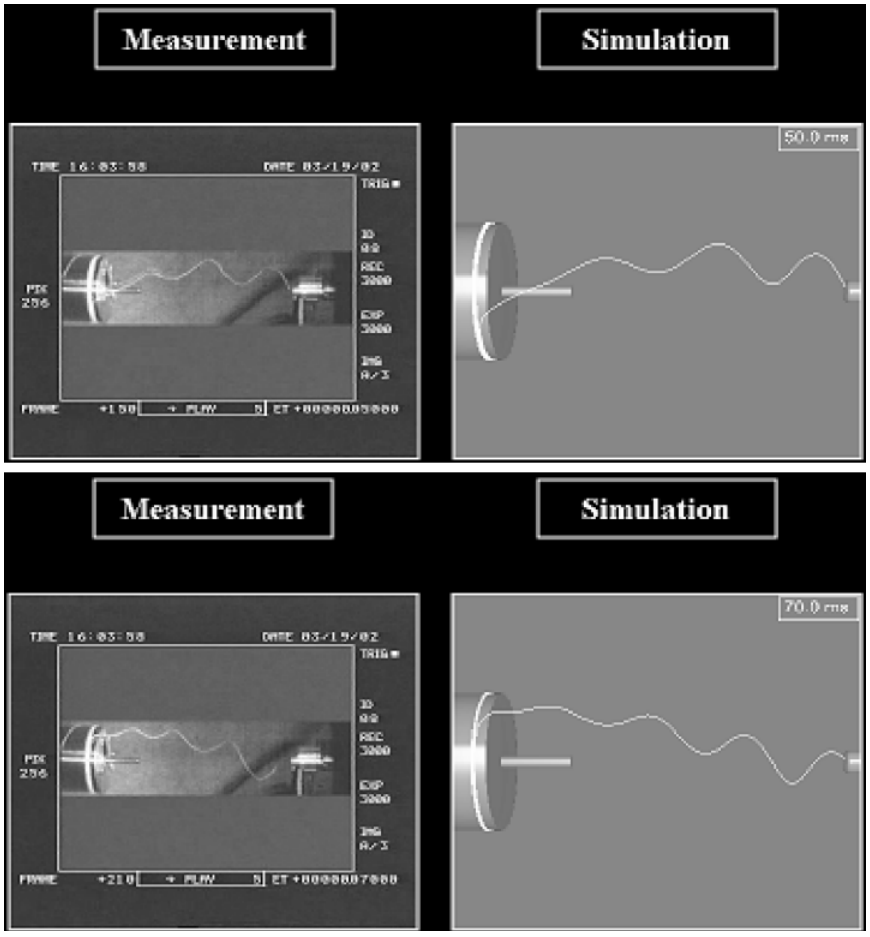

Figure 3.12: Measured and simulated yarn shape during weft insertion.[70]

virtual fibres. The amount of virtual fibres used is found to be between 7 and 100. Increasing this amount would lead to too high computational costs. The fibrous nature is captured by this approach, as it allows for fibre-fibre interaction, fibre realignment, twist, etc. However, small discrepancies could occur, because of the relatively small amount of virtual fibres.

A first discrete model is the one proposed by Wang and Sun [72], which resembles the truss model used in this thesis. They represent a yarn as a flexible 1D component by discretising it in a chain of short cylindrical bars connected by frictionless pins, see Figure 3.13. The cylindrical bars are called *two-node digital rod elements*. Each node has 3 degrees of freedom. These rods are comparable to the truss elements used in conventional FE-software which also consist of two nodes with 3 degrees of freedom. As the length of the rod elements approaches zero, a fully flexible chain is obtained. Contact between yarns is represented by the contact of two nodes. Contact is established when the distance between these nodes becomes smaller than the yarn diameter, and a contact element is placed between them. The global stiffness matrix is constructed and the simulation is computed by an explicit method similar to conventional FE-analysis. A rigid contact is used, where the displacements of two contacting nodes are constrained to be the same. The model is used to obtain the microstructure of a 3D braided preform by simulating the braiding process. A schematic view of their simulation and its results are given in Figure 3.14.

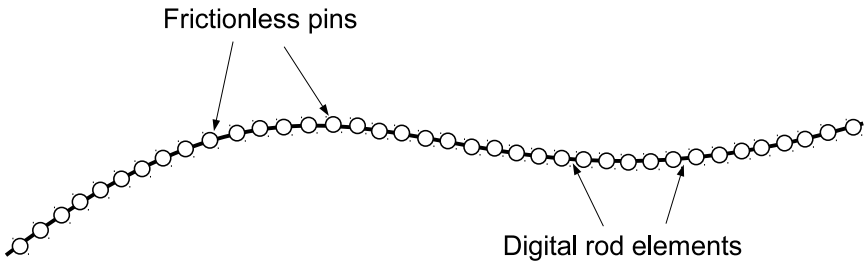

Figure 3.13: Discretising a yarn in a chain of rod elements connected by frictionless pins (after [72]).

Zhou et al. [73] extended the method to a multi-chain method to overcome the weakness of a fixed cross-section. Here, fibres rather than yarns are modelled as flexible chains. The relative displacements between fibres allow for cross-section deformation. The new method differs from the original only in that yarns are now discretised in a number of flexible chains. In real yarns, hundreds or thousands of fibres make up the cross-section, and modelling each fibre would require too much computing power. Zhou et al. argue that 19 - 50 digital chains would suffice in most cases. It seems that this amount of chains yields good results, see Figure 3.15, but the results

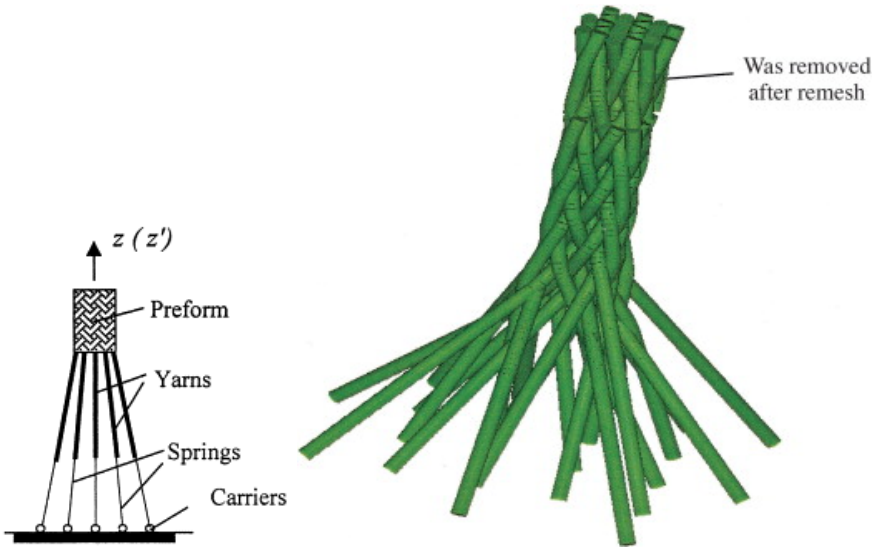

Figure 3.14: Simulation of the braiding process with rod elements: schematic overview (left) and results (right).[72]

are only compared visually to experimental results. Computation time was not mentioned by the authors.

The multi-chain method method is extended by Miao et al. [74], who developed a more efficient contact algorithm and simulation procedure. The textile process is no longer modelled explicitly, but the final fabric structure is obtained through a static relaxation approach. It is claimed this reduces computation time to 1 - 2 % of the original model. Wang et al. [75] extended the method to include failure. They assumed that failure occurs when the stress in an element exceeds the fibre strength. Failed elements are removed from the mesh permanently.

The multi-chain method is used by Wang et al. [75] to simulate impact and penetration of textiles, by Miao et al. [74] to study micro-geometry of 2D and 3D woven and braided structures, by Sun et al. [76] to study the mechanical properties of 3D braided composites and by Tsukrov et al. [77] to study microcracking in 3D woven composites.

A second approach of discrete modelling is that of Durville [78, 79], who modelled fibres as beam elements to study the mechanical behaviour of entangled materials. To overcome contact problems, a special contact algorithm was developed. Durville [80] states that this contact method is more suitable for the modelling of fibrous materials compared to classical methods, which treat contact surfaces as asymmetrical, i.e. a master-slave method. Furthermore, the potentially high curvature of fibres in contact would be handled better. Contact normal and tangential reactions are obtained by

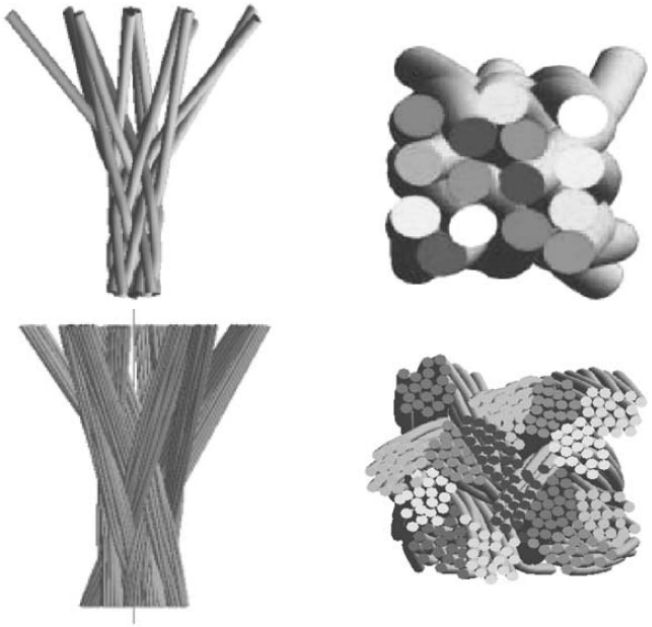

Figure 3.15: Simulation of 3D braided structure with yarns discretised as one virtual fibre (top) and 19 virtual fibres (bottom).[73]

a penalty method and a Coulomb's law respectively. A locally adjusted penalty coefficient controls the maximum penetration between contacting fibres.

Durville [80, 81, 82] applied the beam model to study the behaviour of woven fabrics. The fibres are considered to be linear elastic. The initial fabric configuration is obtained by starting from a structure where all fibres penetrate each other, see Figure 3.16. Subsequently, contact conditions are prescribed between fibres belonging to different yarns according to the prescribed weaving pattern. This pattern states how the yarns cross each other at intersections, i.e. which yarn must be above or below the other yarn. When all fibres of different yarns have separated, ordinary contact conditions are considered between all fibres, and the mechanical equilibrium is computed again. This process results in a woven fabric configuration, see Figure 3.16. The characteristics of the plain weave patch are given in Table 3.1. A simulation of a shear test on this patch took around 60 hours to compute on a cluster using 6 processors [80]. During the simulation, fibres rearrange themselves in a favourable position. It is impossible to simulate this fibre realignment with continuous methods. Hence, the author raises the question whether it is suitable to model yarns as continuous materials [81].

The validity of the beam model was tested by simulating the transverse com-

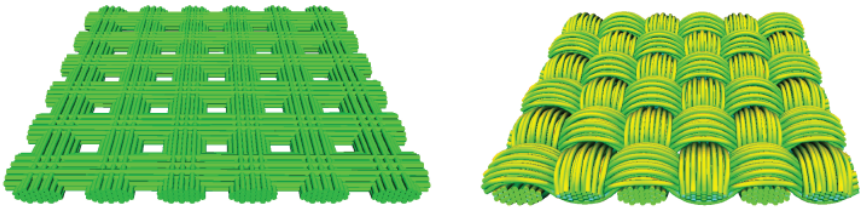

Figure 3.16: Starting configuration (left) and computed configuration (right) of a plain weave fabric.[80]

Table 3.1: Characteristics of the plain weave patch in Figure 3.16.[80]

Yarns	12
Fibers	336
Nodes	$\approx$ 37 000
DOFs	$\approx$ 335 000
Contact elements	$\approx$ 75 000

pression behaviour of nylon 6,6 filament rovings and by comparing this to experimental results. Good agreement between experimental and simulated values were obtained, but several discrepancies still need further investigation [83].

The versatility of the beam model is demonstrated by other recent studies: effect of friction on knot tightening [84]; mechanical modelling at the fibre scale of a multilayer braided scaffold for tissue engineering [85]; mechanical and electrical modelling of superconducting Nb_3Sn strands for cable-in-conduit conductors [86, 87].

Similar beam models are also used by other researchers to study the compaction of 3D woven fabrics. Mahadik and Hallet [88] created a beam model to provide a kinematic representation of a compacted 3D fabric. They chose material properties which minimised the simulations run time, rather than accurately describing the yarn properties. Green et al. [89] used elastic-plastic beam elements. However, the plastic behaviour was used to obtain visually good results and not to describe the actual plasticity of the yarn.

The weakness of the beam models is their bending stiffness. Virtual fibres modelled by beam elements have a higher bending stiffness compared to real fibres, due to their larger diameter. Hence, they are less flexible and the bending stiffness has to be lowered in some way. This is done by artificially decreasing the bending stiffness (e.g. [82]), or by assuming non-physical material parameters (e.g. [88, 89]).

3.2.3 Micro-scale modelling

The meso-scale discrete models are often referred to as micro-scale approaches, because they have the ability to simulate real fibrous behaviour. Nevertheless, the dimensions of the used fibres are still one or two orders of magnitude higher than those of physical fibres. It would therefore not be correct to classify them as microscopic methods.

The use of beam elements for micro-scale modelling is illustrated by Duhovic and Bhattacharyya [90]. They studied and simulated the deformation mechanisms of knitted fabrics for composites. Such fabrics offer a great potential for the forming of complex and highly curved components compared to other fabric structures, like woven or braided fabric. The knitting process can be described as a high-speed dynamic contact problem. Therefore, it was simulated using an explicit dynamics FE-code (PAMCRASH), which is commonly used for crash or forming simulations. The filaments of the yarn were represented by linear elastic circular beam elements. To reduce computing time, only 20 filaments were modelled. The number of filaments in the real yarn was calculated as 120. However, filaments were modelled using their actual dimensions, i.e. a diameter of 17 μm. The filaments were hexagonal close packed and no twist was taken into account. The beam elements' length was chosen as 0.2 mm, which was an optimum between reasonable solving time and accurate fabric geometry. The contact algorithm accounted for self-contact of the filaments, contact with other filaments and contact with the knitting machinery. The forming and tension behaviour of a 1 x 1 rib structure was simulated, see Figure 3.17, and compared to experimental results which showed good agreement. According to the authors, discrepancies were due to frictionless contact between filaments and the fact that only 20 filaments were used. They also studied the components of the deformation energy, i.e. axial energy, torsional energy, contact energy, bending energy and frictional energy, and concluded that bending has the largest contribution to the deformation energy. A video of the simulation can be found in the online version of the article (doi:10.1016/j.compositesa.2005.12.029).

The FE-method has also been used to study the mechanical properties of a yarn, taking into account the properties and arrangements of its fibres, by Van Langenhove [91, 92, 93]. A model was constructed to predict the stress-strain and torque-strain behaviour of a yarn. An idealised cylindrical anisotropic axisymmetric continuous yarn was assumed. The input for the model were appropriate fibre parameters which describe yarn structure, i.e. twist angle, migration angle and packing density, and fibre slippage and fibre breakage. This way, the yarn behaviour could be simulated based on the arrangement and properties of its fibres.

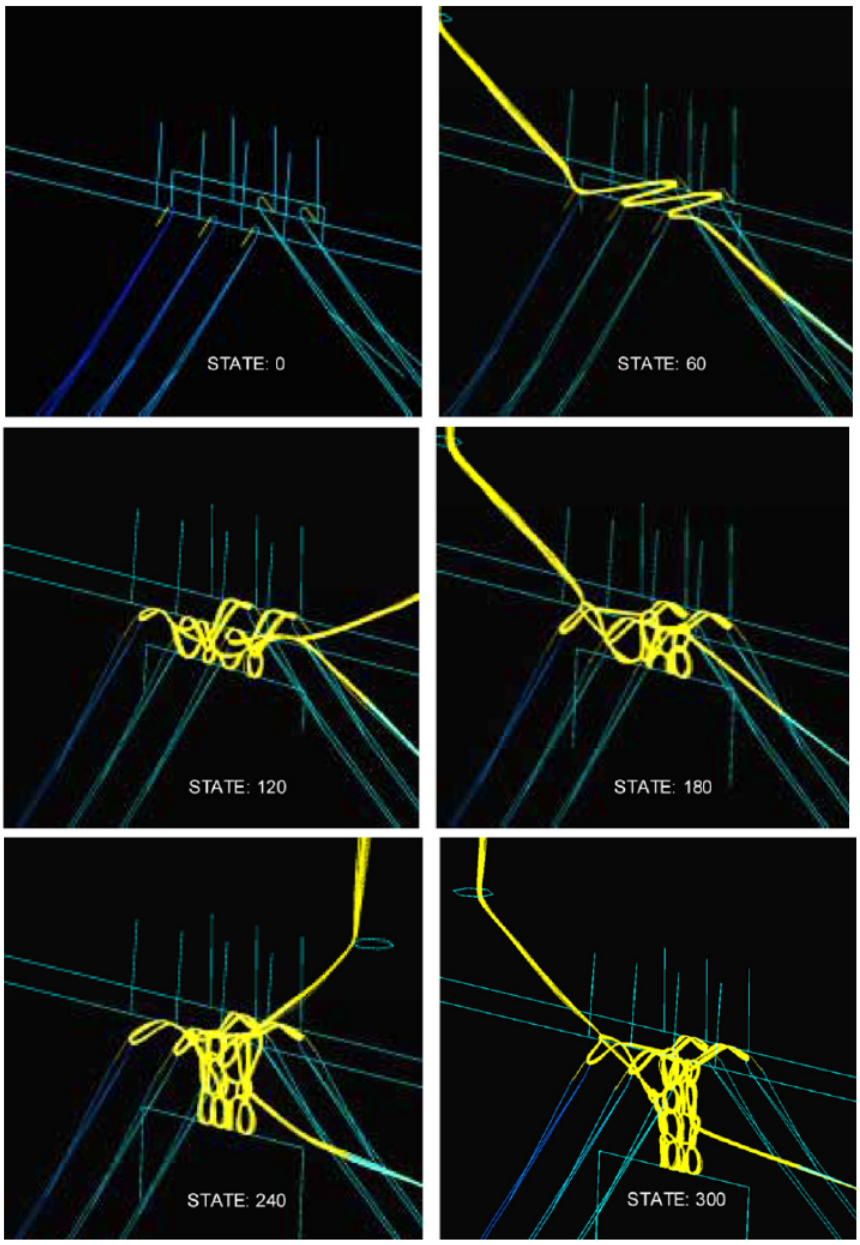

Figure 3.17: Progress of the knitting simulation.[90]

3.2.4 Other methods

The main focus of the literature mentioned above was on finite element modelling. However, several other methods of modelling fibrous materials exist: energy based methods (e.g. [94, 95, 96, 97]), force based methods (e.g. [98, 99, 100]), geometrical methods (e.g. [101, 102]) and mechanistic analytical methods (e.g. [103, 104]). Although these models can be useful for certain applications, they were not usable for this study.

Chapter 4

Modelling the yarn: selecting a model

It became clear after the literature survey that developing a finite element model of a yarn is not an easy task. Most models only concerned describing a specific loading case, such as bending or tension, and a specific textiles structure, such as woven fabrics. However, a generally accepted method to describe a *free yarn* was not readily available. As no articles relating to the FE-simulation of a stitching process were found, the first step of this study was to develop a usable yarn model. Several approaches, some of them mentioned in the literature, were investigated by means of a simple benchmark to assess their feasibility for use in the stitching simulation.

This chapter is divided as follows: first the properties of the yarn are discussed; then, a simple benchmark is proposed and different modelling approaches are investigated with this benchmark. The most suitable model will be worked out in the following chapter.

4.1 Properties of the yarn

A *stretch-broken carbon yarn* from Schappe Technologies is used in the stitching process. In the stretch-breaking process, the filaments of a carbon roving are stretched until breakage. These broken fibres offer a higher flexibility than continuous filaments, as they allow for separation and sliding. For example, when a yarn is bent around a curve, the fibres on the yarn's outside radius are more stressed than those at the centre. However, broken fibres can separate and relax these stresses, which increases the flexibility of the yarn. Furthermore, the stretch-breaking process does not influence the alignment of the fibres, resulting in flexible and highly aligned carbon yarns.

The flexibility is a necessity for stitching, while the alignment ensures good reinforcement properties. The disadvantage of the process is that there is no force keeping the bundle of broken filaments together, since it is essentially untwisted. Therefore, these yarns require some sort of binder or wrapping to hold the structure together. The used yarn consists of a 526 tex carbon roving wrapped by two 76 dtex polyester filament yarns. An image and schematic representation of the yarn is given in Figure 4.1. A 12K Tenax HTS40 carbon filament yarn was used for the stretch-breaking process. The properties of the initial carbon roving and the stretch-broken carbon yarn are given in Table 4.1. The modulus was measured by a static tensile test (ASTM D 2343). The stretch-breaking process decreases the (linear) density, the tensile strength and the tensile stiffness, while it increases the strain at break. The properties will be used to define a material model for the yarn in ABAQUS.

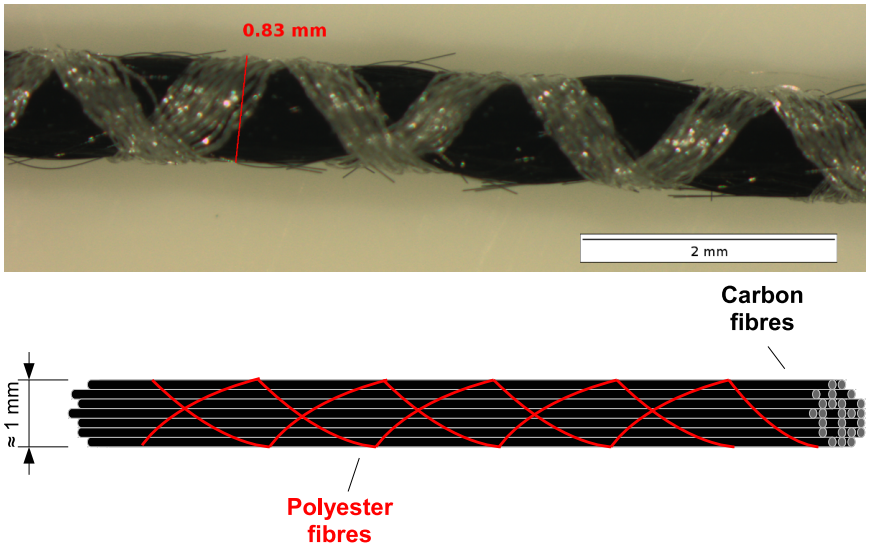

Figure 4.1: Image (top) and illustration (bottom) of the stretch-broken carbon yarn.

4.2 Description of a simple benchmark to test the feasibility of different yarn models

A simple benchmark was constructed and will be used further in this chapter to test different yarn models. The geometry is illustrated in Figure 4.2. A small length of yarn is bent over a curved rigid surface, called the die. It is clamped at the left end and pulled in the y-direction at the other end (displacement controlled). This way, it is possible to see if contact can be

Table 4.1: Properties of the carbon roving and stretch-broken carbon yarn (from manufacturer).

	Carbon roving	Stretch-broken carbon yarn
Composition	12K carbon filaments with diameter = 12 μm	96 % carbon 4 % polyester
Linear density (Tex)	800	521
Density (kg/m^3)	1770	1153[a]
Radius (mm)	0.4[a]	0.4
Strength (N) / (MPa)	1940[a] / 4300	230 / 510[a]
E-modulus (MPa)	240	73[b]
Strain at break (%)	1.8	2.9

[a] Based on the assumption of a circular cross-section.
[b] From ASTM D 2343 tensile test.

defined between yarn and die, and if the yarn model offers enough flexibility. Furthermore, after deformation, the cross-section should be flattened and the stresses should be more or less homogeneous in order to have flexible thread behaviour.

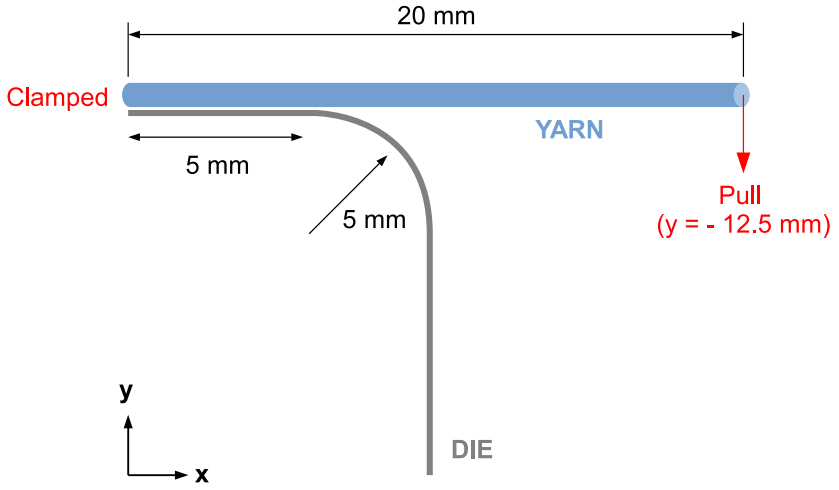

Figure 4.2: Geometry of the benchmark.

All simulations will be performed in ABAQUS/Standard to eliminate dynamic effects. A static solution to the problem is obtained. A rigid body is used to model the die; the yarn thickness and properties are chosen in accordance with the carbon yarn properties depicted in Table 4.1. Contact between yarn and die is assumed to be frictionless, unless stated otherwise.

The benchmark may seem very simple, but it extracts enough information

to assess the feasibility of a certain model for a stitching simulation. The model must fulfil all demands to be usable, i.e. contact with external bodies, flexibility (large deformations), cross-section flattening and realistic stress-states.

4.3 Orthotropic solid model

The first approach was modelling the yarn with general 3D continuum solid elements. Flexible thread behaviour was obtained by assigning appropriate orthotropic mechanical properties to the model [47]. To fully describe orthotropic linear elastic behaviour, 9 engineering constants are required: three Young's moduli E_1, E_2, E_3; three shear moduli G_{12}, G_{13}, G_{23}; and three Poisson's ratios $\nu_{12}, \nu_{13}, \nu_{23}$. The linear elastic stress-strain behaviour is then given by:

$$\begin{bmatrix} \varepsilon_{11} \\ \varepsilon_{22} \\ \varepsilon_{33} \\ \gamma_{12} \\ \gamma_{13} \\ \gamma_{23} \end{bmatrix} = \begin{bmatrix} 1/E_1 & -\nu_{21}/E_2 & -\nu_{31}/E_3 & 0 & 0 & 0 \\ -\nu_{12}/E_1 & 1/E_2 & -\nu_{23}/E_3 & 0 & 0 & 0 \\ -\nu_{13}/E_1 & -\nu_{32}/E_2 & 1/E_3 & 0 & 0 & 0 \\ 0 & 0 & 0 & 1/G_{12} & 0 & 0 \\ 0 & 0 & 0 & 0 & 1/G_{13} & 0 \\ 0 & 0 & 0 & 0 & 0 & 1/G_{23} \end{bmatrix} \begin{bmatrix} \sigma_{11} \\ \sigma_{22} \\ \sigma_{33} \\ \sigma_{12} \\ \sigma_{13} \\ \sigma_{23} \end{bmatrix} \tag{4.1}$$

with subscript $1, 2, 3$ denoting the directions of orthotropy. The engineering constants describing the material model are given in Table 4.2. The transversal behaviour of the yarn was described by a constant transversal Young's modulus. The ratio of longitudinal to transversal modulus was equal to 100.

Table 4.2: Engineering constants for the orthotropic material model.

E_1 (GPa)	E_2 (GPa)	E_3 (GPa)	G_{12} (MPa)	G_{13} (MPa)	G_{23} (MPa)	ν_{12}	ν_{13}	ν_{23}
73	0.73	0.73	1	1	1	0	0	0

The yarn was modelled with 3D solid linear brick elements. The mesh is depicted in Figure 4.3: a total of 1600 elements were used (32 elements in the cross-section). No convergence could be achieved for the simulation and it stopped at about 5 % of the total deformation. To solve this problem, other elements were tried: quadratic brick elements (which are better for simulations involving bending, but have higher CPU costs), reduced integration elements and hybrid elements. None of these elements significantly increased

the convergence, and completion of the simulation was not achieved. The convergence could probably be improved by using finer mesh. However, a finer mesh would mean an extreme amount of elements in the final simulation, where the yarn length easily surpasses the short length of yarn used in the benchmark. Nevertheless, the simulations illustrate an important feature of a solid continuum model: small deformations lead to very high tensile and compressive stresses at the outer surface of the yarn, see Figure 4.4. In real yarns, these stresses would be relaxed by sliding of the fibres. This rearrangement of fibres is not possible when treating the yarn as a solid material. This is a very important finding, as our final simulation will have many large deformations, and in reality the stress would not reach such high values. Another important disadvantage is that the material properties are not measurable physical properties: a real yarn is not continuous and the properties are chosen in such a way that the solid model reacts as a flexible thread.

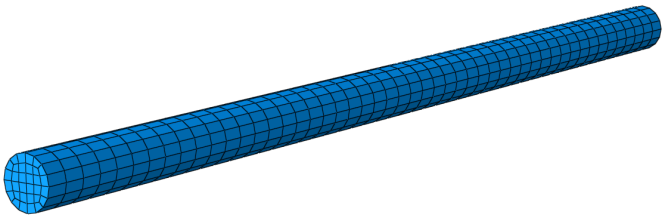

Figure 4.3: Generated mesh for the yarn: 32 x 50 elements.

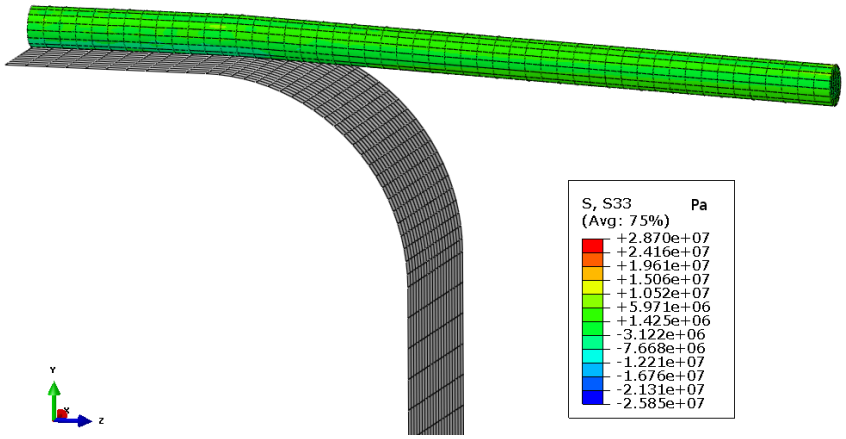

Figure 4.4: Maximum deformation before convergence failed for the orthotropic model (S33 denotes the longitudinal stress of the yarn). The green color represents a stress value of approx. 2 MPa.

The use of an orthotropic material model in which the constants differ several magnitudes and are equal or close to zero, could also lead to convergence

problems [47]. Therefore, an isotropic model was constructed to see if this was really the case. The mechanical properties of the isoptropic model were a Young's modulus of 73 GPa and a Poisson's ratio equal to 0.3. This reduced the problems, but still convergence could not be achieved and the simulation stopped around 70 % of the total deformation, see Figure 4.5.

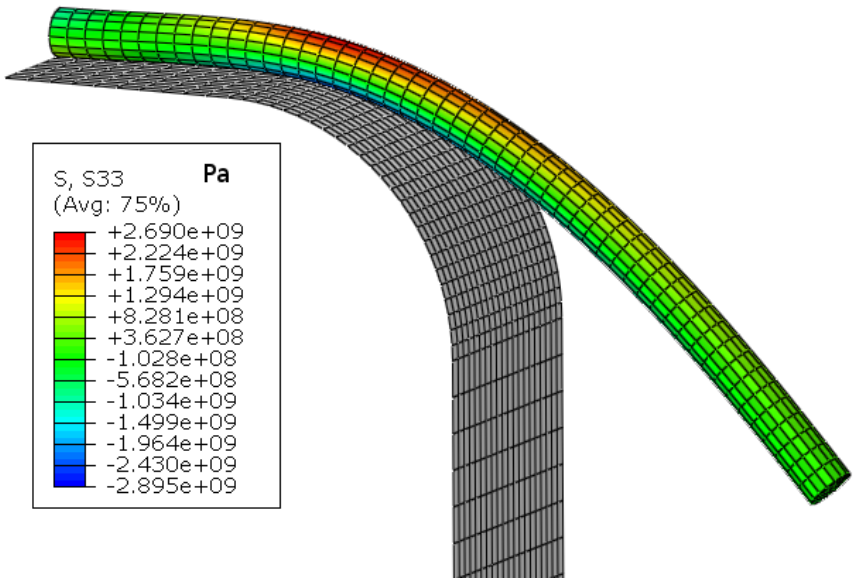

Figure 4.5: Maximum deformation before convergence failed for the isotropic model (S33: longitudinal stress of the yarn).

Numerical problems due to an orthotropic material model combined with low flexibility due to an absence of fibre realignment make this model not useful for simulating the stitching process.

4.4 Two-material solid model

To overcome the problems encountered in the orthotropic solid model, a *two-material* solid model was constructed. By using a combination of two materials, one with high stiffness and one with low stiffness, the yarn's anisotropy could be represented with isotropic materials. Two models were constructed. The first one uses a high stiffness core, while the other one uses a high stiffness shell. This way, no numerical problems related to the orthotropic properties will be encountered, while allowing for an anisotropic behaviour of the yarn.

4.4.1 High stiffness core

The ratio of core diameter on mantle diameter f could be varied anywhere between 0 and 1. The longitudinal Young's modulus E_{long} is determined by the cores modulus E_c and the mantles modulus E_m by a mixing law:

$$E_{long} = v_c\, E_c + v_m\, E_m \tag{4.2}$$

where v_c and v_m are the volume fraction of the core and the mantle respectively. Furthermore, E_m can be approximated by a value of $E_{long}/100$, as the mantle will determine the transverse properties of the yarn. Knowing E_{long} and f, the mixing rule can be rewritten to determine E_c:

$$E_c = [E_{long} - E_m(1 - f^2)]\frac{1}{f^2} \tag{4.3}$$

The ratio f determines the stiffness of the core which should be used. A ratio of $f = 1/2$ was chosen somewhat arbitrarily, which led to a value of E_c equal to 290 GPa. An overview of the used material properties is given in Table 4.3. The result of the benchmark is shown in Figure 4.6. The model was more flexible compared to the orthotropic solid models, but still no convergence could be obtained. An elastic-plastic material was also tried, but this did not improve the results.

Table 4.3: Overview of the material properties used in the two-material stiff core model.

f	E_c (GPa)	ν_c	E_m (GPa)	ν_m
1/2	290	0.3	0.73	0.3

4.4.2 High stiffness shell

Another possible way of representing a yarn is by a hollow cylindrical shell. This shell-structure could be easily compressed, like a real yarn. However, large deformations led to buckling, see Figure 4.7. This problem could be resolved by adding a low stiffness filling to the structure, as is done in real-life with sandwich panels. However, as is also the case with sandwich panels, the combined structure would be very stiff. To determine whether this would pose problems for the flexibility, a first simple yarn model was constructed and tested. The mechanical properties of this model are given in Table 4.4. It was more flexible than the other solid models, see Figure 4.8. Convergence was achieved, but excessive element distortion occurred in the core material.

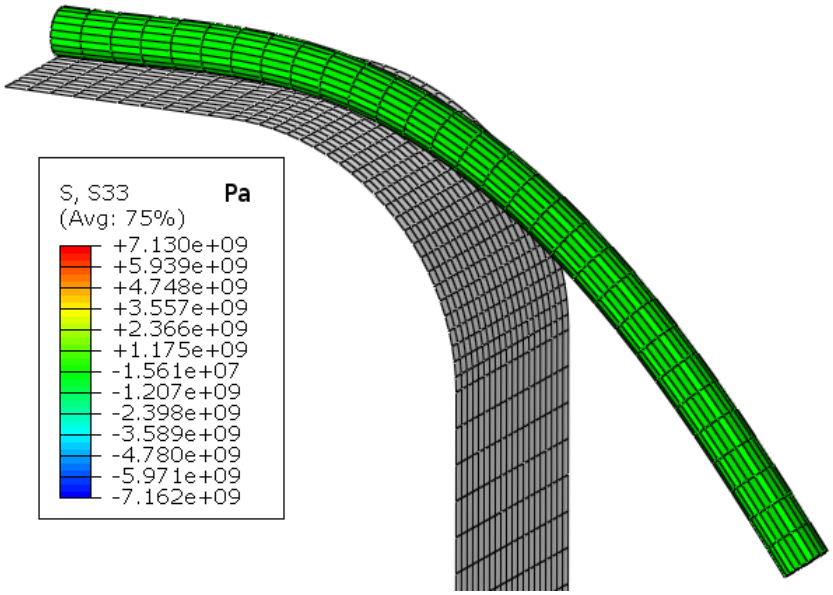

Figure 4.6: The simulation of the two-material model stopped at about 70 % of the total deformation.

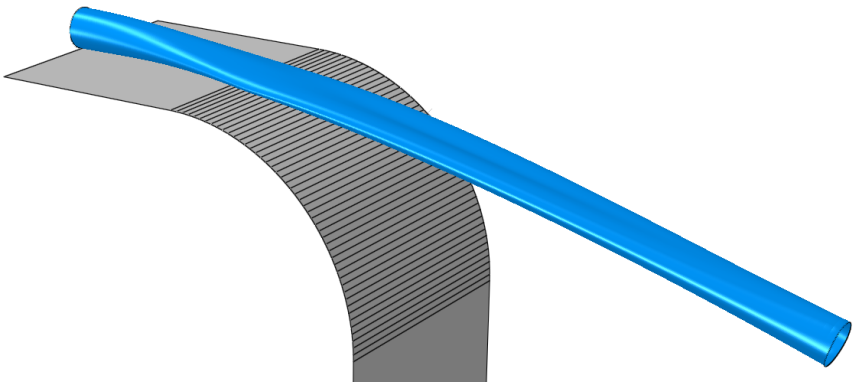

Figure 4.7: Buckling of a hollow cylindrical shell due to bending.

Table 4.4: Material properties of the two-material stiff shell model.

Property	Shell	Core
E (GPa)	73	0.73
ν	0.3	0.3
Thickness (μm)	10	

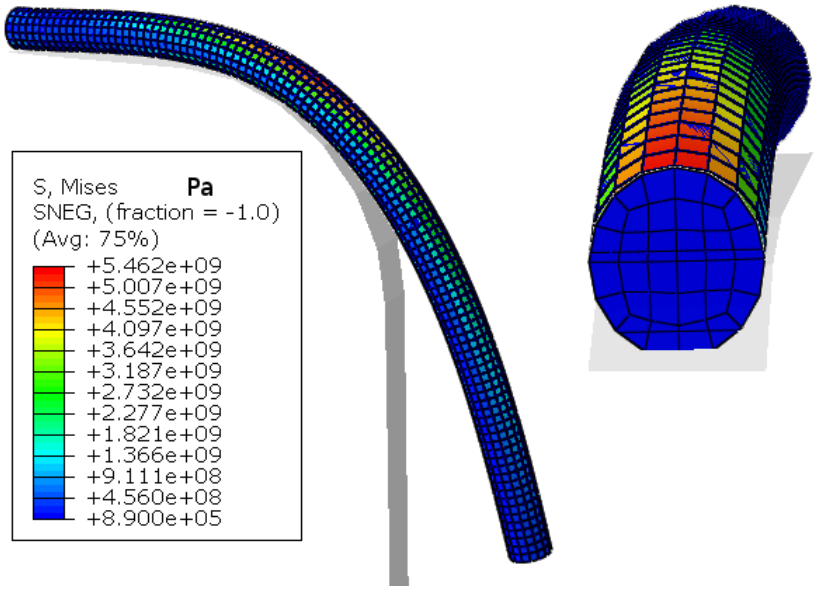

Figure 4.8: Benchmark of the high stiffness shell model and the cross-section deformation.

4.4.3 Conclusion

Although these models are more flexible than the previous ones, they still have many disadvantages. The stress state is not uniform throughout the yarn: the stiff core (or shell) taking up most of the stresses. This would make it difficult to determine the actual tensile stress of the yarn, or to specify a breaking criteria for the yarn. The cross-section deformation is also not very realistic, as no fibre realignment is possible.

4.5 Chain-like models

The chain-like models are similar to the rod element models (e.g. [72, 73, 74, 75]), the beam models (e.g. [80, 81, 82]) and the pin-jointed models (e.g. [37, 38, 39, 40]) described in the previous chapter: a series of elements are connected to each other to obtain a segmented chain-like structure. This structure possesses high flexibility because individual elements can rotate relative to each other at their joints/nodes, see Figure 4.9.

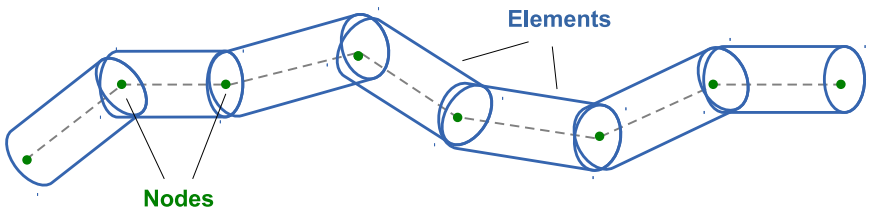

Figure 4.9: Chain-like model.

4.5.1 Segmented rigid cylindrical chain

A first chain-like model that was tested, used spaced rigid cylinders connected by small springs. The rigid elements would provide the chain with a contact surface without high computational costs. The springs connecting the cylinders would provide the chain with elastic behaviour. Adding dashpots to the springs would allow for defining visco-elastic properties. Spring-dashpot models are frequently used to model the behaviour of fibres and yarns (e.g. [105]). Appropriate spring-dashpot combinations would enable the model to describe all kinds of yarn. However, it turned out not to be possible to connect rigid cylinders at both ends in ABAQUS, as these elements are defined by 1 node only. As such, the rigid segments would not follow the path described by the connected nodes, which led to an unconnected surface, see Figure 4.10. The problem could be resolved by using solid element cylinders, but this would increase the complexity of the model beyond the initial intention. Furthermore, creating the connections between nodes is a very time-consuming task in the GUI of ABAQUS. Hence, it would be necessary to write a script which could define the assembly of cylinders.

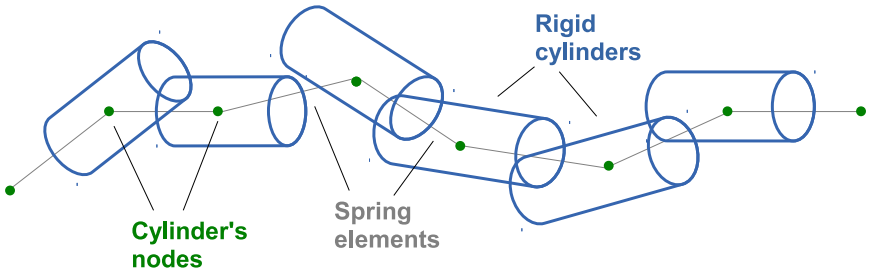

Figure 4.10: Rigid cylinders, defined by 1 node, lead to an unconnected surface.

4.5.2 Truss model

The truss model was much easier to define than the segmented cylindrical chain: truss elements are generated in ABAQUS on a *wire part* by regular meshing techniques. Each truss element is defined by the two nodes at its ends. These elements only transmit axial forces and do not transmit moments. Hence, the nodes react as frictionless pins and the structure inherently has a chain-like behaviour. When the length of truss elements decreases to zero, a fully flexible thread would be obtained.

Four disadvantages are related to truss elements in ABAQUS: (1) it is not possible to define a 3D surface on the elements in ABAQUS/Standard, (2) the cross-section is circular, (3) only isotropic material properties can be assigned to the elements, and (4) a truss element chain possesses no bending stiffness. The first problem could be solved by using the explicit solver ABAQUS/Explicit, see also Chapter 5. By using a bundle of fibres, each modelled by a flexible chain, the anisotropy and cross-section deformation of a yarn could be represented much more realistic. Therefore, the isotropy of the truss elements does not create a real problem. The bending stiffness of yarns is very low due to their long slender structure and fibrous nature, however it is still a positive value. It might be necessary for some applications to take this stiffness into account. Bending stiffness could be obtained by adding angular springs between consecutive elements [26].

The truss model was tested with a slightly modified benchmark in which the yarn is treated as a line. This was necessary because no surface can be generated on the elements in ABAQUS/Standard to represent the thickness of the yarn. A very small preload was also added to the right end of the yarn to overcome numerical problems arising from the lack of stiffness perpendicular to its axis [1]. The preload was obtained by displacing the right end 1 nm to the right. The yarn was modelled with 200 T3D3H truss elements. A linear elastic material was assumed with a Young's modulus of 73 GPa and Poisson's ratio equal to 0. An overview of the deformation at different stages is given in Figure 4.11. These results show the high flexibility of the truss model. The stress stayed small throughout the bending, and was mostly due to the preload and the straining after bending: the yarn was pulled down 12.16 mm which equals an applied tensile strain of approximately 0.07 %. The final stress is then calculated by Hooke's law:

$$\sigma_{11} = E\,\varepsilon \approx 51.1\text{MPa} \tag{4.4}$$

where σ_{11} denotes the longitudinal stress. This value agrees very well with the simulated value of 49.1 MPa, see Figure 4.11.

Until now, the contact was always assumed to be frictionless. When the

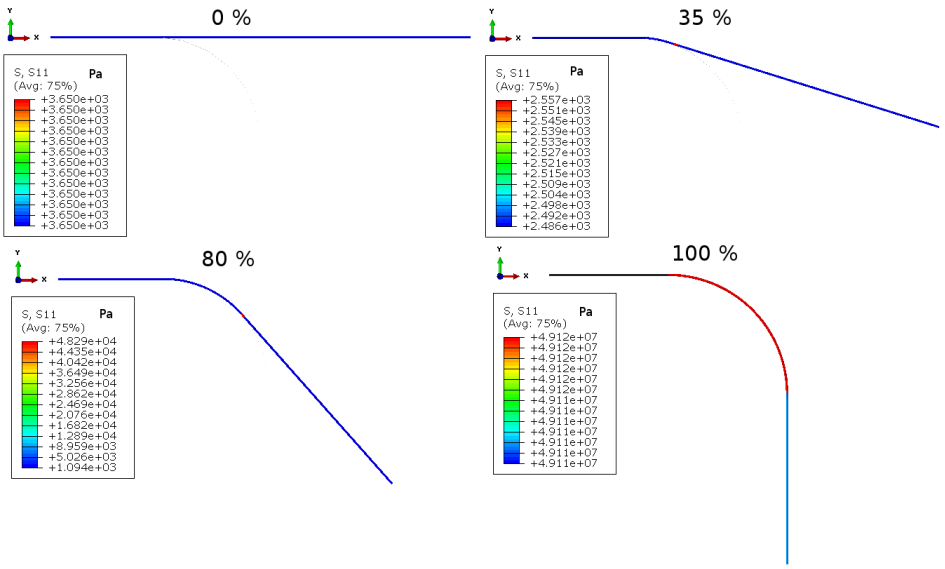

Figure 4.11: Deformation progress of the truss model (S11 denotes the longitudinal stress).

contact would be given by a friction coefficient μ, the longitudinal stress is expected to change over the length of the yarn. Furthermore, the maximum stress σ_{max}, and the minimum stress σ_{min}, before and after the curve would differ. Their relation is given by:

$$\sigma_{max} = \sigma_{min} \exp(\mu\alpha) \tag{4.5}$$

where α denotes the angle of the curve (π for a half circle, 2π for a full circle, etc.). The curved surface in the benchmark has an α equal to $\pi/2$. Figure 4.12 shows the result of the benchmark in which a friction coefficient of 0.3 was assumed. The results correspond well with the theory: the stress changes over the length as expected, and the maximum and minimum stress are related to each other by Eq. 4.5.

These tests showed that the truss model has a high flexibility, which is due to their nodes acting as frictionless pins. Each element acts as a cylindrical segment and together they make up the yarn, see Figure 4.13.

4.5.3 Beam model

The beam model is very similar to the truss model, except for the fact that beam elements do transmit moments. As such, a less flexible chain is

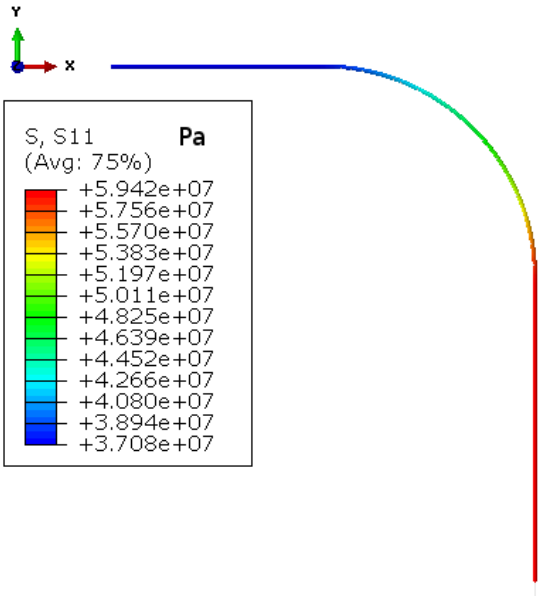

Figure 4.12: Longitudinal stress distribution for the truss model with friction defined between the surfaces ($\mu = 0.3$).

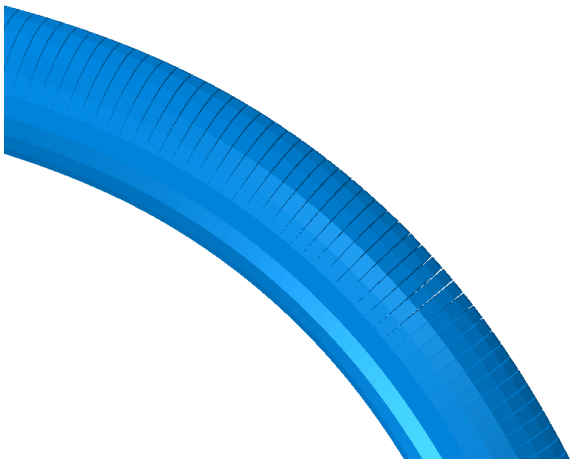

Figure 4.13: Illustration of each truss element acting as a cylindrical segment of the yarn.

obtained, because the nodes no longer act as frictionless pins. A chain of beam elements reacts as one long beam.

Beam elements have a bending stiffness, which is determined by the Young's modulus and the second moment of area. This could lead to a too high bending stiffness if the yarn is represented with only one beam element in the cross-section. The use of a bundle of chains, however, lowers the bending stiffness (as the second moment of area decreases with fibre diameter), which could lead to a viable model.

Truss models and beam models can be easily transformed into each other, essentially only the element type has to be changed. Furthermore, no preload is necessary with beam elements to overcome numerical problems. The results of the benchmark with the beam model is depicted in Figure 4.14. The yarn does not bend completely around the surface, due to its high bending stiffness. Furthermore, there are very high compressive and tensile stresses in the yarn. Although the beam elements are represented as line elements, beam theory equations are used to calculate the stress in the whole beam. The yarn is treated as a solid rod and thus, just as with the solid models, high compressive and tensile stresses are generated during bending. The big difference and advantage compared to solid elements is that beam elements require much less computational resources.

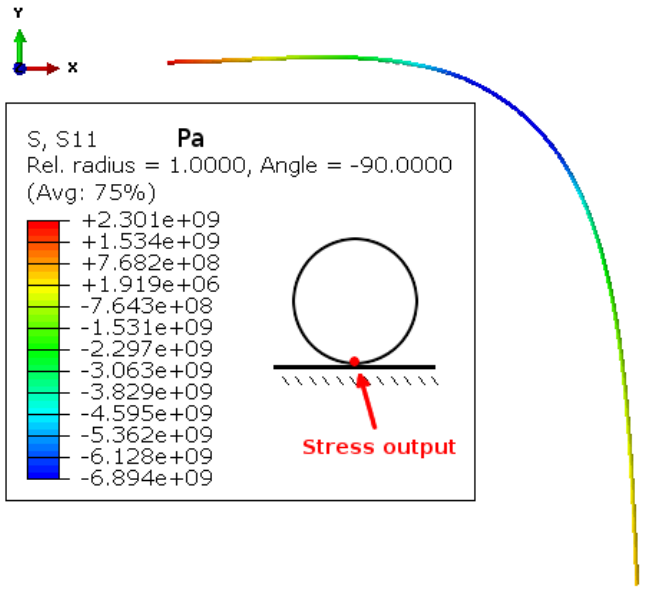

Figure 4.14: Longitudinal stress at the bottom of the beam's cross-section for the beam model. It shows the development of high tensile and compressive stresses during bending.

4.6 Conclusion

Several yarn models were constructed and tested with a simple benchmark. High flexibility and the possibility of defining contact with external bodies is essential for the stitching simulation. The models which made use of solid elements did not possess enough flexibility to be useful. Furthermore, there were several problems with convergence. The chain-like models solved the problem of flexibility, especially the truss model. Furthermore, the calculation times of the truss model were significantly lower than the others. As the truss model showed the best results, it was chosen to model the yarn in the stitching simulation. However, it was not possible to define contact with the outer surface of truss elements. The truss model and its contact problem are further explained in the next chapter.

Chapter 5

Modelling the yarn: the truss model

The previous chapter showed that truss elements offer a good way of representing a flexible yarn. However, it was not possible to define a 3D contact surface on the elements in ABAQUS/Standard, which makes the truss model useless if this problem cannot be resolved.

In this chapter, the truss model will be further explained. By using the explicit solver ABAQUS/Explicit, it is possible to define a 3D contact surface on truss elements. The explicit algorithm treats the problem as a dynamic equilibrium, and is mostly suited for high-speed dynamic events, complex contact problems, highly nonlinear quasi-static problems or problems concerned with degradation and failure of materials. This makes it especially useful for simulating the stitching process, where many complex contact conditions arise, e.g. fibre-fibre, fibre-needle, needle-foam and fibre-foam interactions. Furthermore, the foam material fails when it is penetrated by the needle. The possibility of simulating dynamic effects is also of interest to Acrosoma, whom encounter these effects during the production.

First, the basics of the model are developed by using one truss element chain, further referenced to as a (virtual) fibre, in ABAQUS/Explicit. Contact is defined between the fibre and a curved rigid surface. Then, the model is expanded to a bundle of fibres in order to account for the fibrous behaviour of the yarn. Finally, the model is validated by a frequency analysis.

5.1 Explicit algorithm [1]

ABAQUS/Explicit integrates the equations of motion explicitly through time. The kinematic conditions at one time increment are used to calculate those at the next increment. Time is a real physical property in this approach. In order to obtain accurate results, the time increments should be very small. Hence, simulations often require many increments. Fortunately, the calculations are computational inexpensive compared to those in ABAQUS/Standard, since there is no system of linear equations which has to be solved simultaneously. The size of the largest stable time increment Δt_{stable} is usually very small in order not to obtain numerical instabilities. ABAQUS/Explicit uses a simplified stability limit and automatically calculates the time incrementation. The simplified stability limit is given by:

$$\Delta t < \Delta t_{stable} \propto \frac{L}{c} = L\sqrt{\frac{\rho}{E}} \tag{5.1}$$

where L denotes the length of the smallest element in the model, and c, ρ and E are the wave speed, the density and the Young's modulus of the material, respectively.

The stability limit is important because it determines the amount of increments needed in the simulation, and thus, the run time of the simulation. For example, suppose an event of 1 s is simulated and that $\Delta t_{stable} = 10^{-6}$ s. Assuming that Δt_{stable} remains fixed throughout the simulation, a total number of 1 000 000 increments is necessary. When the same event is simulated with a stiffer material, Δt_{stable} decreases to 10^{-7} s and the simulation will require 10 000 000 increments. Hence, the simulation's run time will take approximately 10 times as long as that of the original model. To obtain a larger stability limit, and thus computationally feasible results, the material's Young's modulus used in this chapter was chosen to be 3 GPa. This has no significant influence on the conclusions drawn from the preliminary tests in this chapter.

5.2 One fibre model

For simulations where cross-section deformation of the yarn is unimportant, it would suffice to use 1 virtual fibre. In such cases, the fibre and yarn diameters would be the same. As explained above, the stable time increment is proportional to the smallest element length. Hence, it is important to choose the largest element possible, without sacrificing flexibility of the chain. This length was estimated to be about 1 mm, see Section 5.4. Furthermore, to obtain good contact definitions, the element's length should be less than its

diameter. The same benchmark as in Chapter 4 was used to develop the truss model. Thirty truss elements (T3D2) were defined over the length of the yarn, leading to an element length of 0.67 mm. A radius of 0.5 mm was used to represent the yarn. The tangential friction coefficient for all contacts was taken as 0.3.

The definition of a 3D surface on a truss element does not offer any problems in ABAQUS/Explicit, it is generated automatically, based on the radius of the elements. Truss elements are normally used to define long slender structures, where the element's length is far greater than its diameter. The element's diameter is often referred to as its thickness. In order to obtain a flexible thread, the element's length is usually much smaller than its thickness. This could lead to spurious self-contacts when defining *general contact* in ABAQUS. General contact is a penalty contact algorithm which automatically considers contact between all surfaces in the model, including the self-contact of parts. It is commonly used in complex contact problems, where contact could occur between many parts, e.g. crashing simulations of cars. Therefore, it is well suited to define contact between all the parts in the stitching simulation, i.e. needle-fibre, needle-foam, fibre-foam and fibre-fibre interactions. The contact surface of truss elements in ABAQUS is constructed as a sphere on each node of the elements. These spheres have a diameter equal to the thickness of the element. Since the element's length is smaller than its thickness, the spheres of two successive connected truss elements contact each other. These contacts are called spurious contacts, and do not represent physical contact. Therefore, ABAQUS automatically reduces the element's thickness, so that the spheres no longer overlap, see Figure 5.1. In order to disable this *contact thickness reduction*, self-contact of the fibre has to be excluded from the general contact domain, and contact controls have to be assigned, see Figure 5.2.

5.2.1 Contact with rigid bodies

The results of the benchmark for the 1 fibre model are given in Figure 5.3. The parameters used for this test are given in Table 5.1. It is clear that contact with the outer truss surface is no problem in ABAQUS/Explicit. Furthermore, the stress agrees well with Eq. 4.5.

Table 5.1: Parameters for the simulation in Figure 5.3.

E (GPa)	ρ (kg/m^3)	time (s)	friction
3	1153	0.01	0.3

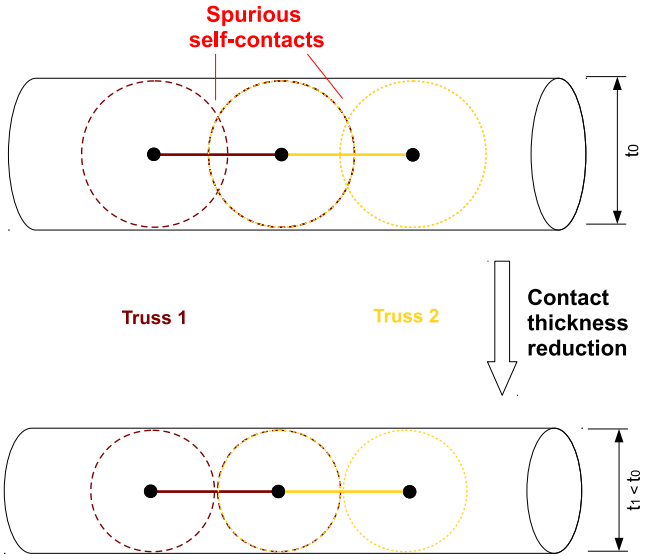

Figure 5.1: The truss element's thickness is automatically reduced to avoid spurious contacts by the contact thickness reduction algorithm.

Figure 5.2: Disabling of the contact thickness reduction through the input-file.

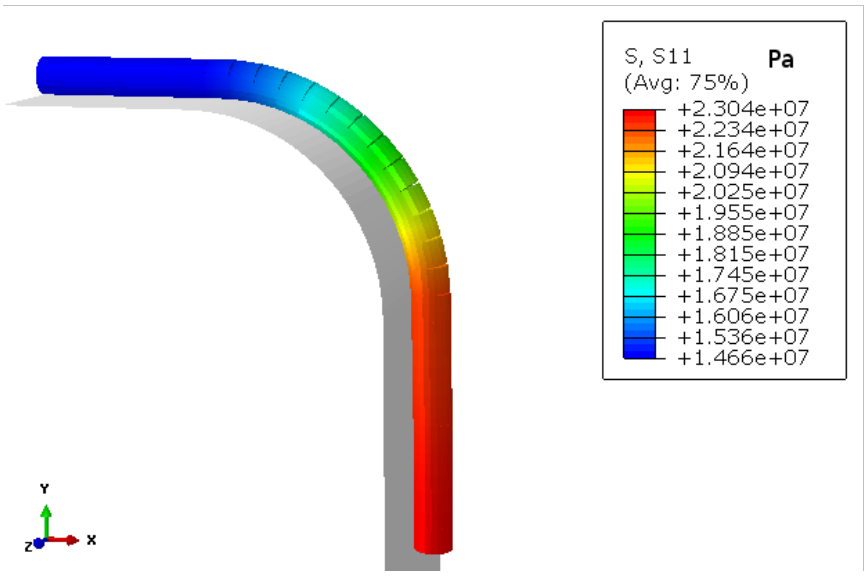

Figure 5.3: Longitudinal stress in the yarn with the 1 fibre model.

5.2.2 Influence of the simulation time

Time is very important for explicit methods, as it represents the real time scale of the process. In the previous test, the *simulation time* was taken as 0.01 s. This corresponds to the yarn being pulled 12.2 mm in one hundredth of a second. At these speeds, the dynamical phenomena become very important. A stress wave is generated in the yarn, which leads to inaccurate longitudinal stresses. This is illustrated in Figure 5.4, which shows the stress distribution during the benchmark simulation for a yarn deformed at low speeds (quasi-static) and at high speeds (dynamic). The low deformation speed was obtained by a simulation time of 1.0 s. In the quasi-static simulation, the longitudinal stress remains close to zero throughout most of the analysis, as compared to the dynamic simulation. However, the run time of the quasi-static simulation took much longer, as explained in Section 5.1. A process should ideally be simulated in its real time scale, but this often leads to a high amount of time increments. It is common practise in explicit simulations to decrease the simulation time in order to obtain computationally feasible models. A simulation time of 0.1 s was found to give good results, while keeping the run time short.

5.2.3 Influence of the preload

In contrary to ABAQUS/Standard, a small preload is usually not necessary to overcome numerical instabilities in ABAQUS/Explicit [1]. Although it is

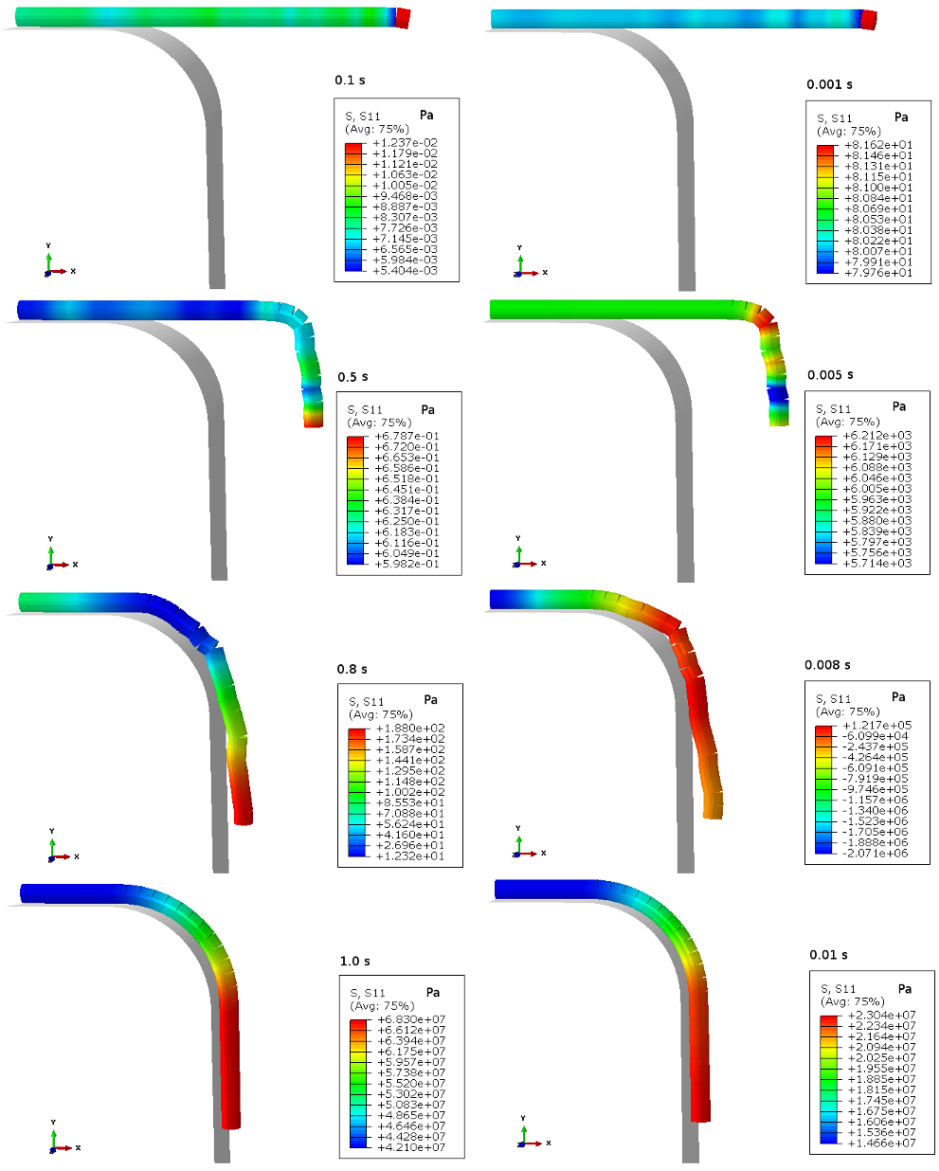

Figure 5.4: Influence of the simulation time on the longitudinal stress in the yarn.

often neglected, fibres do possess some bending stiffness, albeit small. The truss model, however, has no bending stiffness, due to the nodes acting as frictionless pins. By adding a small load to the fibre prior to the simulation, a *preload*, the effect of a bending stiffness can be somewhat imitated. It leads to a small amount of tension in the yarn, which prevents the bending of the yarn to some extent. Adding a small preload resulted in more kinematical correct models, see for example Figure 5.5, and it often solved numerical problems. Hence, a preload of 1 mN was given to the yarn in most models.

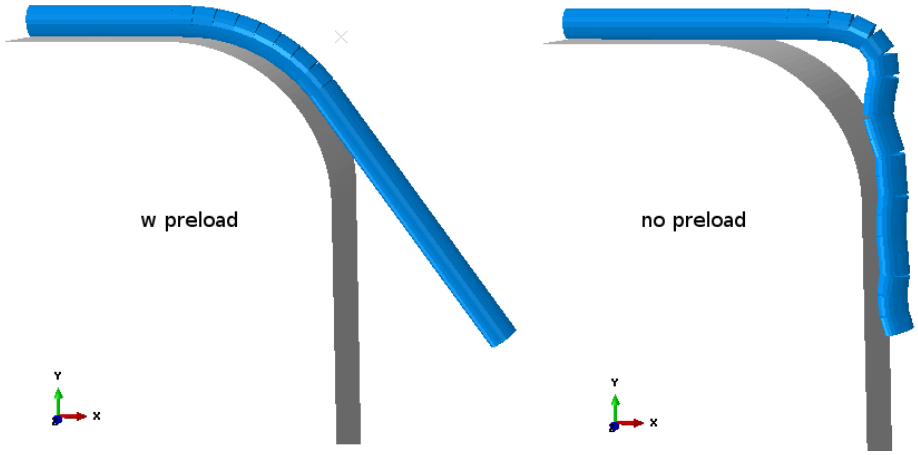

Figure 5.5: Deformation of a yarn with preload (left) and without preload (right).

5.2.4 Contact with deformable elements

In the stitching process, contact between the yarn and the foam core is an important issue, as it determines the denting of the foam due to yarn tension. Therefore, it must be possible to define contact between truss elements and deformable solid elements, i.e. 3D continuum elements. For a first test, a simple ideal elastic-plastic material replaced the rigid surface of the benchmark. The material properties of the elastic-plastic material are given in Table 5.2. The resulting geometry is illustrated in Figure 5.6. It clearly shows that contact with solid elements is possible. The material deforms and dents under the tension of the yarn.

Table 5.2: Material properties of the perfectly elastic-plastic material model.

E (MPa)	ν	ρ (kg/m^3)	σ_y (MPa)
70	0	500	0.8

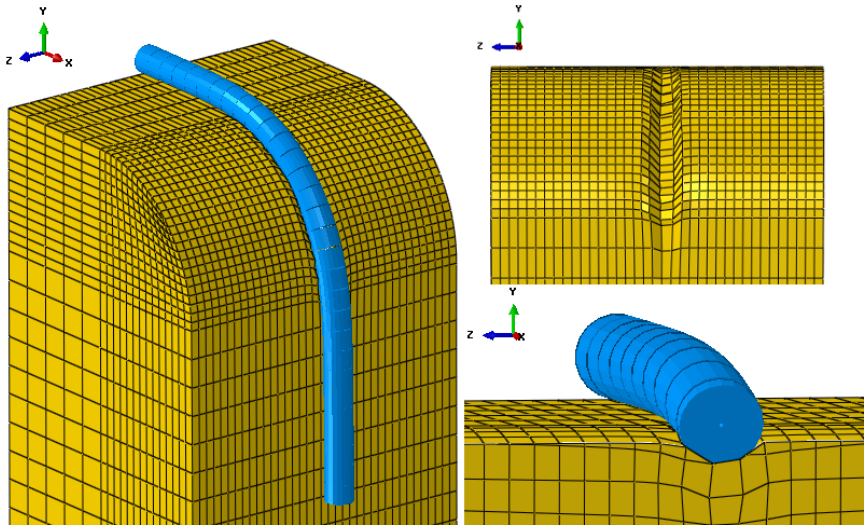

Figure 5.6: Different views of the denting in a deformable material caused by yarn tension.

5.3 Fibre bundle model

The 1 fibre model can easily be expanded to a bundle of fibres by decreasing the fibre diameter and by arranging them into a packing. Open and closed packing of the fibres were used, because these were easily defined in the GUI of ABAQUS. The aspects of the fibre bundle model are depicted in Figure 5.7.

5.3.1 Amount of fibres

The influence of the amount of fibres was tested by discretising the yarn in 7, 19 and 37 fibres. It was assumed that the fibre ends remain fixed in their initial shape. This has no significant effect on the deformation of the bundle around the curved surface, which is relatively far away from the yarn boundaries. The final geometry of the benchmark is given in Figure 5.8. The longitudinal stress is not uniform over the yarn, but the fibres rearrange themselves in such a way that their tension is minimised. In Figure 5.8 can be seen that most of the fibres have a low tensile stress (dark blue), while this stress is high in one or two fibres. The simulation time was equal to 0.1 s for all tests. The amount of fibres used by other researchers varies between 7 - 51. From the results in Figure 5.8, it seems that 19 fibres already give a good view of the yarn deformation.

Since all of the fibres could possibly touch each other, the amount of contacts increases rapidly with increasing amount of fibres in a bundle. Hence, the

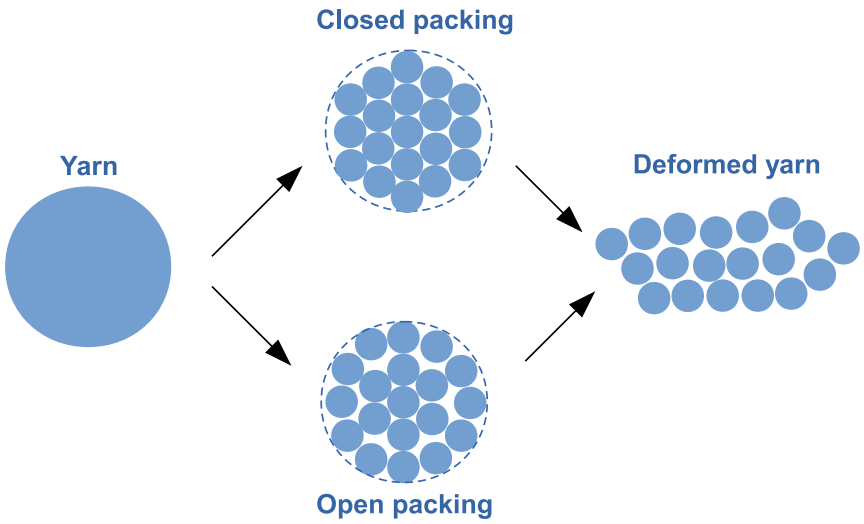

Figure 5.7: Discretising the yarn as a bundle of fibres.

run times also increases, because the contact search algorithm has to take every fibre-fibre interaction into account. The influence on the run time of adding fibres to the bundle is given in Table 5.3. The calculation of the model with 37 fibres took about 15 minutes on a notebook with an Intel i3 processor (1 core used) and 4 GB RAM memory.

Table 5.3: Normalised run time of the benchmark with 1, 7, 19 and 37 fibres.

# fibres	norm. run time
1	1.0
7	1.5
19	3.8
37	7.0

The fibres in real yarns are not perfectly arranged, but have a stochastic packing. However, the packing of filaments in rovings typically used for composite applications can be approximated by a closed packing. Furthermore, Miao et al. [74] have showed that the initial packing has no significant influence on the final geometry for a similar model. Nevertheless, it is worth looking at the differences between the open and closed packed models. Both packings are illustrated in Figure 5.7. The benchmark was performed for a bundle of 19 fibres, but no significant differences were seen between both packings. The spreading is a little different, see Figure 5.9, but the tensile stresses and contact pressures remain similar. Hence, the influence of the packing could be ignored in preliminary tests.

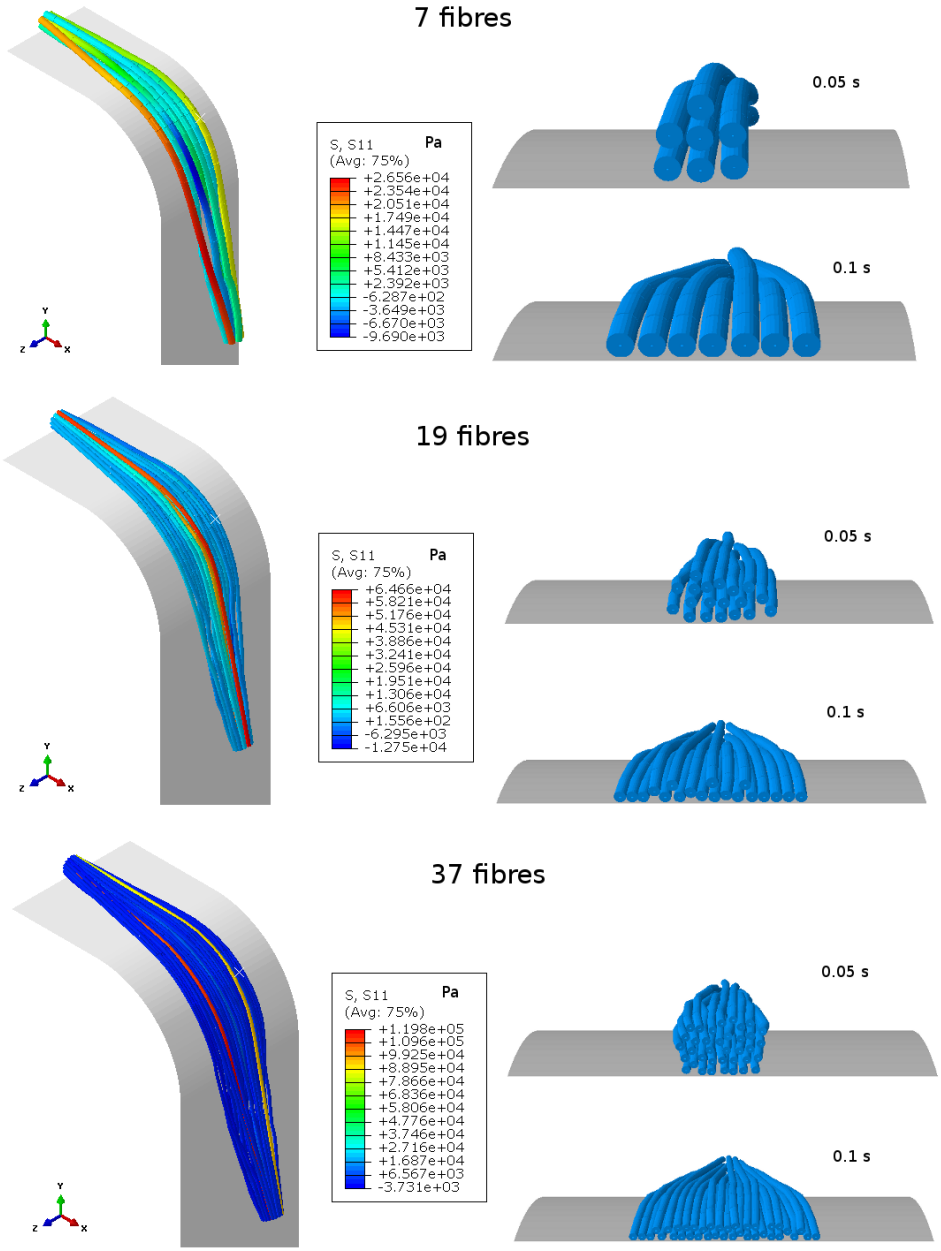

Figure 5.8: Longitudinal stress (left) and cross-section deformation at two points in time (halfway and final) (right) for three bundle models.

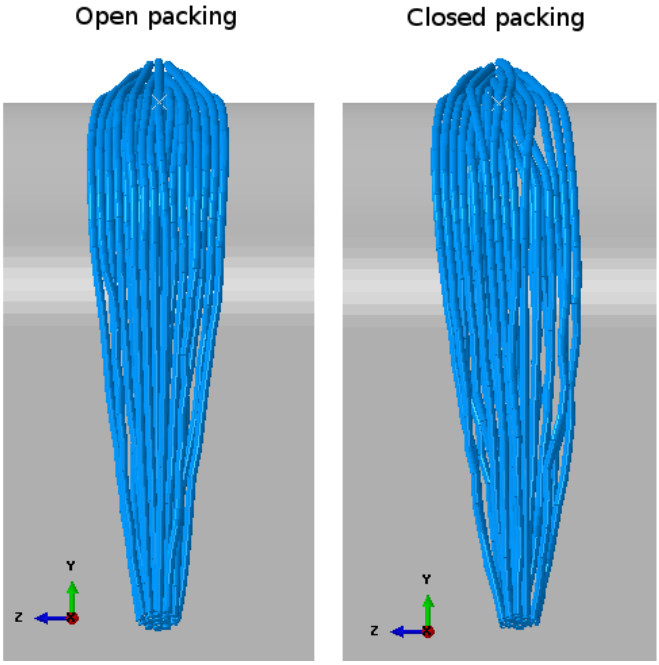

Figure 5.9: Deformation of a 19 fibre bundle with open packing (left) and closed packing (right).

5.3.2 Energy balance and viscous dissipation [1]

The energy balance is a great way to analyse the results of an explicit simulation. ABAQUS automatically outputs several energy components for the whole model. The conservation of energy for the benchmark can be expressed as follows:

$$E_{total} = E_I + E_{KE} + E_{VD} + E_{FD} - E_W \approx constant \tag{5.2}$$

The *internal energy* E_I is the total strain energy, mainly due to elastic and plastic deformation. The *kinetic energy* E_{KE} is the kinetic energy of the system. The *viscous dissipated energy* E_{VD} is the energy dissipated by damping mechanisms in order to damp out high frequency dynamical phenomena, which stabilises the numerical results. Despite its name, this does not include energy dissipated by visco-elastic material properties. The *frictional dissipated energy* E_{FD} describes the energy which is dissipated due to frictional effects. The *external work* E_W is the work done by external applied loads.

The energy balance can be used to check whether a simulation is dynamic or quasi-static. When the kinetic energy of the deformable material does not exceed a 5 - 10 % fraction of its internal energy throughout most of the

simulation, it can be regarded as quasi-static. Numerical energy contributions, such as viscous dissipation, should be low compared to the physical contributions for an accurate simulation.

The energy balance of the benchmark for the 1 fibre model is given in Figure 5.10. Only the last part of the simulation, where the yarn tightens around the curved surface, is important in energy contributions. The model has no initial energy, thus E_{total} is zero throughout the simulation. Hence, the energy balance can be written as:

$$E_W = E_I + E_{KE} + E_{FD} + E_{VD} \tag{5.3}$$

The frictional dissipated energy E_{FD} and internal energy E_I form the greatest contributions to the external work. This is to be expected, as the yarn is stretched a little after it has bent around the curved surface. The energy balance seems to indicate good results, see the close-up Figure 5.11. The kinetic energy and artificial energy contributions are negligible.

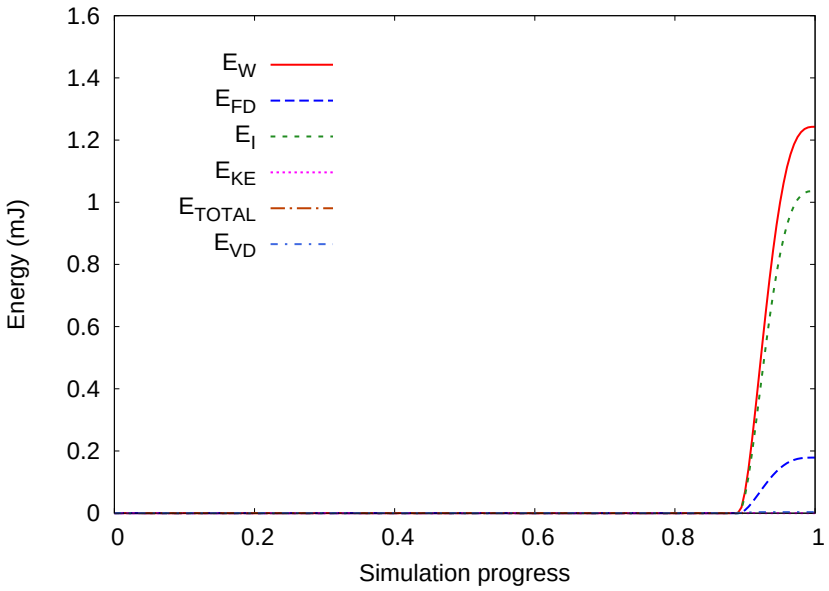

Figure 5.10: Energy balance of the 1 fibre model.

The fibre bundle models show a completely different energy balance, see Figure 5.12. There is almost no strain energy, because the fibres rearrange themselves to relieve most of the stresses. Furthermore, a significant amount of viscous dissipated energy is present in the model. The shapes of the frictional dissipated energy and viscous dissipated energy seem to be similar. Hence, the phenomena leading to both energies is probably the same. ABAQUS/Explicit's general contact algorithm uses a softened contact. Small penetrations of contacting surfaces are allowed, and a small

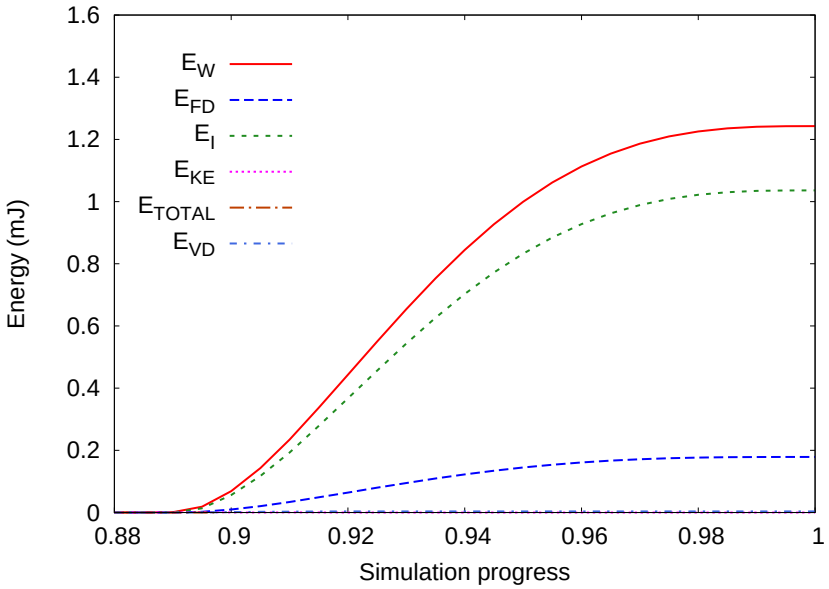

Figure 5.11: Close-up of the energy balance of the 1 fibre model.

amount of viscous contact damping is applied in order to reduce solution noise due to high frequency vibrations [1]. Due to the higher amount of fibres, more contacts take place, which is probably the main reason why the viscous dissipation is higher in the fibre bundle models.

By analysing the time where the viscous dissipation increased substantially, it was found that the perfect arrangement of fibres on top of each other led to one fibre being highly stressed, while the other fibres experienced much lower stresses. This fibre then snagged at substantial speed between the other fibres, see Figure 5.13, which caused a stress wave in the fibres. This effect can be avoided by changing the geometry of the packing a little, which decreased the amount of viscous dissipation significantly. For example, the ratio of viscous dissipation on external applied work decreased E_{VD}/E_W from 18 % to about 6 % by changing the geometry of the 19 fibre bundle so that no stacking of the fibres occurred.

Increasing the amount of fibres leads to more contacts. It was expected that this would increase the viscous dissipation. The ratios E_{VD}/E_W for different fibre bundles are shown in Table 5.4. The results indicate that the viscous dissipation increases with increasing amount of fibres. However, the fraction of viscous dissipation for the 7 fibre model was large compared to the other models, because the fibres could not rearrange themselves enough to relieve their stresses. In the 19 and 37 fibre bundle models, the fibres are thin enough to easily pass each other and rearrange themselves in a favourable position.

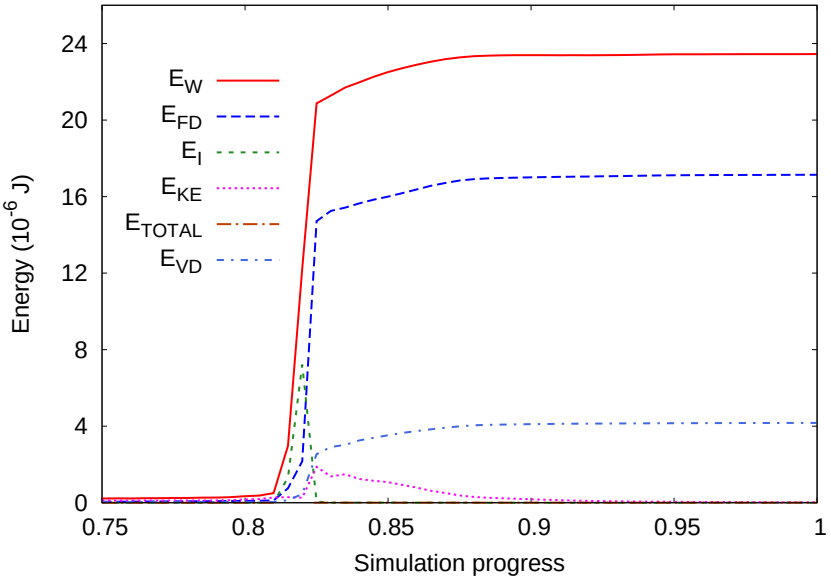

Figure 5.12: Energy balance of the 19 fibre bundle.

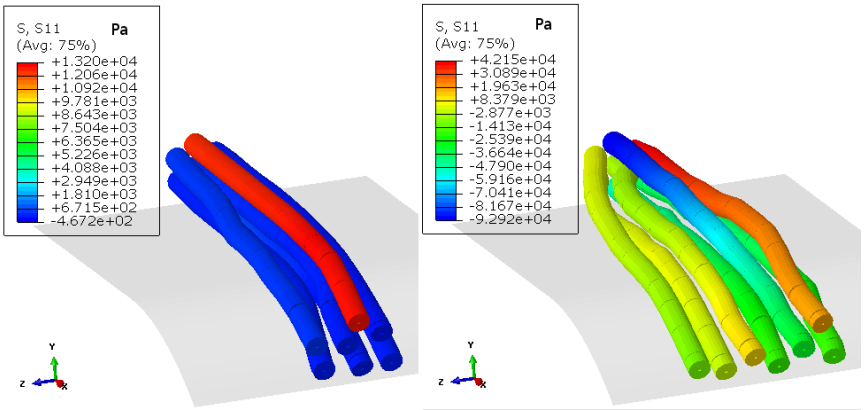

Figure 5.13: The tension builds up in a fibre which is located on top of the others (left) and is released when the fibre suddenly snags between the others (right) leading to the generation of a stress wave in the fibres.

Table 5.4: Influence of the amount of fibres in a yarn on the viscous dissipation fraction.

Amount of fibres	E_{VD}/E_W (%)
1	0.5
7	13
19	6.0
37	11

The viscous dissipation is important, since it is an artificial energy and should be low compared to other energy contributions: no more than 10 % of the external applied work. Furthermore, it was found that a high amount of viscous dissipation often went hand in hand with large penetrations of the fibre surfaces. No easy solution to this problem was found, but minimising the dynamical effects did decrease the viscous dissipation substantially.

5.3.3 Contact with deformable elements

In the stitching simulation, contact will also take place between the fibres and the foam core. From Section 5.2.4 it was clear that contact between truss and solid elements is possible. However, when using a bundle of fibres, the diameter of each truss element is reduced. For example, for a bundle of 19 fibres, the element's thickness reduces from 1 mm to 0.2 mm. If the same length, i.e. 0.67 mm, for each truss element would be used, this would lead to small contact spheres on the truss element's nodes. However, contact with a truss element only occurs with the contact spheres and zones of no contact are developed, see Figure 5.14. This poses no real problems when the bundle of fibres stays aligned and the contact spheres stay in close vicinity to each other, nor when contact with rigid bodies occurs. However, when the fibres do not align, or contact with deformable elements occurs, this can lead to penetrating surfaces, see Figure 5.15. The problem can be resolved by using a denser mesh on the fibres, so that the element's length is equal to or smaller than its thickness, see Figure 5.14. However, Δt_{stable} scales linearly with the element's length, and can be reduced significantly.

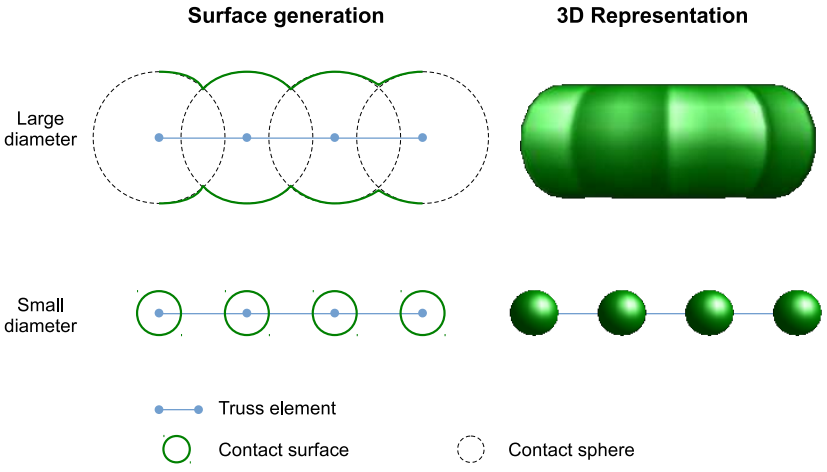

Figure 5.14: Generation and 3D representation of the contact surface on a fibre with a large or a small diameter (with fixed element length). Small element diameters lead to a discontinuous surface.

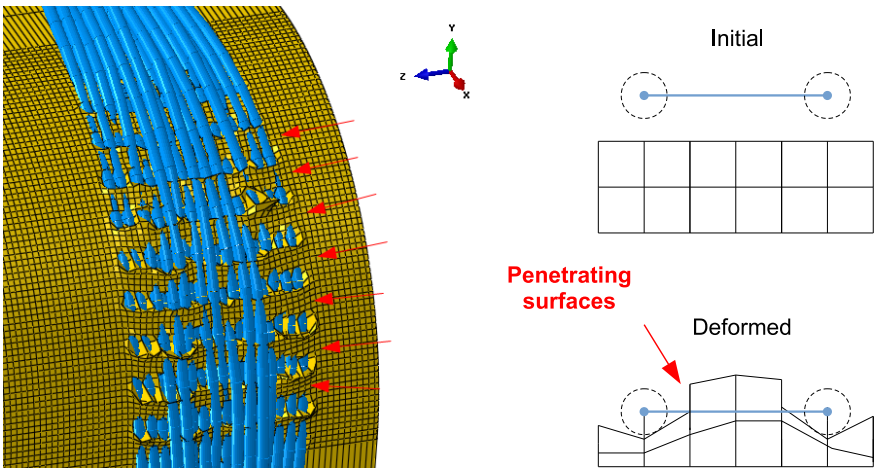

Figure 5.15: Small diameter to length ratio of the truss elements leads to penetrating surfaces.

5.4 Frequency analysis validation

A frequency analysis can be used to validate the truss model. The hypothesis is that the model should behave as a flexible thread without bending stiffness, i.e. an ideal string, which can be described by the theory of standing transversal waves on a string. The wavelength λ of a standing wave on a string with length L, and with both ends fixed is given by Eq. (5.4), where n denotes the mode of the wave. The longest wavelength is obtained for the fundamental mode, with $n = 1$. The overtones are obtained for $n = 2, 3, 4, \ldots$.

$$n\lambda = 2L \tag{5.4}$$

The velocity of the wave c is related to the wavelength by its frequency f as follows:

$$c = \lambda f \tag{5.5}$$

The velocity can be written in terms of the tension T acting in the string, the cross-sectional area A and the density ρ as $c = \sqrt{T/(\rho A)}$. By combining equations (5.4) and (5.5), an expression for the frequency in function of model's properties is obtained:

$$f = \frac{n}{2L}\sqrt{\frac{T}{\rho A}} \tag{5.6}$$

A string with fixed ends was simulated with the truss model. The parameters of the simulation are given in Table 5.5. A frequency analysis was used to test the hypothesis of a flexible thread, but it also provided information about an appropriate element size. Smaller elements lead to a more flexible chain, but

decrease the stable time increment. However, elements which are too large will lead to a chain that is unable to represent the flexible behaviour of a yarn. The built-in frequency analysis of ABAQUS was used to automatically determine the natural frequencies of the system. The influence of the truss element's length was investigated by comparing simulated frequencies to those obtained from Eq. (5.6) for different element sizes, see Figure 5.16. The fundamental frequency converges rapidly, while that of the 4th overtone converges when more than 100 elements are used. This is to be expected, as the shape of an overtone wave is more curved than that of the fundamental. When too few truss elements are used, they cannot accommodate for this curvature, see Figure 5.17. The string behaves less flexible, leading to lower frequencies. The same model is used to obtain the 4th overtone frequencies of a fixed string modelled with 100 truss elements for different tensions, see Table 5.6.

The results of the frequency analysis show that the truss model behaves as a flexible thread. Hence, it is suited to model flexible yarn behaviour. The size of the elements depends on the demanded flexibility: more elements are necessary for higher curvatures. It seemed that elements smaller than 1 mm suffice in most cases.

Table 5.5: Parameters for the fixed string frequency analysis.

L (mm)	E (GPa)	ρ (kg/m^3)	A (mm^2)	T (mN)
100	73	1153	0.785	537

Table 5.6: Results for a fixed string of 100 mm modelled with 100 truss elements.

Strain	Tension (N)	Theoretical freq. (Hz)	Simulated freq. (Hz)	Error (%)
$1.00\ 10^{-7}$	$5.73\ 10^{-3}$	50.32	50.29	0.07
$1.00\ 10^{-6}$	$5.73\ 10^{-2}$	159.14	159.03	0.07
$1.00\ 10^{-5}$	$5.73\ 10^{-1}$	503.24	502.90	0.07
$1.00\ 10^{-4}$	$5.73\ 10^{0}$	1591.23	1590.1	0.07
$1.00\ 10^{-3}$	$5.73\ 10^{1}$	5027.39	5022.8	0.09

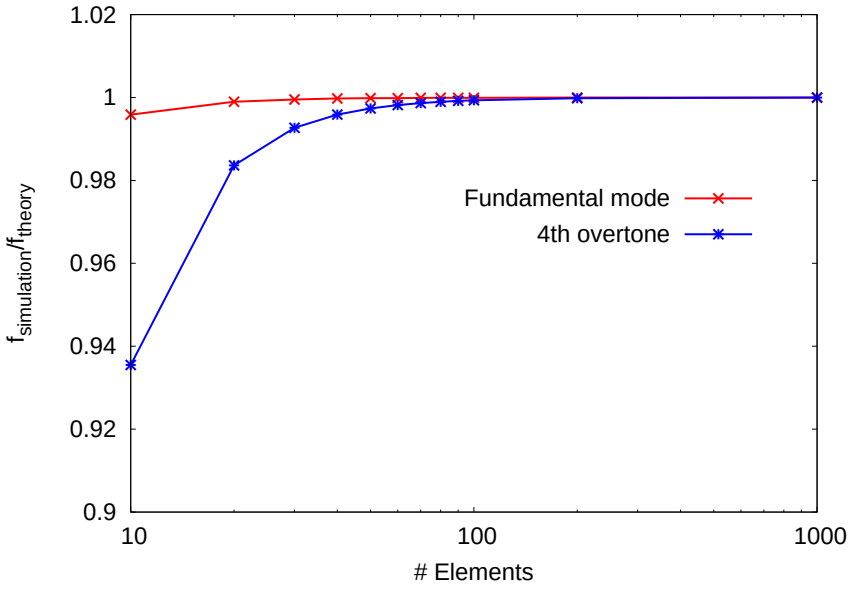

Figure 5.16: Element length versus relative frequency.

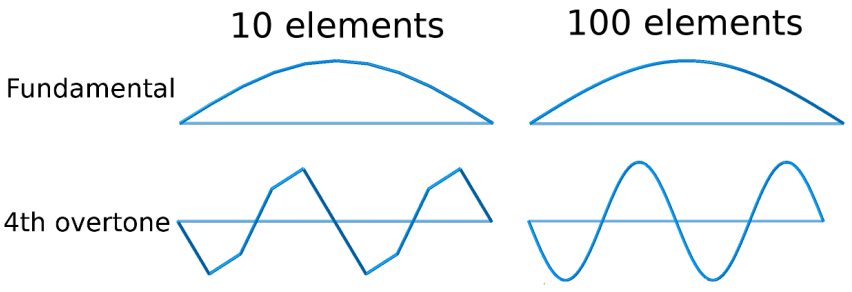

Figure 5.17: Shape of the standing wave using 10 and 100 truss elements over the length of the string.

Chapter 6

Modelling the foam core

Conventional metal components are more and more replaced by composite sandwich panels, mainly to reduce the weight of the components. Polymer foams are especially well suited to be used in the core of such panels, due to their high specific strength and stiffness, as well as their good durability. Their applications range further than only sandwich panels and they are also used for their thermal insulation properties or in energy absorbing structures.

This chapter deals with the modelling of the foam core in the Acrosoma stitched sandwich panel. A short introduction to their structure and behaviour is given first, since foams are not conventional materials. The introduction is followed by the implementation of a foam material model in ABAQUS.

6.1 Structure and mechanical behaviour of polymer foams

Foams could be classified under the cellular solid materials. The presence of voids, also referred to as cells, in these materials leads to their low weight and characteristic mechanical behaviour. Honeycomb structures and wood are other materials which are part of the cellular solids. Generally speaking, foams could be divided into two groups, based on their cellular structure: open cell foams and closed cell foams. Open cell foams have interconnected voids, while closed cell foams have voids which are completely surrounded by solid material. The difference between these two structures is visualised in Figure 6.1. The micromechanics of both groups are somewhat different, because they are governed by different deformation mechanisms. However, both groups show similar stress-strain behaviour on macroscopic scale.

Foams used in sandwich panels are typically closed cell polymer foams [106].

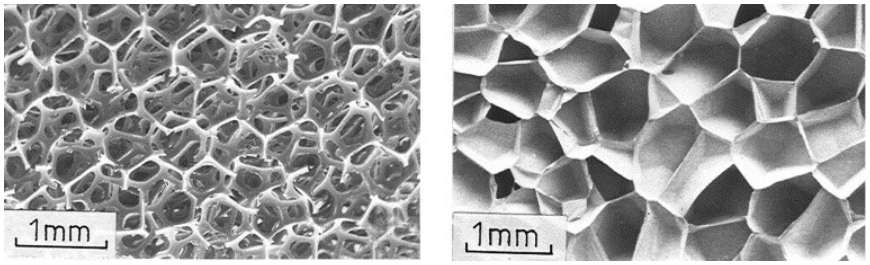

Figure 6.1: Cellular structure of open cell (left) and closed cell (right) foams.[107]

The progressive collapse of cells during compression is characteristic for foams. Therefore, they are often referred to as *crushable foams*. The progressive crushing leads to a very distinct stress-strain curve in compression, in which there is a relatively long zone of nearly constant stress, i.e. the plateau zone. The crushing of foam could be best understood by looking at the crushing of honeycomb structures, which are easily visualised in 2D, see Figure 6.2. The compressive stress-strain curve shows three distinct zones of deformation, see Figure 6.3. At small compressive stresses the foam reacts linear elastic. This elastic response is controlled by cell wall bending and cell face stretching. At higher compressive stresses, the cell walls progressively collapse, leading to a long collapse plateau where the stress remains approximately constant. When the cells are almost completely collapsed, opposite faces of the cells start to touch each other and the stress rises quickly. This regime is called the densification. The behaviour in tension is quite different. At small tensile stresses, the foam also reacts linear elastic. However, the foam is brittle in tension and failure occurs at relatively low strains. As explained in Chapter 2, failure of the foam core at 45 ° to the shear direction is often observed. This is the direction of maximum tensile stress. Hence, the tensile strength controls the failure in shear loading cases [108].

6.2 Crushable foam material model in ABAQUS

Just like fibrous materials, foams are multi-scaled. At the macroscopic scale, the foam could be approximated by a continuous solid material. At the microscopic level, however, the material consists out of cells. The scale ranges from several micrometers to millimeters, depending on the size of the cells. Foam materials are modelled at both scales. Local deformation behaviour of the cell and cell walls could be obtained from modelling the foam at the microscopic scale, see Figure 6.4. However, this requires very fine meshes, and thus, many elements are necessary which increases the calculation times. Therefore, only small volumes of foam could be modelled. On the

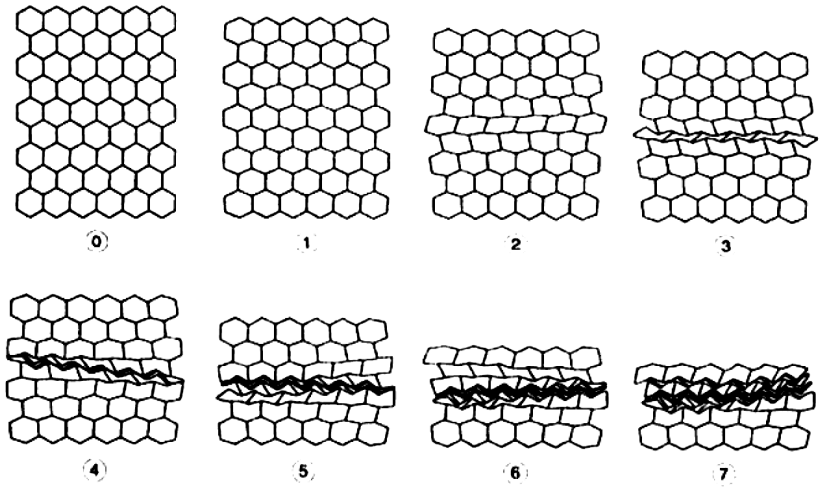

Figure 6.2: Progressive collapse sequence of a honeycomb structure under compression.[109]

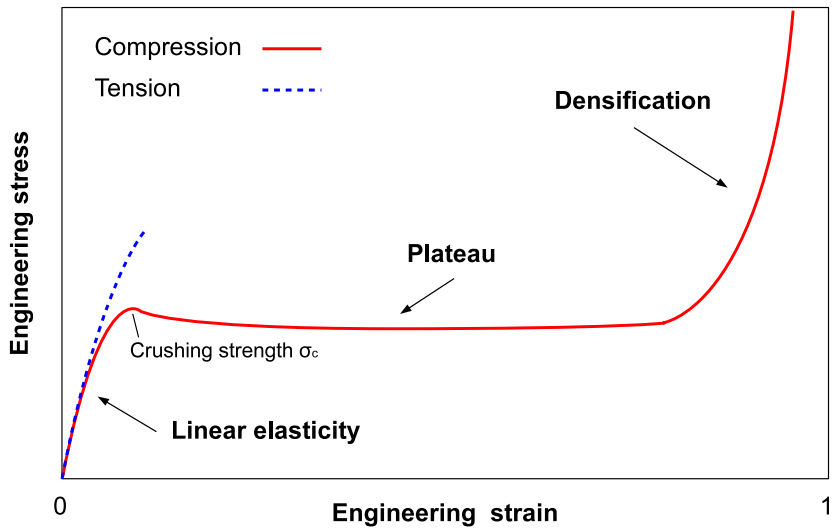

Figure 6.3: Stress versus strain for a polymer foam in compression (solid line) and tension (dashed line).

other hand, by using appropriate constitutive laws, the material can be homogenised and modelled as a continuum material. This would require much less computing power, and it is also easily implemented into conventional FE-software. Furthermore, microscopic models require precise experimental determination of the cell size distribution, their arrangement, etc., to define a FE-model, which is very difficult and time consuming. Macroscopic models, however, require precise determination of the constitutive laws to account for their cellular behaviour. ABAQUS already possesses a crushable foam material model to simulate these kind of materials.

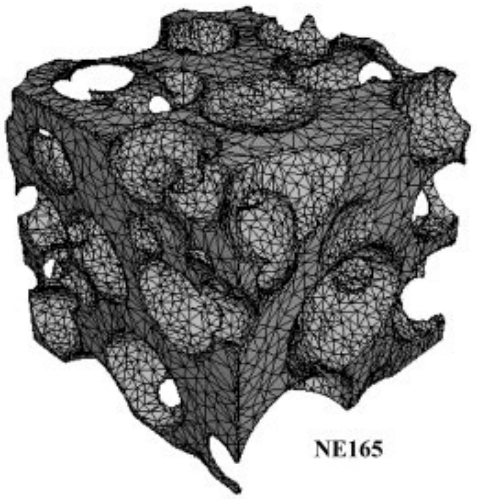

Figure 6.4: Microscopic modelling of a small elementary foam volume.[110]

The crushable foam material model is a plasticity model which is used to model crushable materials such as foams [1]. It takes into account the foam's ability of deforming in compression due to cell wall buckling. The crushable foam material model only simulates the plastic response of the foam; the elastic response is modelled by assigning a linear elastic behaviour to the material. The material model was first validated to see if its compression behaviour is similar to the one observed experimentally. The intensively studied Rohacell 51 WF foam was used for the validation, because its mechanical data are readily available [108, 106, 111, 112]. If the crushable foam material model is suited for Rohacell 51 WF, it can also be used to model Rohacell 71 RIST, as both foams are very similar.

6.2.1 Validation with Rohacell 51 WF foam data

Polymethacrylimide (PMI) foams, commercially known as Rohacell foams, are produced by Evonik Industries. The parent polymer has a density of

1200 kg/m^3 [108]. The manufacturer's data of the foam is given in Table 6.1. The data agrees well with the experimental obtained data [108]. The average cell-wall length and cell-wall thickness are 300 μm and 12.0 μm respectively [108]. The microscopic structure of the foam is shown in Figure 6.5.

Table 6.1: Rohacell 51 WF manufacturer's data.

Density (kg/m^3)	52
Compressive strength (MPa)	0.8
Tensile strength (MPa)	1.6
Shear strength (MPa)	0.8
Elastic modulus (MPa)	75
Shear modulus (MPa)	24
Strain at break (%)	3.0

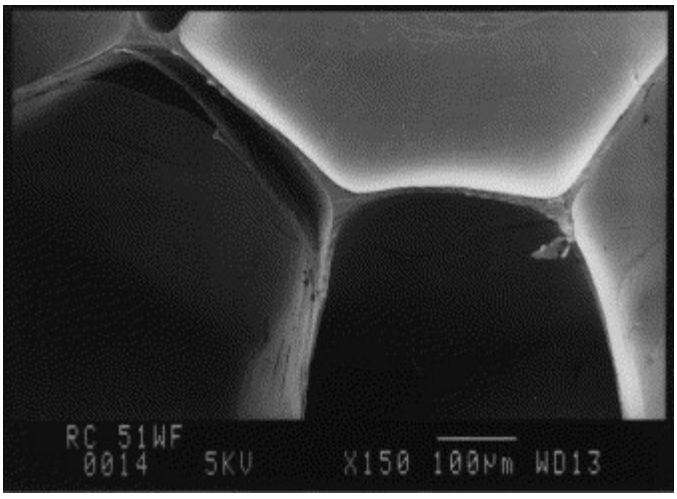

Figure 6.5: Microstructure of Rohacell 51 WF foam.[108]

Definition of the model in ABAQUS

The compressive behaviour of Rohacell 51 WF foam for three mutually perpendicular directions is given in Figure 6.6. The figure shows that the foam can be assumed isotropic. The linear elastic response is modelled by assigning a linear elastic material behaviour to the foam, which requires a Young's modulus E and a Poisson's ratio ν. The Poisson's ratio is often obtained from the relationship between the Young's and shear modulus of an isotropic material:

$$\nu = \frac{E}{2G} - 1. \tag{6.1}$$

The use of this relation is however questionable, as it is only valid for continuous isotropic materials. In cellular solids, compressive deformation is governed by cell wall bending and buckling and is very different from the deformation behaviour in tension. Li et al. [108] noted the inconsistency between the Poisson's ratio obtained from compressive and tensile moduli. Gibson and Ashby [109] showed that the Poisson's ratio for open and closed cell foams could be approximated by 1/3. However, they noted that the property is difficult to measure and their data showed large scattering. Different Poisson's ratios were tried in ABAQUS, and it was concluded that a ratio equal to 0 showed the best results. A compressive Young's modulus of 75 GPa was used.

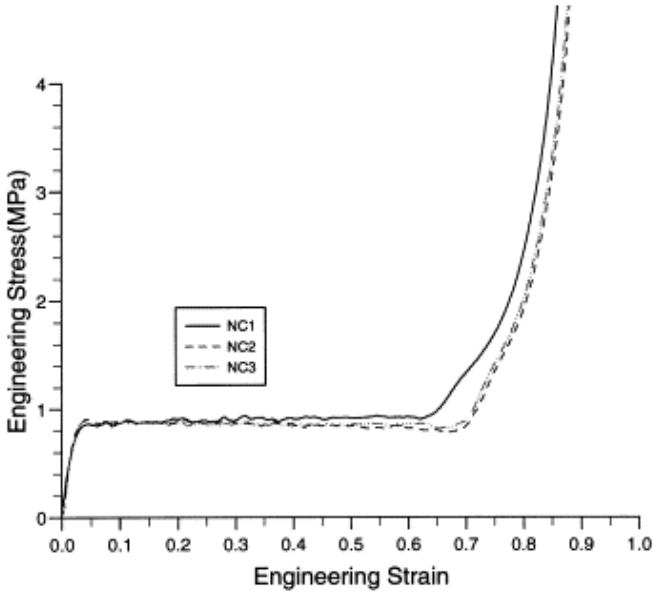

Figure 6.6: Compressive behaviour for three mutually perpendicular directions of Rohacell 51 WF showing low anisotropy.[108]

The plastic response was modelled using the crushable foam material model. Two models are available in ABAQUS: one that uses volumetric hardening, and one that uses isotropic hardening. The isotropic hardening model is based on the constitutive model for metallic foams developed by Deshpande and Fleck [113]. According to the authors, the model is also suited to describe the behaviour of polymer foams [114]. The difference between the isotropic and volumetric hardening models is their behaviour in hydrostatic tension [1]. However, the crushable foam material is namely used in compressive loading and there should be no significant differences between both models in compression. Therefore, the volumetric hardening model was chosen. The model requires the ratio of initial yield stress in uniaxial compression σ_c^0 on initial yield stress in hydrostatic compression p_c^0 and the ratio of

yield strength in hydrostatic tension p_t on initial yield stress in hydrostatic compression p_c^0. Li et al. [108] determined that $\sigma_c^0/p_c^0 \approx 1$. Foams are rarely tested in (hydrostatic) tension, because these tests are difficult to perform. A common approximation is to use a p_t equal to 10 % of p_c^0 [1]. Li et al. [108] remarked that this is probably not a correct assumption, however, the exact value of p_t has no significant influence on the compressive stress behaviour. Assuming that the foam is mainly stressed in compression during stitching, a value of p_t equal to $0.1p_c^0$ was chosen.

The crushable foam material model also requires the strain hardening data, i.e. the progression of the yield stress with strain. The stress-strain curve from Figure 6.6 was used to define the strain hardening. Stress-strain data for foams are often given in engineering stress s and engineering strain e. The crushable foam model in ABAQUS, however, requires the progression of the true stress σ with true plastic strain ε_{pl} (in absolute values). The data from Figure 6.6 was transformed using following equations:

$$\sigma \approx s \tag{6.2}$$

$$\varepsilon_{pl} = \ln(1+e) - \frac{\sigma_c^0}{E} \tag{6.3}$$

where s, e and σ_c^0 are negative in compression, σ_c^0 is the initial yield stress in compression and E is the compressive Young's modulus. Eq. 6.2 is valid because the plastic Poisson's ratio during crushing is found to be around zero [111]. A summary of the crushable foam material model is given in Table 6.2.

Table 6.2: Summary of the crushable foam material model for Rohacell 51 WF.

E (MPa)	ν	σ_c^0 (MPa)	e_d (%)	σ_c^0/p_c^0	p_t/p_c^0
75	0	0.8	70	1	0.1

Quasi-static compression tests were performed in ABAQUS/Explicit by compressing solid foam disks with rigid plates. The disks had a height and radius of 1 cm, and were assigned the Rohacell 51 WF material model described in Table 6.2. Due to symmetry, only one quarter of the disk had to be modelled. The course of the simulation is visualised in Figure 6.7, and the corresponding compressive stress-strain curve is plotted in Figure 6.8 for both hardening models. Figure 6.7 shows the progressive collapse of cells in the foam. Comparison of Figure 6.8 to Figure 6.6 validates the use of the crushable foam model for simulating foam compression behaviour as the

simulated stress-strain diagram corresponds very well to the experimental stress-strain diagram.

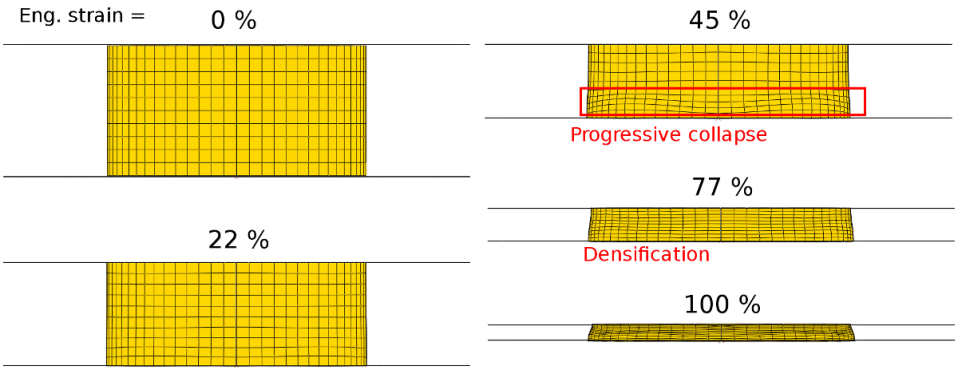

Figure 6.7: Compression of a foam disk at different engineering strains showing the progressive collapse of cells in the material.

Mesh distortion controls

Large deformations of the foam can lead to a distorted mesh, and thus, inaccurate results. Hence, in simulations where there is significant deformation of the foam, e.g. stitching, some sort of mesh distortion control should be used. Two methods of distortion control are available in ABAQUS: element distortion control and adaptive meshing techniques.

Adaptive meshing in ABAQUS makes use of an arbitrary Lagrangian-Eulerian (ALE) method. In a Lagrangian model, the mesh moves with the material, making it easy to track surfaces and boundary conditions of the model. Most simulations in ABAQUS make use of a pure Lagrangian description. In a Eulerian model, the material flows through a fixed mesh. However, the use of a fixed mesh makes it difficult to track the free surfaces of the model. The ALE method combines the features of both methods: at free surfaces the material motion is fixed to that of the mesh (Lagrangian), otherwise both motions are independent of each other (Eulerian). A schematic representation of the Lagrangian, Eulerian and ALE method is given in Figure 6.9. The ALE method generates a smoother mesh at regular intervals, which reduces the mesh distortion. The extra computational cost for this operation in ABAQUS/Explicit, is made up by the increase of the stable time increment Δt_{stable}. When no adaptive meshing is used, the distorted mesh elements can become very small. This can lead to a very small Δt_{stable}, as it scales linearly with the smallest element size.

The other method of distortion control is *element distortion control*. Element distortion control prevents solid elements from inverting or distorting excessively. However, the technique does not attempt to maintain a high-

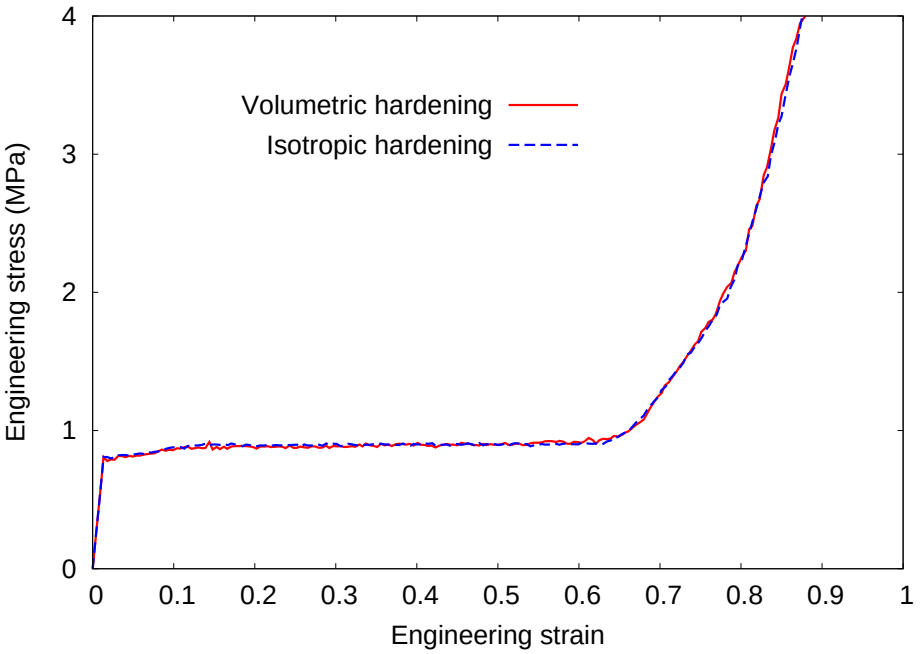

Figure 6.8: Simulated engineering stress-strain diagram for the quasi-static compression of Rohacell 51 WF foam for volumetric and isotropic hardening models. No significant difference between both hardening models is observed.

quality mesh during a simulation, as is the case with adaptive meshing. It should be used in simulations where the mesh is coarse relative to the amount of compression. Furthermore, element distortion control is especially well suited to model volumetric compacting materials, such as crushable foams [1].

The final deformed structure of the compressed foam disks for both types of distortion control are shown in Figure 6.10. Element distortion control seemed to yield the best results. Therefore, it was used in all simulations which made use of the crushable foam material. To overcome numerical instabilities of the reduced integration solid elements (C3D8R), the enhanced hourglass setting was used, as recommended for crushable materials [1]. C3D8R elements are the default solid elements used by ABAQUS/Explicit.

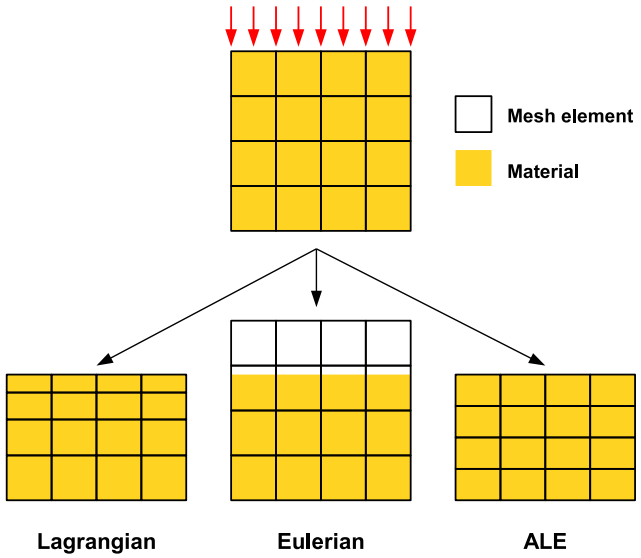

Figure 6.9: Schematic representation of the pure Lagrangian, pure Eulerian and ALE mesh method.

Strain rate dependent behaviour

A last characteristic of the crushable foam material model is its capability to represent strain rate behaviour of foams. Strain rate dependent input is given by a power law, or by specifying the ratio of the yield stress at different strain rates. The strain rate behaviour of Rohacell foams depends on the foam's density [111]. Arezoo et al. [111] reported mild strain rate sensitivity for the Rohacell 51 WF foam: the plateau stress increases about 30 % when the strain rate changes from 10^{-3} s^{-1} to 10^{3} s^{-1}. This increase in yield stress was provided as tabular data in the crushable foam material model. The resulting compressive stress-strain curve at low and high strain rate is

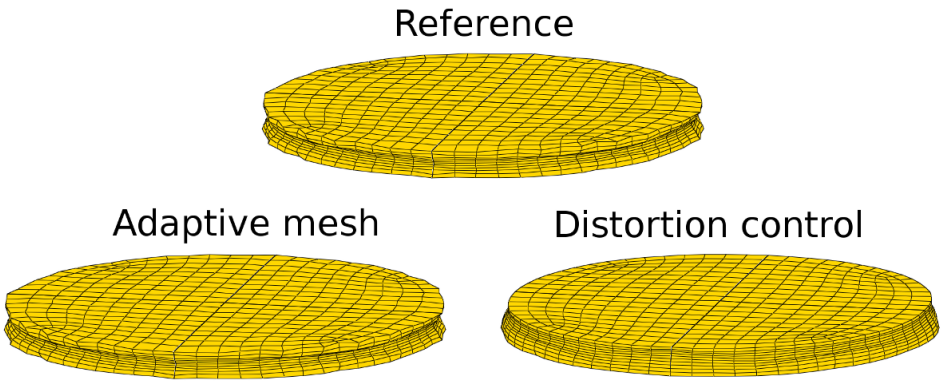

Figure 6.10: Deformed structure after compression with and without distortion control techniques. The element distortion control seems to yield the best results.

shown in Figure 6.11. It shows that the crushable foam material model is capable of incorporating strain rate dependent behaviour.

The results showed that the crushable foam material model available in ABAQUS is a good constitutive model to simulate Rohacell 51 WF foam. Therefore, it is also used to model Rohacell 71 RIST foam, which, according to the manufacturer, is not that different from the WF foams.

6.2.2 Rohacell 71 RIST material model

In the previous section, the crushable foam material model was validated by simulating compression tests on a model of Rohacell 51 WF foam. The mechanical properties of Rohacell 71 RIST are, however, not extensively researched. Therefore, the mechanical properties for the Rohacell 71 RIST foam were taken from the manufacturer's data sheet. The densification strain of Rohacell 71 RIST was not available, but most PMI foams show a densification engineering strain between 60 and 70 % [111]. The compressive stress-strain input for the crushable foam material model is depicted in Figure 6.12 together with the stress-strain curve obtained from a quasi-static simulation. At engineering strains above 70 %, small discrepancies are observed between the input and output. Table 6.3 summarises the mechanical properties of the Rohacell 71 RIST material model.

Table 6.3: Summary of the crushable foam material model for Rohacell 71 RIST.

E (MPa)	ν	σ_c^0 (MPa)	e_d (%)	σ_c^0/p_c^0	p_t/p_c^0
105	0	1.6	70	1	0.1

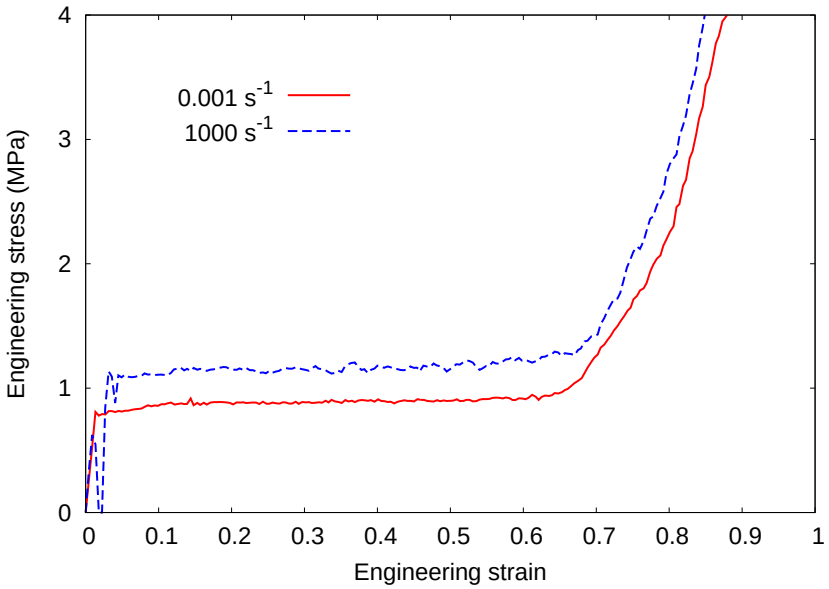

Figure 6.11: Engineer stress-strain curve for low and high strain rates. The zero stress value at small engineering strains for the high strain rate compression test was due to dynamical effects.

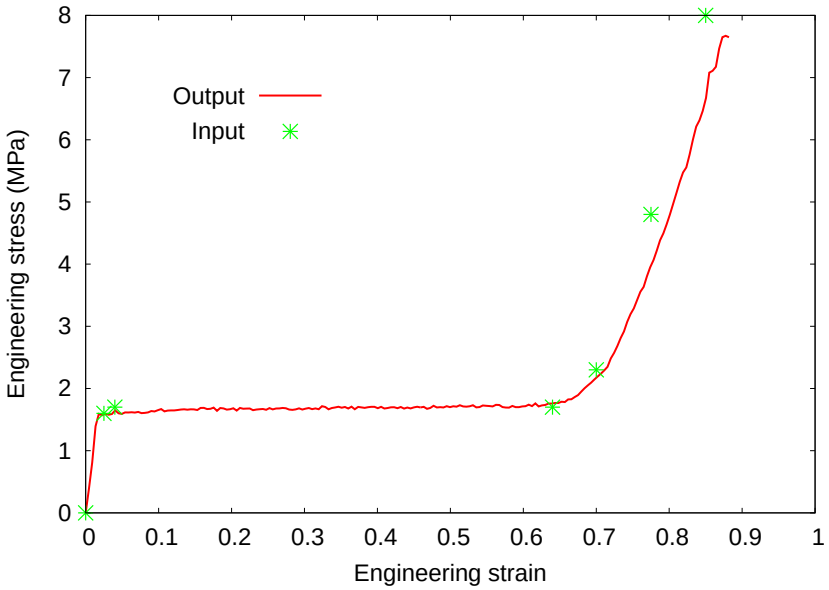

Figure 6.12: Input of stress-strain values and the resulting compression stress-strain output.

The material model created in this section is used to simulate the behaviour of Rohacell 71 RIST foam used by Acrosoma as a core in their sandwich panels.

6.3 Needle penetration in the foam

During stitching, needles penetrate the foam, making way for the yarn. The needle tip tears the foam and pushes it to the sides. A cylindrical hole is created through the thickness of the foam. To obtain similar results in a FE-model, the tearing should be included in the material model. In default FE-analyses, finite elements stay bonded to each other at their shared nodes at all times. No matter how much distortion of the mesh occurs, the elements stay fixed to each other. A damage model gives the ability of FE-elements to fail. For example, when an element reaches a certain amount of strain or stress, the element is said to have failed. Failed elements are deleted from the mesh, resulting in a gap, and this can lead to inaccurate results when the mesh is very coarse. Before implementing a damage model in the Rohacell 71 RIST material model, needle penetration in crushable foams is investigated. Two specific cases are studied: penetration by a blunt needle and penetration by a sharp needle.

6.3.1 Penetration by an axisymmetric blunt needle

It is assumed that a blunt needle could be represented by a rigid cylinder. The cylinder has the same radius as the needle, however, it has no pointed tip. When a foam is penetrated by a rigid cylinder, two major mechanisms occur that determine the force exerted on that cylinder: (1) tangential friction of the cylinder's side with the foam, and, (2) crushing of the material underneath the cylinder's face. The force due to tangential friction increases linearly with the displacement of the cylinder in the material, because the contact surface increases linearly. The force due to crushing is related to the compression strength of the material. For crushable foams, which have a zone of nearly constant crushing strength, this force remains approximately constant throughout the displacement. At a certain displacement value, the shear strength of the foam column underneath the cylinder is reached, and the column is pushed out. The mechanisms are illustrated in Figure 6.13. The force-displacement curve is shown in Figure 6.14. The friction force F_{fric}, crushing force F_{crush} and the shear failure force F_{fail} are summarised in Equations (6.4) - (6.6), where σ_N is the normal pressure on the needle, μ is the friction coefficient, d is the displacement in the foam, σ_c is the crush strength of the foam, r is the radius of the cylinder, f_{shear} is the shear strength of the foam and H is the height of the foam.. From Eq. (6.4) and

Eq. (6.5) follows that the main parameters that determine the total force exterted on the needle are the friction coefficient μ, the normal pressure on the needle σ_N and the crush strength of the foam σ_c.

$$F_{fric} = \mu\, \sigma_N\, A_1 = \mu\, \sigma_N\, (2\pi r)\, d \tag{6.4}$$

$$F_{crush} = \sigma_c\, A_2 = \sigma_c\, (\pi r^2) \tag{6.5}$$

$$F_{fail} = f_{shear}\, A_3 = f_{shear}\, (2\pi r)\, (H - d) \tag{6.6}$$

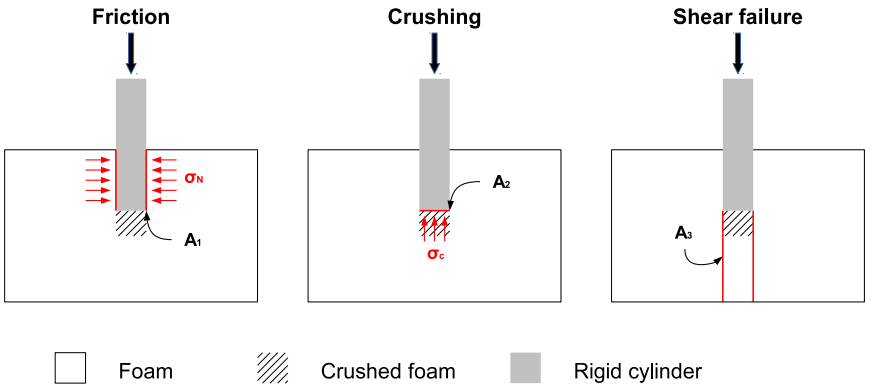

Figure 6.13: Mechanisms occurring when a foam is penetrated by a rigid cylinder (blunt needle).

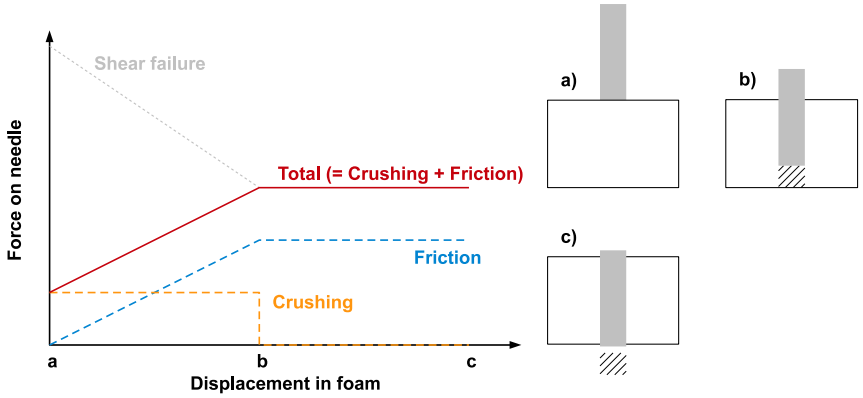

Figure 6.14: Force-displacement curve for a rigid cylinder penetrating a foam.

6.3.2 Penetration by an axisymmetric sharp needle

When a sharp needle penetrates the foam, the mechanisms contributing to force exerted on the needle are similar to those occurring for a blunt needle. There is still a tangential friction force due to contact between the needle body and the foam. However, crushing of the foam now occurs more laterally, due to the needle tip geometry. Furthermore, no column of foam material gets pushed out by shear failure. The sharp point tears the material, resulting in an opening in the foam. The penetration of a needle tip into a foam is illustrated in Figure 6.15. The two major mechanisms that determine the force exerted on the needle are shown in Figure 6.16. The friction contribution can be divided in two parts: force due to friction with the needle tip and force due to friction with the needle body. The normal pressure acting on the needle tip is higher than that acting on the needle body, because the latter is only coming from the elastic recovery of the foam. The normal pressure on the needle tip, however, is also due to the crushing strength of the foam. Crushing of the foam only takes place around the tip, as is illustrated in Figure 6.15. Therefore, once the needle tip has penetrated the foam completely, the force due to crushing stays constant, until the tip reaches the bottom side of the foam. An illustration of a general force-displacement curve for a sharp needle penetrating a foam is given in Figure 6.17. The total force exerted on the needle is mainly determined by the friction cofficient μ, the normal pressures on the needle σ_{N1} and σ_{N2} and the crush strength of the foam σ_c. The tearing of the foam by the needle tip also contributes to the total force. However, this fraction is probably negligible when the needle tip is sharp. Furthermore, the exact geometry of the needle tip will have an influence on the force-displacement curve.

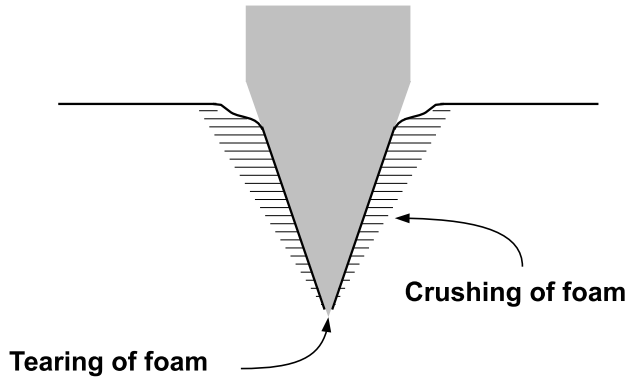

Figure 6.15: Penetration of a sharp needle tip into foam causes lateral crushing around the needle tip.

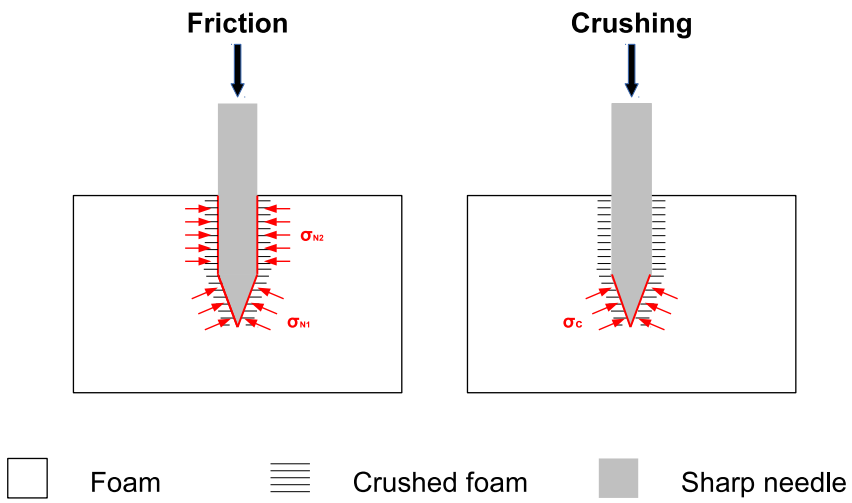

Figure 6.16: Mechanisms that occur when a sharp needle penetrates a foam.

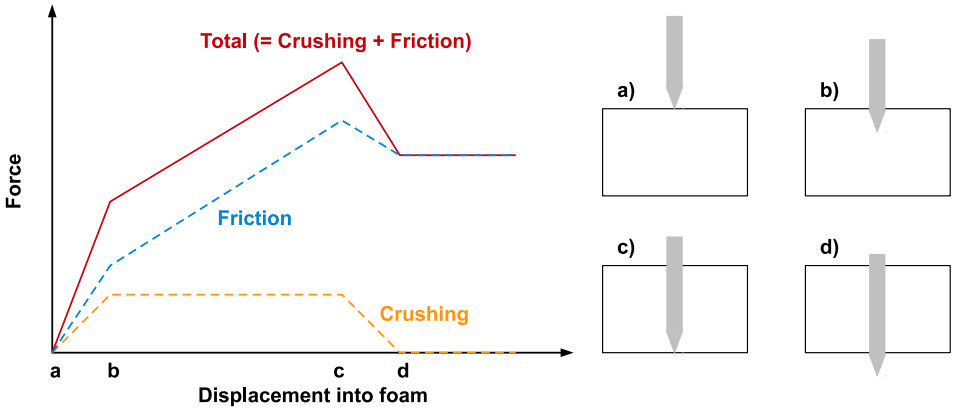

Figure 6.17: Force-displacement curve for a sharp needle penetrating a foam.

6.3.3 Penetration of Rohacell 71 RIST: experimental

The indentation of Rohacell 71 RIST with a real stitching needle has been done by Acrosoma for different types of needles at different penetrating speeds. It could be expected that, depending on the needle tip geometry, mechanisms belonging to sharp needle or blunt needle penetration will be observed. It was confirmed by Acrosma that a small column of crushed foam is pushed out by a blunt needle. Furthermore, they noticed that the elastic recovery of the foam after the needle had been removed, led to high frictional forces when the needle was again inserted in the same place.

Acrosoma measured the force-displacement curve for the penetration of a needle in Rohacell 71 RIST foam. The needle had a diameter of 3 mm, but the exact needle tip geometry is not known. This could have an effect on the exact shape of the force-displacement curve. However, the measured curve seems to be very similar to the one proposed in Section 6.3.2, see Figure 6.18. The foam specimen had a thickness of 30 mm. The force increases almost linearly to its maximum value of 60.3 N at 29 mm, where the needle tip just touches the bottom side of the foam. As the needle tip is pushed out of the foam, the force decreases to 46 N. The measurement was stopped at a needle displacement of 38 mm. Most likely, the force falls to a certain value at further displacements, and stays constant when the needle tip is completely out of the foam. The same test was performed for different needle penetrating speeds, ranging from 30 mm/min to 1800 mm/min. The increase on the maximal exerted force was only 5 - 7 %. Furthermore, the force-displacement curves were very similar in shape. This small increase could be due to the strain rate sensitive behaviour of the foam or due to dynamic effects. This was, however, not further investigated.

6.3.4 Penetration of Rohacell 71 RIST: simulation

The penetration of a needle through Rohacell 71 RIST must be simulated, as it is a key part of the final stitching simulation. As mentioned in the beginning of this section, the finite elements in a mesh stay connected at their nodes at all times. This would make it impossible for the needle to pass through the foam. Therefore, it is necessary to include a damage model to the material model. This is done in ABAQUS by defining a damage initiation and a damage evolution criterion, which control the failure of mesh elements. When the criteria are met, an element is said to be failed. Failed elements are removed from the mesh and do no longer contribute to the structure's stiffness.

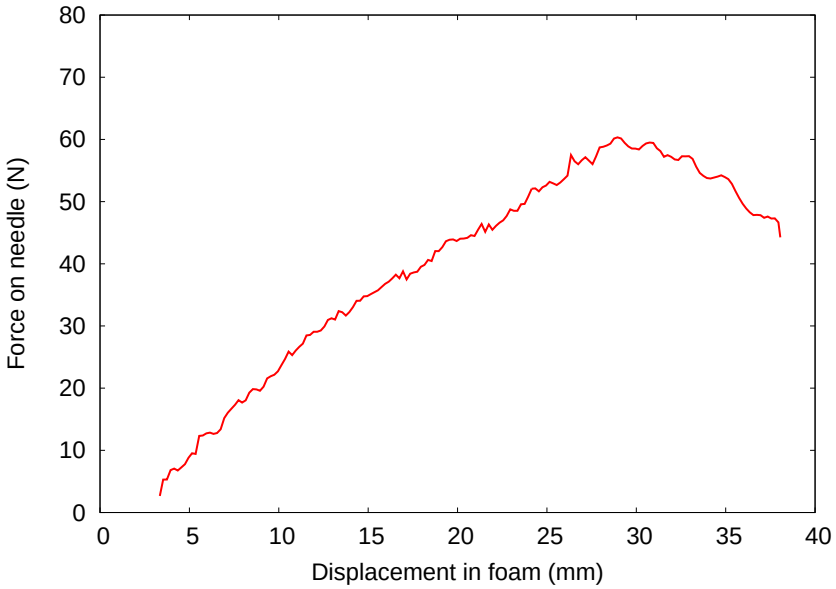

Figure 6.18: Force-displacement curve for a needle penetrating through a Rohacell 71 RIST foam specimen with a thickness of 30 mm.

Damage initiation and evolution

A damage initiation criterion specifies the strain at which damage begins, while a damage evolution criterion specifies the response of the damaged material. This is illustrated in Figure 6.19. Several damage models are available in ABAQUS for simulating different kinds of failure, e.g. brittle cracking of concrete, ductile damage for metals, damage models for fibre reinforced composites. However, there is no damage model intended for crushable foams, which are brittle in tension, but not in compression. Therefore, the ductile damage model, intended for ductile metals, was used.

The ductile damage model simulates the fracture of metals due to void nucleation, coalescence and growth [1]. Most likely, the fracture mechanism in polymer crushable foams is different, however, the damage model is still useful as it provides a failure mechanism to mesh elements. The parameters of the damage model can be inversely determined to obtain good results. The ductile damage initiation criterion is specified by three parameters: plastic strain at damage initiation, stress triaxiality and strain rate. The stress triaxiality is defined as the negative ratio of pressure stress on Mises stress. Normally, the plastic strain at damage initiation should be given as a function of stress triaxiality at different strain rates. However, these parameters were not available for Rohacell foams. Several values of stress triaxiality and strain rate were tested, but these parameters had negligible influence on the

needle penetration results. Therefore, the stress triaxiality and strain rate were set to an arbitrary value of 1. The ductile damage evolution criterion requires a fracture energy to describe the damaged response of the material. The fracture energy of Rohacell 71 RIST was not available, but was inversely determined from the needle penetration simulation as 1 J/m^2 at a plastic true strain of 1.1. The damage model is summarised in Table 6.4. It represents brittle failure at a strain which is just a little higher than the onset of densification. Figure 6.20 shows the compressive engineering stress-strain curve for the Rohacell 71 RIST material model with and without damage, obtained from a quasi-static compression simulation.

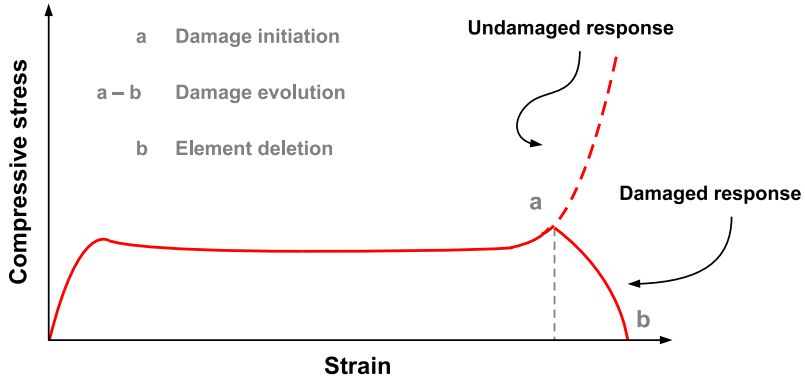

Figure 6.19: Damage initiation and evolution criteria.

Table 6.4: Ductile damage initiation and evolution used for the Rohacell 71 RIST material model.

Parameter	Initiation	Evolution
Plastic strain at failure	1.1	
Stress triaxiality	1.0	
Strain rate	1.0	
Fracture energy (J/m^2)		1.0

Simulation

A quasi-static penetration of a needle in Rohacell 71 RIST was simulated with ABAQUS/Explicit. The needle was assumed rigid, as the stiffness of steel is much higher than that of Rohacell 71 RIST foam. For simplicity's sake, the needle was assumed to be a sharp axisymmetric needle. Therefore, only one quarter had to be simulated with appropriate symmetry boundary conditions. The curvature and size of the needle tip was taken similar to that of a real needle. The foam is modelled as a disc with a height of 30 mm

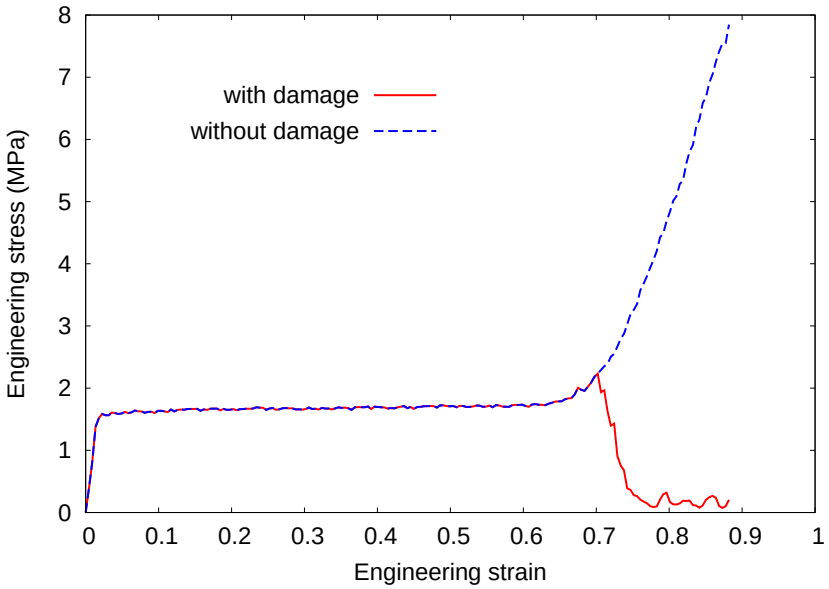

Figure 6.20: Compression engineering stress-strain curve for the Rohacell 71 RIST material model with and without damage specified.

and a diameter of 40 mm. A tangential friction coefficient of 0.3 was used. The initial geometry of the simulation is shown in Figure 6.21. The needle was displaced vertically in the foam at a constant velocity of 5 m/s, while movement in other directions was restricted. This velocity may seem very high for a quasi-static analysis. However, simulating at the natural time scale is often not necessary in explicit simulations [1]. The foam's outer surface was fixed in all directions.

The simulation is very sensitive to the mesh geometry, due to the element deletion. It is important that the simulation captures the friction of the needle body with the foam once the needle tip has passed. If too many elements are deleted, contact between the needle body and the foam disappears, because the new exposed foam surface does not touch the needle body. Furthermore, the elements that do touch the needle body should be deformed. Otherwise, there is no elastic recovery, and thus no normal pressure and no tangential friction. The mesh sensitivity problem is illustrated in Figure 6.22. Several mesh geometries were tested. They varied mainly in element size and element geometry around the perimeter of the needle. Most mesh geometries resulted in an uneven distribution of tangential friction with the needle body, or in a loss of contact. The mesh geometry which resulted in a good contact surface is shown in Figure 6.23.

The energy balance indicated that frictional dissipation and strain energy were the two major contributions to the work applied on the needle. The

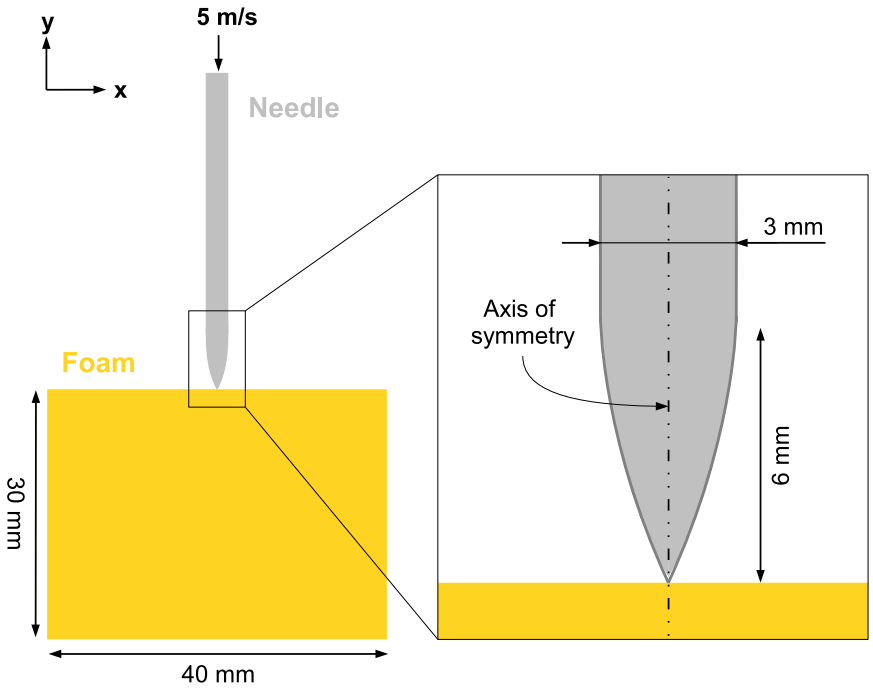

Figure 6.21: 2D Sketch of the needle penetration simulation.

frictional energy dissipation fraction is related to the amount of dissipated energy due to friction between the needle and the foam. The strain energy fraction is related to the elastic and plastic straining of the foam material. The results from the energy balance are a validation of the sharp needle case proposed in Section 6.3.2, where it was stated that friction and crushing were the two governing mechanisms to the force exerted on the needle. The external loading was applied only in y-direction, hence, the following equation is valid:

$$E_W(y) = \int F_{total}(y)\,\mathrm{d}y \tag{6.7}$$

where $E_W(y)$ is the work applied on the needle (from the energy balance), $F_{total}(y)$ is the vertical force exerted on the needle and y is the displacement in the foam. The force exerted on the needle is a function of the displacement, as was explained in Section 6.3.2. From Eq 6.7 follows that $F_{total}(y)$ can be obtained from the energy balance by differentiating $E_W(y)$ with respect to displacement y. The force-displacement curve obtained by this method has less noise than the signal obtained by directly outputting the force acting on the needle's reference node, see Figure 6.24. Good agreement was found with the experimental force-displacement curve provided by Acrosoma, see Figure 6.24. Discrepancies are most likely due to a difference

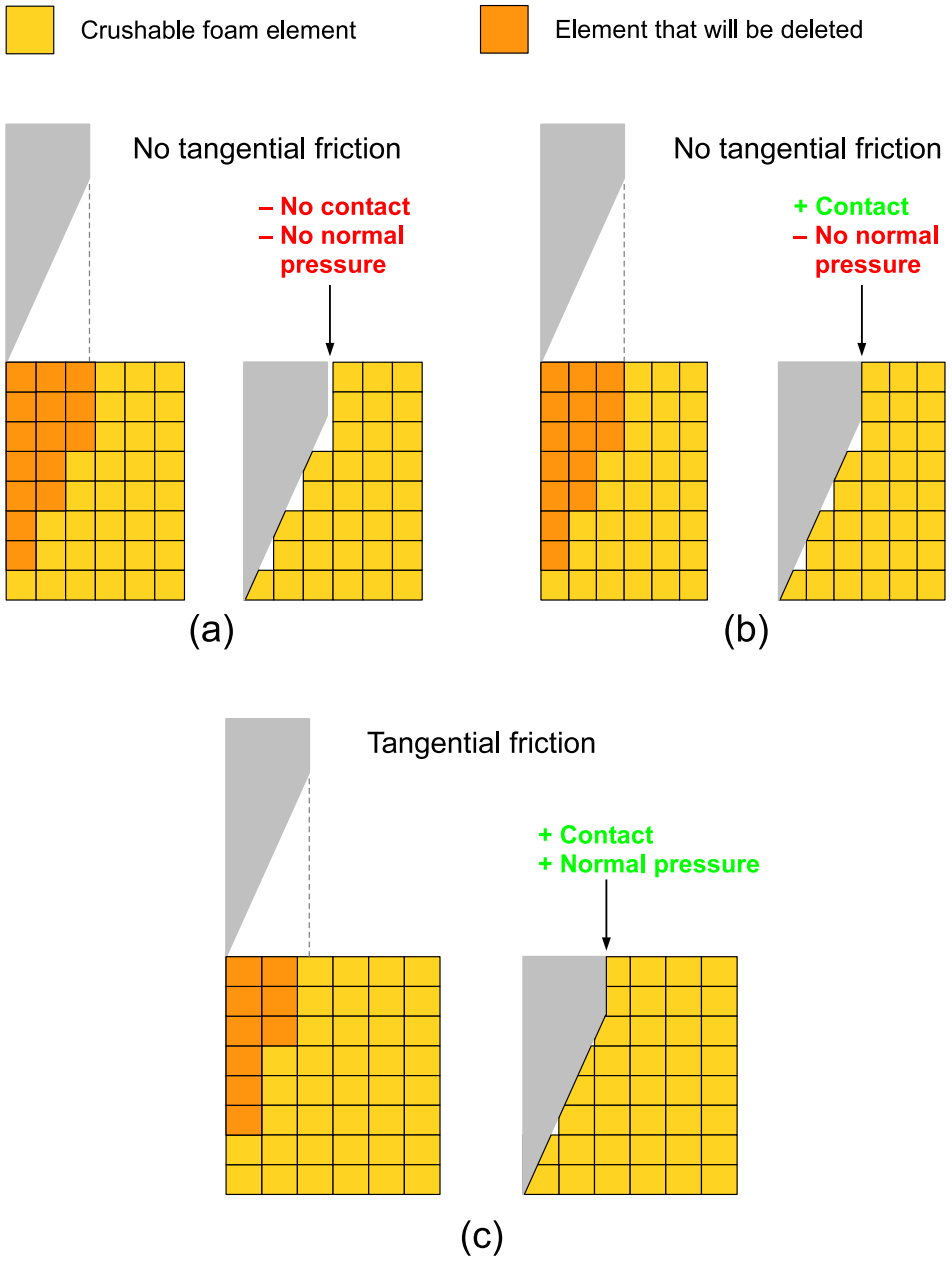

Figure 6.22: Illustration of the mesh sensitivity to obtain tangential friction between the needle body and the foam.

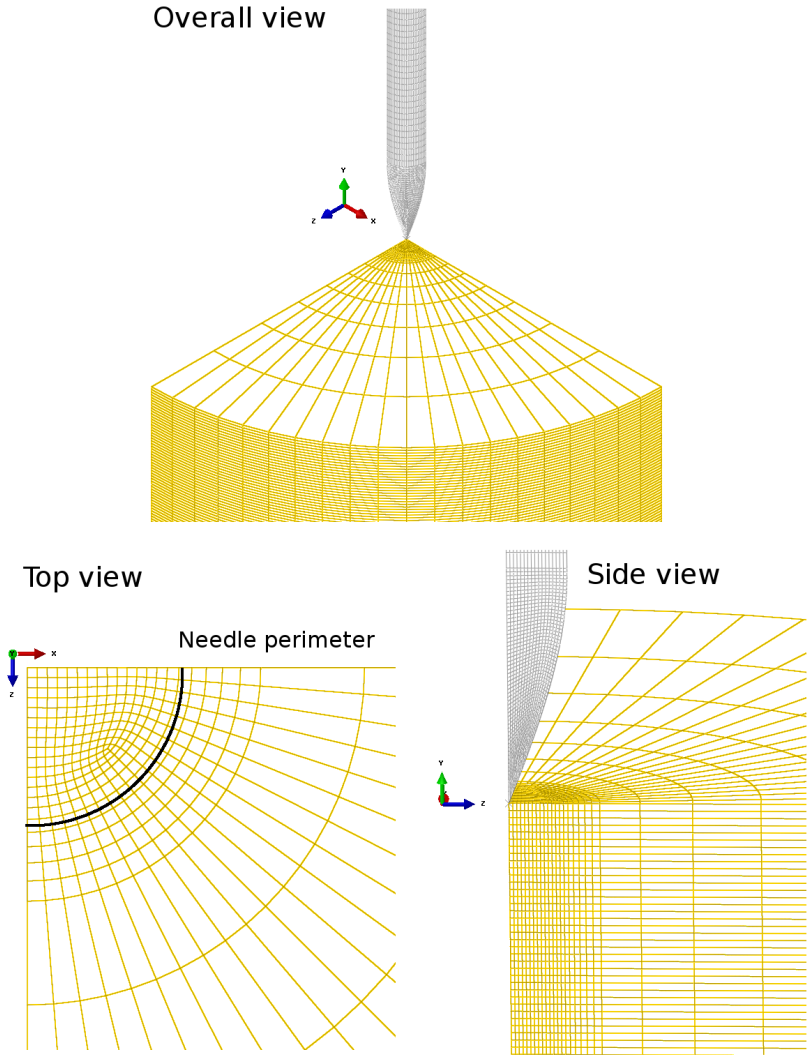

Figure 6.23: Several views of the mesh geometry that resulted in a good contact surface.

in needle geometry and a difference in friction coefficient.

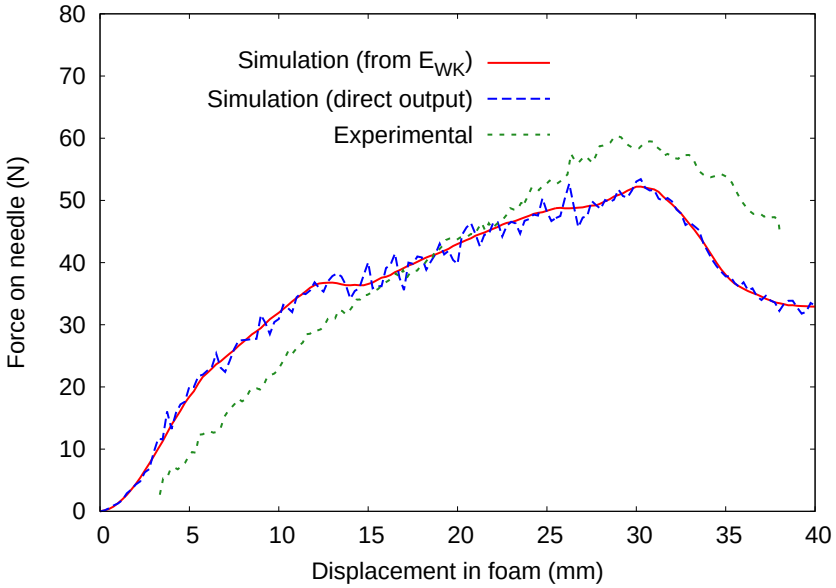

Figure 6.24: Total force exerted on the needle: experimental and simulated.

The force fraction due to friction and due to crushing can be obtained by differentiating the frictional energy dissipation and strain energy, respectively. Figure 6.25 shows that the friction and crushing force are very similar to those hypothesised in Section 6.3.2, see Figure 6.16. Furthermore, it seems that friction between the needle and the foam mainly determines the total force acting on the needle.

Deformation behaviour

The deformation behaviour of crushable foams is very different from that of other materials. During crushing of cells inside the foam, the volume of the material changes. This behaviour is very different from the plastic deformation common to metals, where the plastic Poisson's ratio is 0.5, resulting in a conservation of volume. As the plastic Poisson's ratio of crushable foams is approximately zero, the deformations and the accompanying stresses stay very local. The plastic deformation of the foam in the needle penetration is illustrated in Figure 6.26. It shows that the crushing of the foam occurs close to the needle. However, this is probably also due to element deletion, which deletes highly crushed elements. Hence, there is more loss of volume in the simulation than in real life.

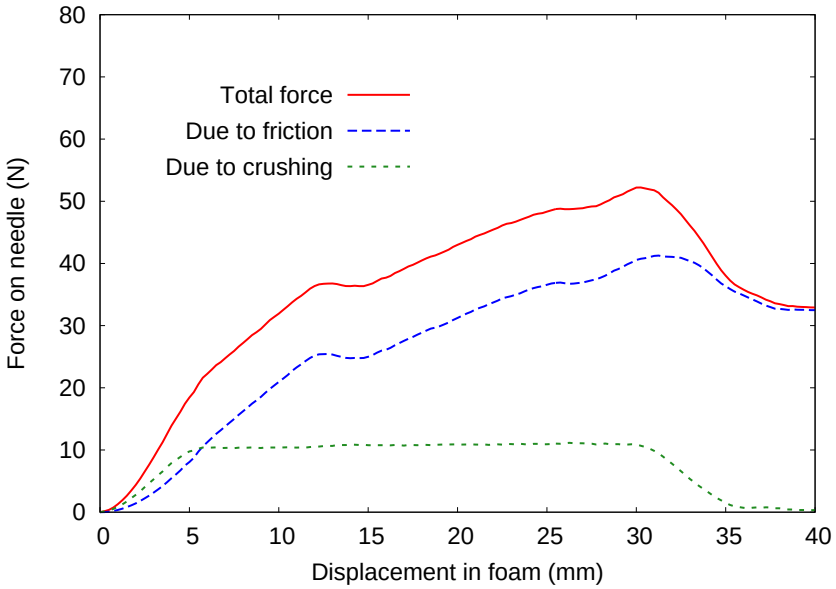

Figure 6.25: Total force exerted on the needle and its fractions due to friction and crushing.

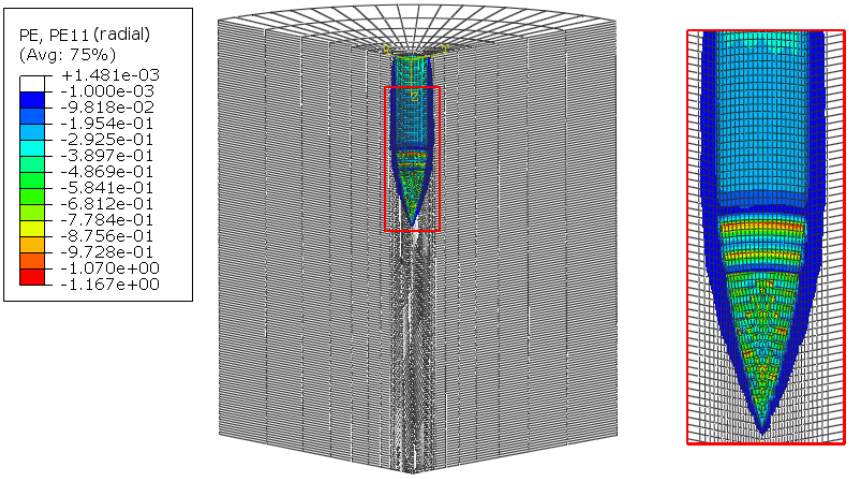

Figure 6.26: True plastic strain of the foam in radial direction during penetration of a needle.

Mass scaling

The stable time increment of the penetration simulation is very small, due to small mesh elements, low Young's modulus and low density. Retaking the stable time increment formula defined in Chapter 5:

$$\Delta t_{stable} \propto L\sqrt{\frac{\rho}{E}} \tag{6.8}$$

It follows that an increase in stable time increment can be achieved by increasing the density of the material. This method is often used in explicit simulations to obtain feasible computation times, and is referred to as *mass scaling*. By increasing the density, the dynamics of the system are changed, which can lead to inaccurate results. However, in quasi-static simulations the effect should be negligible, as the inertia effects related to the mass of the material are negligible. There is an upper limit to the possible mass scaling, as increasing the density also increases the kinetic energy, making the simulation less quasi-static. The penetration simulation described in the previous section, was done for different densities of the foam. The resulting force-displacement curves are shown in Figure 6.27. A summary of the results is given in Table 6.5. The differences in the total exerted force are due to a change in frictional dissipated energy, probably due to the increase of kinetic energy. The force due to crushing remains the same in all simulations. When the ratio of kinetic energy on internal energy of the foam E_{KE}/E_I remains small during the simulation, i.e. 5 - 10 %, the solution is quasi-static. Table 6.5 shows that a density of 375 kg/m^3 is the upper limit to obtain a quasi-static simulation. However, the time scale of the stitching process is several orders of magnitude higher than the one used in these tests. Hence, the effect of mass scaling on the total force is probably less prominent in the stitching simulation.

Table 6.5: Summary of the mass scaling results for the needle penetration simulation.

Density (kg/m^3)	Δt_{stable} (10^{-8} s)	Max. force (N)	Norm. run time	E_{KE}/E_I (%)
75	2.61	52	1.00	1.7
150	3.69	52	0.79	2.7
375	5.84	59	0.54	5.8
750	8.25	67	0.43	11
1000	9.53	69	0.39	13

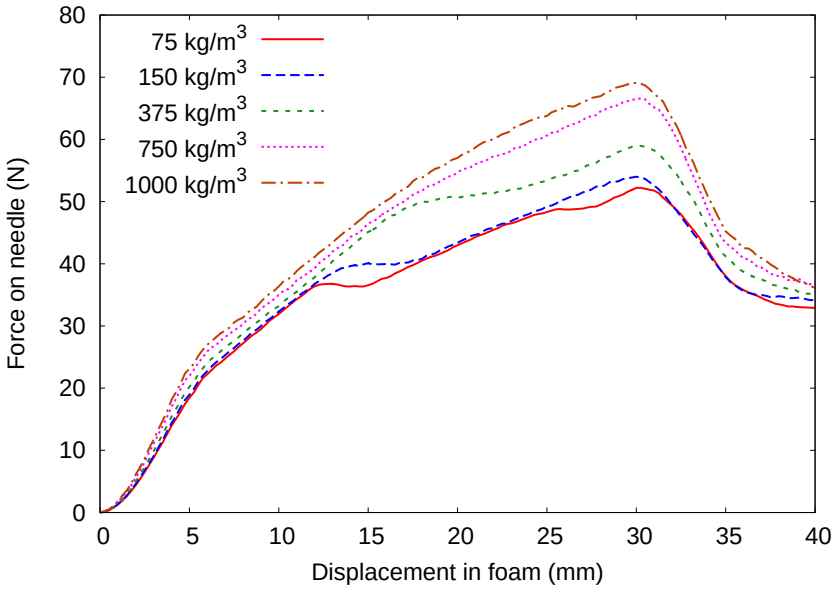

Figure 6.27: Force-displacement curve for different mass scalings of the foam.

6.4 Conclusion

The behaviour of Rohacell 71 RIST can be simulated by the crushable foam plasticity model in ABAQUS. Ductile damage can be used to delete mesh elements, in order to simulate needle penetration. Simulated results of quasi-static compression and needle penetration tests showed good agreement with experimental results. The force exerted on the needle during penetration is mainly determined by the friction between the needle and the foam. Mass scaling can be used to increase the stable time increment, which is small due to the low density and small mesh element size of the foam model. A reduction of calculation time by 20 - 50 % is possible without large differences in the force-displacement curve.

Chapter 7

Modelling the needle system

7.1 Stitch needle

7.1.1 Geometry

Acrosoma makes use of needles designed for their production process. The geometry of the needle is shown in Figure 7.1. The needle is about 130 mm long, the needle tip approximately 6 mm. The diameter of the needle is 3 mm. The needle body has shafts on either side which act as a guide for the yarn during stitching. Furthermore, when the yarn lies in the shafts, its contact with the foam is minimised. This way, the friction acting on the yarn is very small, which leads to better results during stitching. The yarn is put through the eye, which is located just above the needle tip.

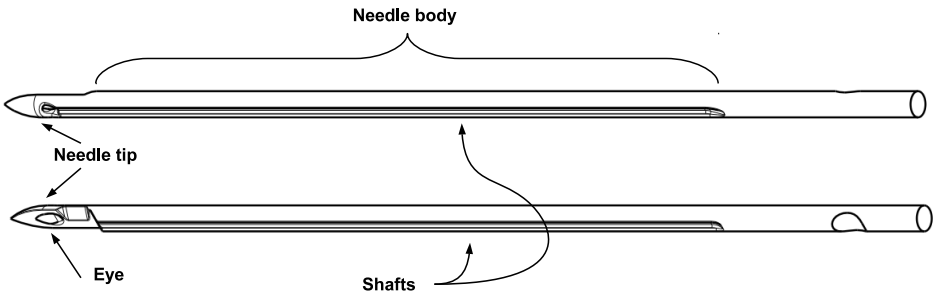

Figure 7.1: Geometry of a stitch needle used by Acrosoma.

7.1.2 Implementation in ABAQUS

Acrosoma provided a 3D CAD image of a real needle. This file can be imported to ABAQUS to be meshed and used in simulations. However, due to

the complex geometry, the constructing of a simplified needle model based on the real geometry was chosen. Therefore, several simplifications were made, especially to the needle tip and yarn shafts. These are illustrated in Figure 7.2. Curved surfaces are replaced by flat ones, which makes the meshing of the needle much easier. The needle was meshed with tetrahedral mesh elements, because these are better suited to fit the curved geometry of the needle tip. Steel material properties, i.e. Young's modulus and density, were assigned to the needle. A rigid body constraint was used on the mesh elements to make the needle behave as a rigid body. This is a valid assumption, as the stiffness of the needles is much higher than that of the yarn and the foam. Although the needle geometry was changed substantially, the simplified model captures the specificities of a real stitch needle, i.e. needle tip, eye and shafts, making it useful for a first model.

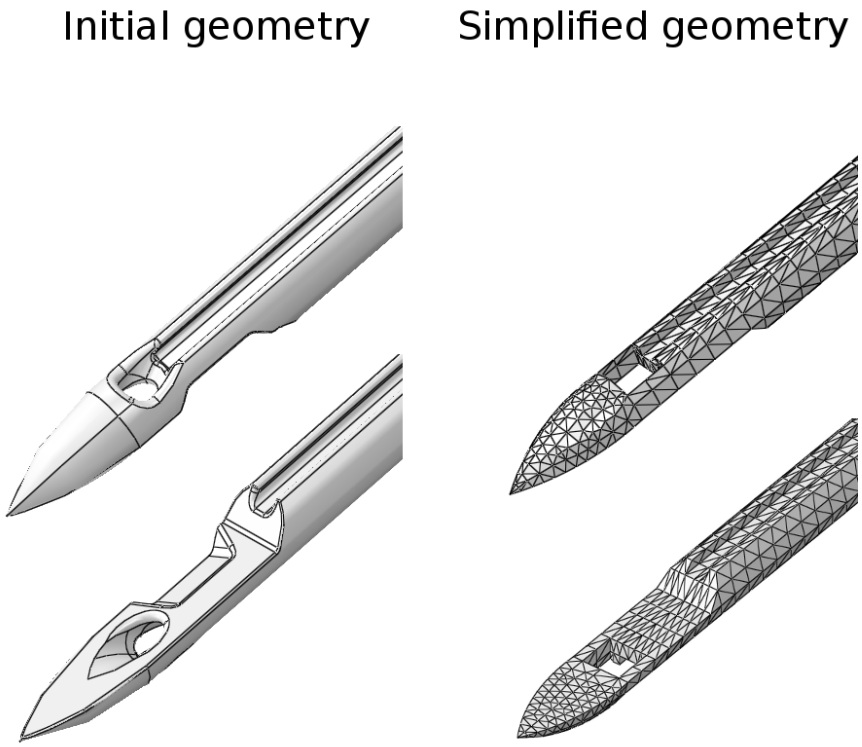

Figure 7.2: Simplification of the needle geometry.

7.2 Looping hook

Once the needle has perforated the foam panel, the yarn is transferred to a looping hook. The geometry of the looping hook was provided as a 3D CAD

image by Acrosoma. The looping hook does not have a complex geometry and it can be used without simplifications. The meshed part is shown in Figure 7.3. Steel material properties were used, and the part was constrained to act as a rigid body.

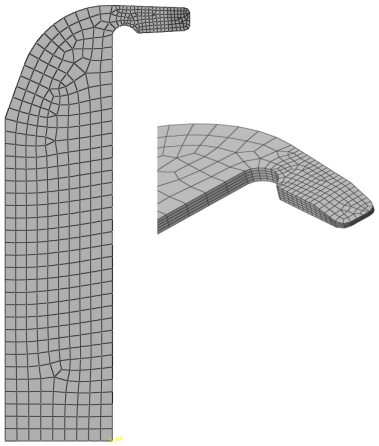

Figure 7.3: Geometry and mesh of the looping hook.

Chapter 8

Modelling the Z-stitching process of Acrosoma

Simulating the stitching process can provide useful information on the stress acting in the yarn and the forces acting on the needle. This information can be used to tune the process in order to reduce the amount of stitch faults or to reduce the denting of the foam by yarn tension. However, simulating the complete process is a challenging task because it is rather complex "FEA-wise". The causes of this complexity are:

(i) The large natural time scale, which is in the order of seconds;

(ii) The degradation and failure of the foam, which requires very fine meshes;

(iii) The yarn feed mechanism;

(iv) The dynamical effects of the yarn, which have to be reduced;

(v) The many contact interactions;

(vi) The sliding of the yarn through the needle eye, which requires a smooth geometry.

These factors will have an unfavourable effect on the simulation's run time. Small finite element sizes combined with low material properties will decrease the stable time increment significantly. Furthermore, the relatively large natural time scale of the problem requires a long simulation time. Hence, many time increments are needed.

8.0.1 The Z-stitch

As explained in Section 2.3.1 of Chapter 2, Acrosoma produces stitched sandwich panels with different stitch angles. The simplest process is that of Z-stitched sandwich panels, which have a stitch angle equal to 0°. The different steps in the process were illustrated and explained in Chapter 2. The illustration is shown again in Figure 8.1. The Z-stitch used by Acrosoma is similar to a basic chain stitch used in textiles [22].

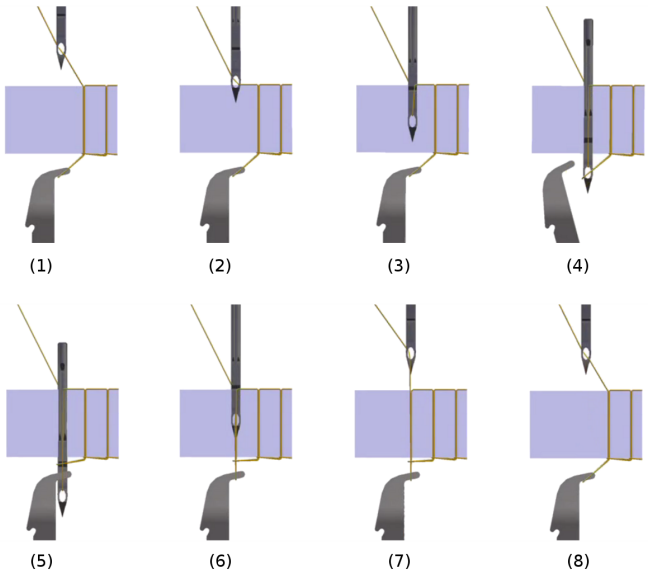

Figure 8.1: Illustration of the different steps in the Z-stitching process (images from Acrosoma).

8.1 Geometry and boundary conditions

The geometry of the model that was used to simulate the forming of one Z-stitch is shown in Figure 8.2. The foam core was modelled as a block of crushable Rohacell 71 RIST foam material with a width of 10 mm, which is similar to the stitch spacing used by Acrosoma, and a thickness of 30 mm. The carbon yarn was modelled with only 1 fibre for preliminary tests and had a diameter of 0.8 mm. It consisted out of 450 truss elements, each with a length of 0.67 mm. The yarn feed mechanism actually requires that truss elements are added to the chain in each step in order to be physically correct. This is, however, difficult to obtain in a FE-simulation. Therefore, the yarn feed mechanism was simplified to an excess length of yarn (20 mm) with a preload of 0.1 N attached to its end. The Z-stitch was formed by moving the needle system in a series of steps similar to those in Figure 8.1. These

movements were displacement controlled. Each step occurred in 0.05 s or 0.1 s. The average needle speed was 500 mm/s, which is about 10 times higher compared to the real process. This speed was chosen in order to reduce computational expenses, while keeping the dynamical effects of the yarn limited. General contact was used for all contact interactions with a tangential friction coefficient of 0.3.

The following boundary conditions were used:

- The sides of the foam were fixed in all directions.
- The needle was fixed in all directions, except in the z-direction during movement.
- The yarn end at the surface of the foam was fixed in all directions.
- The other yarn end was fixed in all directions, except the z-direction.

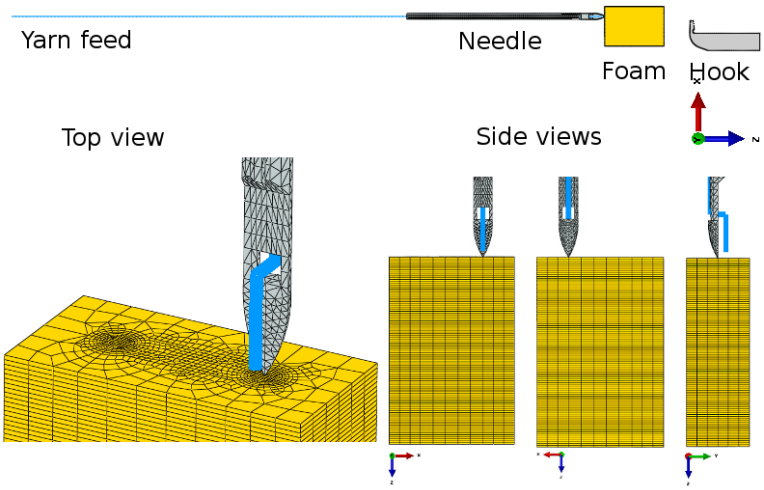

Figure 8.2: Initial geometry of the Z-stitch simulation.

8.1.1 Problem with excluded self-contact

As explained in Chapter 5, self-contact has to be excluded for the fibre surfaces. Hence, when only one fibre is used to represent the yarn, the formation of a stitch would be impossible. This problem was easily avoided by defining several different surfaces on the fibre, each with a length of about 100 mm. This way, the self-contact of a yarn with only one fibre is possible if the contact occurs between two different surfaces of the fibre.

8.1.2 Minimising computational expenses

Mass scaling was used to increase the stable time increment. Depending on the size of the foam elements, Δt_{stable} was determined either by the truss elements or the foam elements. For the finest mesh of foam elements used, Δt_{stable} was of the order of magnitude 10^{-8} s, which is very small. Increasing the density of the foam by a factor of 10 and using elements which were not smaller than 0.2 x 0.2 x 0.2 mm, increased Δt_{stable} significantly. For the same reason, the density of the yarn was increased in some models, but only by a factor of 2.

Reducing the amount of elements is also a good way of reducing computational expenses. However, this must not have an effect on the results. Small foam elements are mainly required to model the penetration of the needle correctly. Hence, the mesh was created with fine elements at the place where the needles will penetrate the foam.

Another possibility to minimise run time is to reduce the simulation time. However, this makes the model's behaviour more dynamically. Especially the yarn suffered from dynamic effects, see also Section 8.3. Adding damping to the truss elements seemed to have an insignificant effect on this behaviour.

A last possibility is to decrease the stiffness of the materials. This has the same influence on the stable time increment as mass scaling. However, it leads to stresses and strains in the materials which are not comparable to those observed in the real process.

8.1.3 Predrilling the foam

Sometimes, Acrosoma predrills foam cores before stitching, in order to facilitate the stitching process. Although it was not intended to simulate this stitching process, it actually is much easier. The foam element size can be increased, because small elements were mainly necessary to model the damage during needle penetration. Furthermore, there is less volume of foam material which has to be modelled. Hence, the amount of finite elements needed for the foam is reduced, while Δt_{stable} is increased. These two factors reduce the computational costs to a great extent. An illustration of a (coarse) full foam mesh and a (coarse) predrilled foam mesh is shown in Figure 8.3. The hole had a diameter equal to that of the needle.

Another factor favouring the predrilled models is the change in Δt_{stable} during penetration of the needle. In predrilled foams, the mesh elements are much less crushed than the elements in regular foams. Hence, the reduction of Δt_{stable}, due to smaller element lengths, is also smaller.

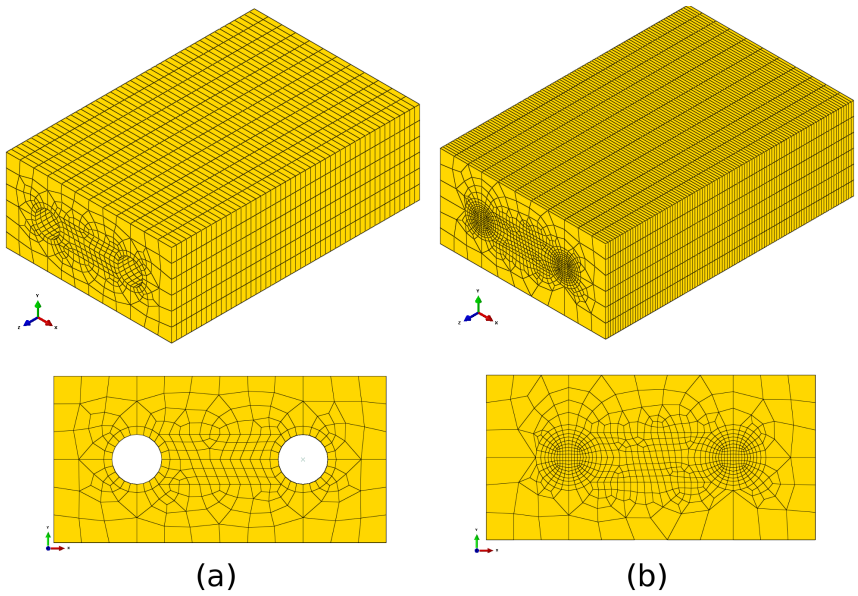

Figure 8.3: Illustration of the (coarse) mesh density for (a) a predrilled foam (≈ 41 000 elements) and (b) a regular foam (≈ 78 000 elements).

8.2 Simulations

Several simulations were carried out with different parameters in order to choose the most efficient models. Tests with predrilled foams have a name beginning with *P*, those with regular foams have a name starting with *F*. A small letter *x* indicates that the simulation was run on a workstation in the Department of Materials Science.

8.2.1 Predrilled foam (P.X)

P.1x: fine mesh

A fine mesh was used around the holes in the foam. The properties of the carbon yarn and the Rohacell foam were not changed, except for the mass scaling of the foam.

P.2: coarse mesh, low yarn Young's modulus

To reduce the locking of truss elements in the needle, see Section 8.3, a finer needle mesh was used and the Young's modulus of the yarn was decreased to 7.3 GPa. This reduction of Young's modulus also increased the stable time increment.

P.3: coarse mesh, low yarn Young's modulus, deformable needle

This simulation was used to see if deformable needle elements reduced the locking of truss elements. General contact could have difficulties with the contact between deformable truss elements and rigid elements. It uses a penalty method which assigns forces opposing the penetration of nodes. These forces are related to the penalty stiffness (automatically assigned by ABAQUS) and the depth of penetration. The penalty stiffness of rigid bodies is different from deformable elements and can lead to a difference in penetration between the two surfaces [1].

P.4: coarse mesh, low yarn Young's modulus, frictionless contact

The locking of truss elements can also lead to numerical difficulties which increase the computation time. Another possibility of reducing this locking is to assign a frictionless contact.

8.2.2 Regular foam (F.X)

F.1x: very fine mesh

A fine mesh was used for the foam, especially at the region of penetration. The properties of the carbon yarn and the Rohacell foam were not changed, except for the mass scaling of the foam.

F.2x: normal mesh, gravity, smaller simulation time

Adding gravity to a model can have a positive effect on its stability, especially for models which include elements with no bending stiffness. The idea was that adding gravity limited the dynamical effects of the yarn. The gravity field was applied in the negative z-direction, so that the yarn is tensioned by its own weight. To reduce the run time, the simulation time for each step was reduced by a factor of 5 and mass scaling was applied to the foam and the yarn.

F.3: coarse mesh, low yarn Young's modulus

This simulation was used to reduce the locking of truss elements.

8.3 Results and discussion

8.3.1 Encountered problems

Truss element locking

Truss element locking was encountered in all the models to some extent, mainly at sharp needle edges. The main cause for truss element locking is the incompatibility between the yarn's surface and the sharp surface of the simplified needle geometry. As explained in Chapter 5, contact spheres are created on the nodes of the elements. Hence, the surface is not a smooth cylinder, but has a sort of wavy form, which leads to the truss elements not slipping smoothly over sharp edges. This is illustrated in Figure 8.4. As a result, the stress in the yarn does not smoothly increase (or decrese) during stitching, but it stutters. This does not form a real problem when the stuttering is small, but in some occasions the truss elements are almost completely locked behind a sharp edge, leading to physically incorrect results, see Figure 8.5.

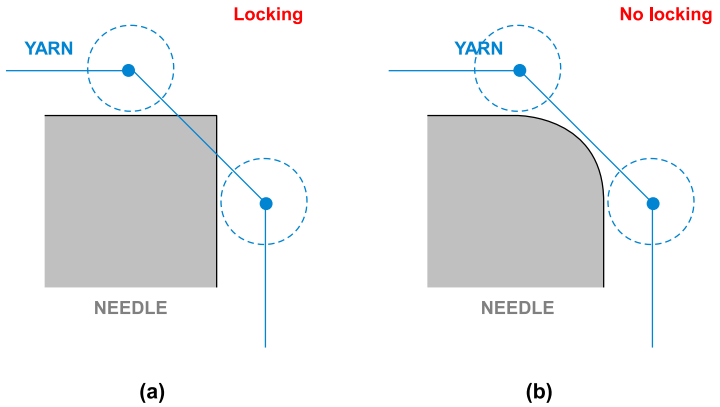

Figure 8.4: Illustration of truss element locking with the sharp needle edges (a) and a possible solution by smoothing the edges of the needle (b).

Simulations that show severe truss element locking are unusable for three reasons: when the stress rises to high magnitudes in the locked elements, they can (1) slip at a certain moment, leading to a stress wave propagating in the yarn, (2) loose contact with the needle system, so that no stitch can be produced, or (3) influence the forces acting on the needle. To overcome this problem, the truss element length can be made smaller, or the needle surface can be smoothed, see Figure 8.4. However, shorter truss elements cause a decrease in the stable time increment. It was noticed that decreasing the yarn's Young's modulus can prevent the locking to some extent.

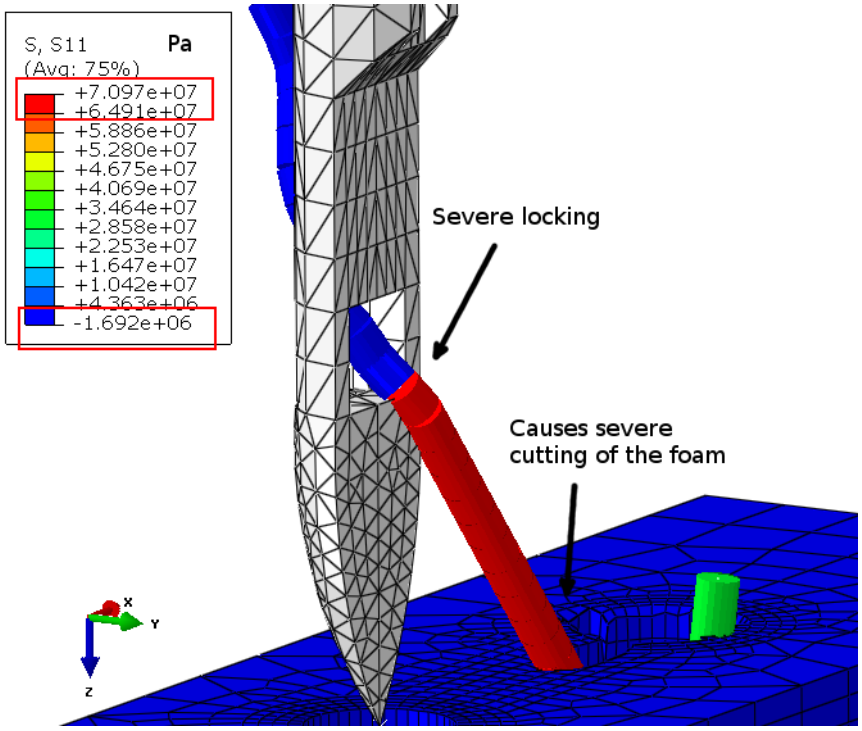

Figure 8.5: Severe truss locking causes the stress to go from compressive to tensile in just 1 - 2 truss elements. Furthermore, it causes severe damage to the foam.

Nevertheless, a smoothed needle geometry probably leads to much better results.

High inertial effects

When the simulation is accelerated, dynamic effects become more and more important. For example, simulation F2.x accelerated the reference simulation by a factor of five. This decreased the simulation's run time. However, the yarn gathered at the foam's surface when the needle went down due to its inertia, see Figure 8.6. This did not happen in the real process and it damaged the foam's surface. Hence, the results were unusable. Accelerating the simulation cannot be used to minimise computational expenses with the geometry of this simulation.

Run time too high

Simulation F.1x ran on a workstation at the Department of Materials Science for more than four days, but only reached about 15 % of the total stitch

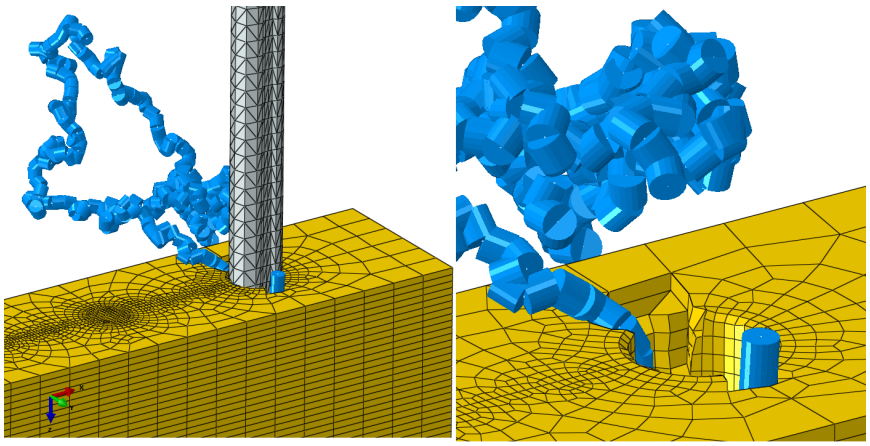

Figure 8.6: The yarn gathers at the foam's surface when the needle goes down due to its inertia and results in unwanted damage.

formation. Simulation P.3 used a deformable needle. This reduced Δt_{stable} to about 10^{-9} s, due to the small size and high Young's modulus of the elements, which led to very high computational costs. The other simulations needed about 24 hours to form a stitch, which is acceptable.

8.3.2 Results

The results of the simulation are shown in Table 8.1. An illustration of the course of simulation P.4 is given in Figure 8.7. The final form of the Z-stitch is illustrated in Figure 8.8.

8.3.3 Discussion

Truss element locking seemed to form a problem in most simulations, especially in the simulations that used the regular yarn's Young's modulus of 73 GPa. This could be avoided by using frictionless contact. However, this lowers the forces acting on the needle substantially, because they will only be determined by the crushing of the foam and the yarn tension. Hence, the results from simulation P.4 are less suited to study the production process. Nevertheless, they indicate that it is possible to simulate the process, especially if truss element locking can be avoided.

Frictionless contact had negligible effect on the total computational costs, which indicated that truss element locking did not introduce extra computational costs.

Table 8.1: Overview of the results from the stitching simulations.

Simulation	Characteristics	Results
P.1x	Fine mesh, normal material properties	Severe truss locking leading to a loss of contact
P.2	Coarse mesh, low E_{yarn}	Truss locking leads to high tensile stresses in the yarn, which damages the foam
P.3	Coarse mesh, low E_{yarn}, deformable needle	Run time too high: very small Δt_{stable} due to small needle elements
P.4	Coarse mesh, low E_{yarn}, frictionless	No truss locking, but frictionless contact not realistic
F.1x	Very fine mesh, normal material properties	Run time too high
F.2x	Normal mesh, gravity, accelerated simulation	Inertial effects of the yarn damages the foam's surface
F.3	Coarse mesh, low E_{yarn}	Truss locking, contact difficulties between needle and foam (possibly due to too large foam elements)

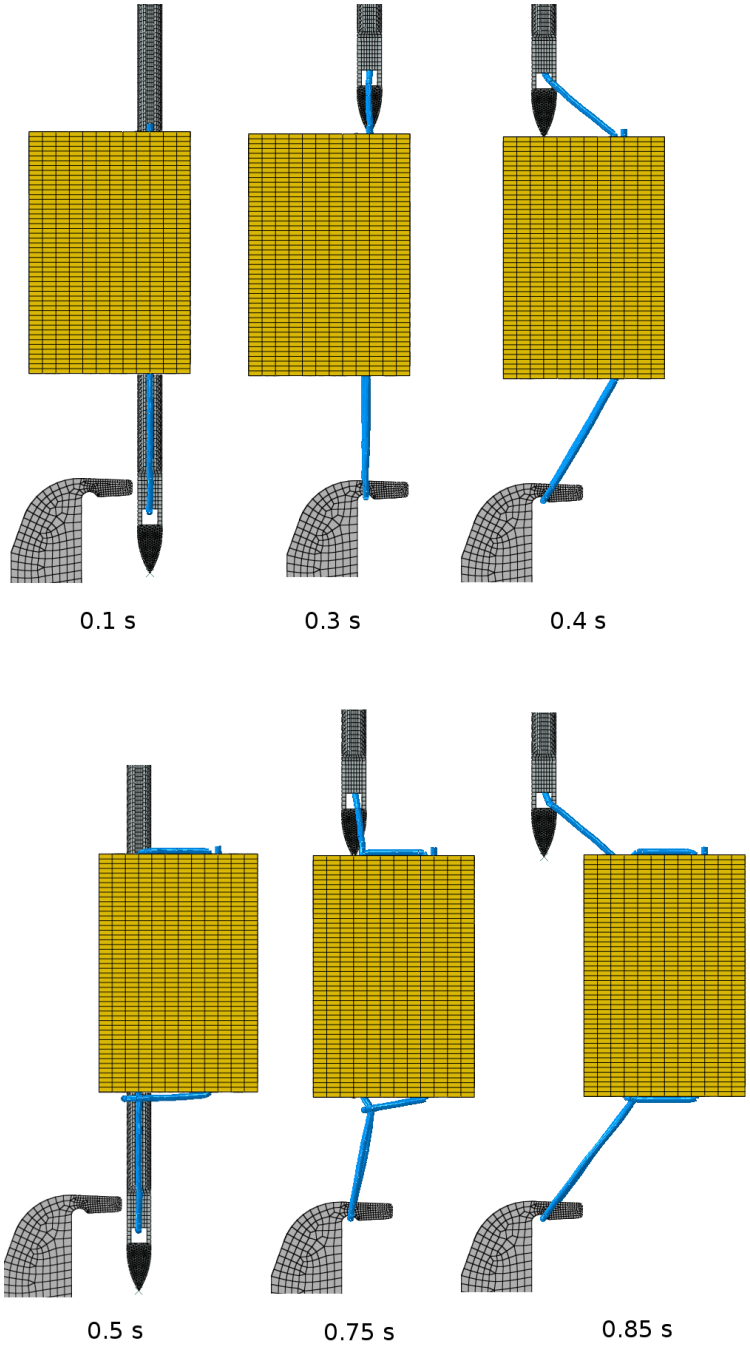

Figure 8.7: Formation of the Z-stitch (simulation P.4).

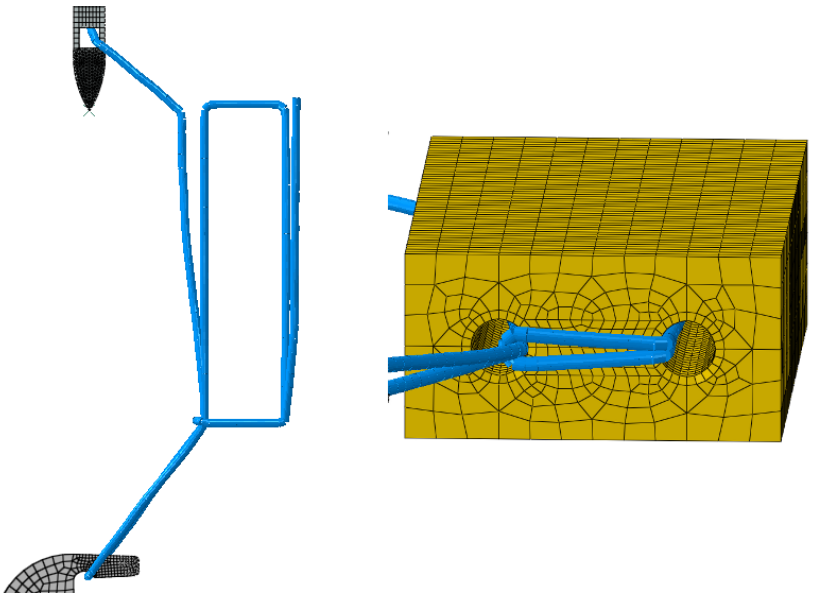

Figure 8.8: The formed Z-stitch (simulation P.4).

The order of magnitude of Δt_{stable} for the coarse models was about 1 - 3 10^{-7} s, while that of the finer meshes was one order of magnitude lower, around 2 - 6 10^{-8} s. This made it possible to run the coarse models on a regular notebook with a reasonable run time.

8.4 Conclusion

The Z-stitching of a Rohacell 71 RIST foam core was simulated using the truss model to represent the yarn, and the crushable foam model to represent the foam core. The tests showed that it is certainly possible to realistically model the process itself. However, due to difficulties concerning computation time, modelling specific stages of the proces, e.g. the penetration of a needle in the foam, the influence of yarn tension on foam crushing, etc., would be advisable.

The main limiting factor of the model is its run time, which is too high to be feasible for today's computational powers. The run time is mainly determined by the large natural time scale of the problem and the small Δt_{stable}. The use of mass scaling on the foam, the use of large mesh element sizes and the use of 1 fibre to represent the foam, decreased the computational costs significantly. However, they also changed the physical behaviour of the problem to some extent, and the results are not directly applicable to the real process.

Although it may seem that simulating the whole stitching process provides little directly useful information, these tests were mainly constructed to assess the feasibility of using FE-analysis to study the process. Several simplifications and assumptions were used to obtain all the necessary information for a full stitch, because detailed data were not yet available. Furthermore, more detailed analyses are necessary when a specific problem has to be investigated. For example, an investigation of the denting/cutting of the foam by yarn tension can probably be done with a much simpler simulation, especially when the regions of interest can be identified by a crude stitching simulation.

A useful foundation for modelling the stitching process has been constructed here. More research and some creativity could lead to a promising method for simulating the problems that occur in the production of stitched sandwich panels.

Chapter 9

Other applications of the truss model

The truss model developed in this work is a general way of modelling fibres, yarns or other fibrous materials, which can be used for all sorts of simulations. To illustrate its versatility, a few interesting examples of other research topics that would benefit from this model are given. The examples were constructed during the development of the truss model to test its capabilities. These examples are just a tip of the iceberg, and many more applications can be thought of.

9.1 Twisting process

Yarns are made by twisting fibres together, for example by ring spinning, resulting in an entangled fibrous structure. Twisted fibres follow helical paths around the yarn's neutral axis. Their distance to the neutral axis is not constant, the fibres migrate towards and away from the centre. When a bundle of fibres is twisted, the trajectories of fibres at the surface are longer than those of other fibres. Hence, higher stresses develop in the outer fibres, and they migrate towards the center of the yarn, where their stress is relieved. This process exposes new fibres at the surface, which will in turn migrate towards the centre. This process can be simulated by twisting a bundle of parallel fibres. Both ends of the yarn were twisted in the opposite direction, while they were gradually moved inwards to relieve some of the stresses. The final configuration of the yarn is given in Figure 9.1. The migration of fibres can be seen by looking at the cross-section at different locations.

The illustrated example is rather simple, and may seem unnecessary. How-

ever, adding fibres with different material properties, varying the twist speeds, etc. can lead to interesting results.

Figure 9.1: Twisting of the yarn leads to a migration of the fibres.

9.2 3D woven compression

The compression of 3D woven fabrics is of great importance in the field of composites, and is usually simulated with continuous materials or beams, as seen in Chapter 3. However, these methods have important disadvantages. Representing the yarns as continuous materials leads to inaccurate cross-section deformation, because there is no realignment of fibres possible. Beams suffer of a high bending stiffness, due to the relatively large diameter of virtual fibres. The truss model is an ideal candidate to model the compression of 3D woven fabrics, because it is able to simulate fibre realignment without the problems of beam elements.

The 3D woven structure was constructed out of yarns that consisted out of 12 fibres. Figure 9.2 shows the initial structure of the model. The fabric was compressed in the z-direction by rigid plates. No periodic boundary conditions were used, the structure was boxed in by rigid plates at the sides. Small preloads were assigned to the fibres to overcome numerical instabilities. Furthermore, the magnitude of the preload can be used as a fitting parameter for the waviness of the fibres after compression. An example of a compressed structure is shown in Figure 9.3. The amount of artificial energy contributions in the model was negligible.

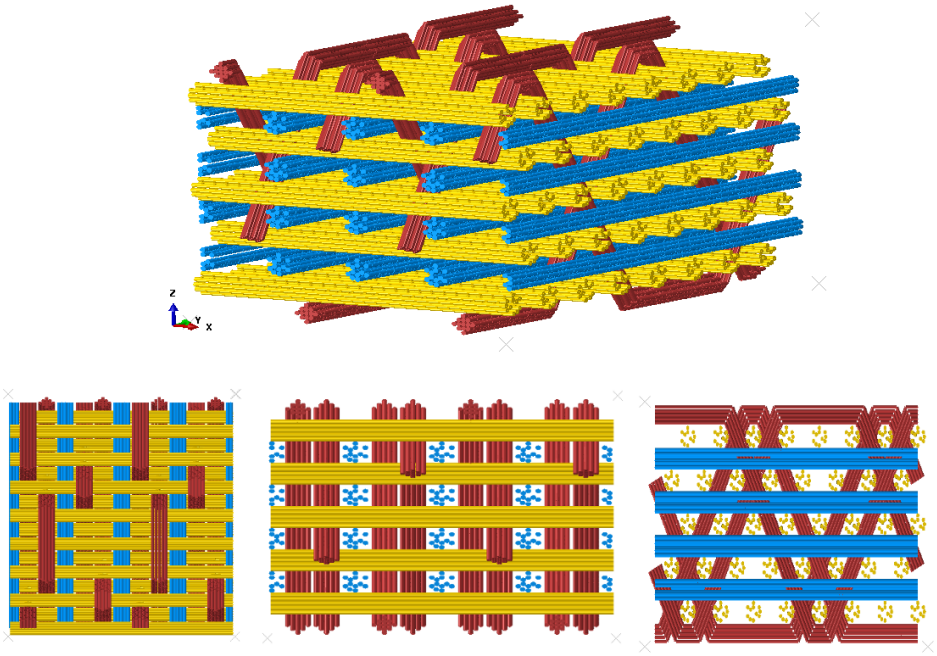

Figure 9.2: Initial structure of the 3D woven model.

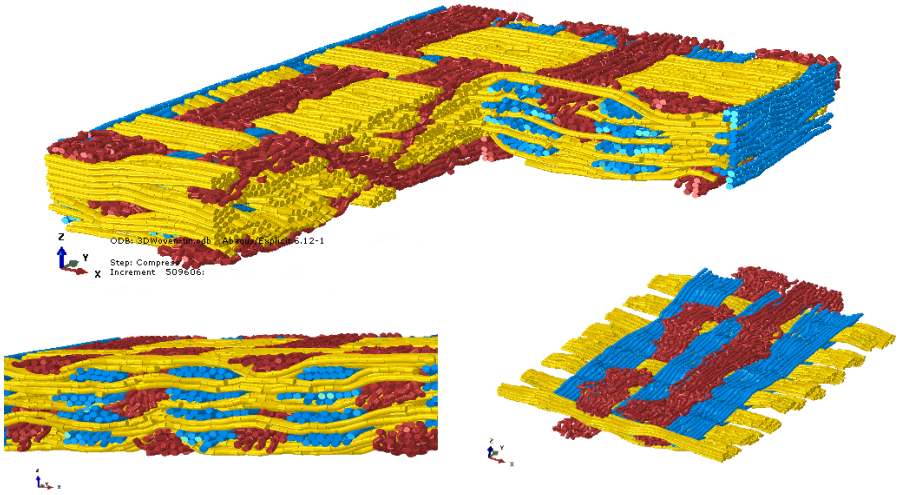

Figure 9.3: Compressed structure of the 3D woven model.

9.3 Fibre layer penetration

In Chapter 2 was mentioned that resin rich zones, so-called resin eyes, can occur in stitched sandwich panels, in particular in FRP composite skins. These zones have a detrimental effect on the in-plane properties of the skins. The truss model can be used to model the dry fibrous skins and investigate the formation of resin eyes due to stitching. Simulations can shed light on the influence of friction, stitching speed, needle geometry, etc. on the formation and structure of resin eyes.

As an example, the penetration of the stitching needle through a unidirectional layer of fibres was simulated. The fibres were modelled with truss elements and a preload of 0.1 N was added to each fibre end. Figure 9.4 shows several results from the simulations. Friction between the fibres and the needle displaces the fibres not only to the sides, but also pulls them down.

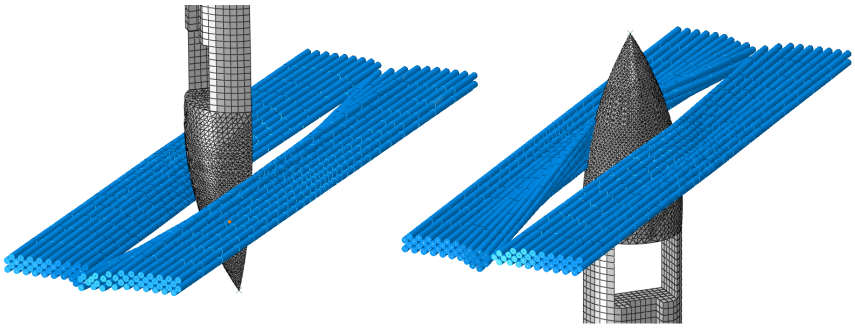

Figure 9.4: Penetration of a stitching needle through a unidirectional layer of fibres.

Chapter 10

Conclusion

The aim of this thesis was to assess the feasibility of using ABAQUS to simulate the stitching process of sandwich structures. The emphasis laid on the construction of a model that is able to simulate the yarn behaviour during this process. Simulating the stitching process required models for each component, in particular for the fibrous yarn, the crushable foam core and the needle system. Therefore, each component of the process was modelled separately at first and then combined to simulate the stitching process.

The constructed yarn model was made up of chains of truss elements. Truss elements only transmit axial loads and their nodes act as frictionless pins, which resulted in high flexibility of the chains. A physically correct cross-section deformation was obtained by arranging the chains in a bundle, representing the fibres of a real yarn. A frequency analysis showed that the yarn behaved as an ideal string.

The Rohacell 71 RIST foam material model was constructed with the crushable foam plasticity model of ABAQUS. It showed good agreement with experimental data, both in compression and during the penetration of the needle. However, a damage model intended for ductile metals had to be used due to the lack of a foam failure model. The parameters for the ductile damage model were chosen in order to obtain the best possible results.

The difficulty in modelling the needle system laid in meshing the complex geometry of the needle. Therefore, a simplified geometry was used. However, this simplification led to the locking of truss elements with sharp needle edges. This had a detrimental effect on the results of the stitching simulation.

Finally, the Z-stitching process was simulated using the three constructed models mentioned above. However, its use was limited by computing power.

Hence, predrilled foams where used to reduce computational costs. Frictionless contact was necessary to prevent the locking of truss elements.

The work done in this thesis can provide useful information on the yarn behaviour during the stitching of sandwich panels. However, the truss model offers a versatile way of modelling fibrous materials and can be used for other research to, for example for the compression of 3D woven fabrics.

10.1 Further research

This thesis lays the foundation for further research. The truss model was developed from scratch and is therefore still quite simple. Further research could investigate the possibility of defining twisted fibre bundles in ABAQUS, which will require the use of CAD software. Another possible topic is the reduction of the dynamical behaviour of the yarn, which would make the simulations much more computationally efficient. The yarn was modelled as a linear elastic material. Further determination of the yarn's mechanical properties is necessary to construct a physical correct model. This would also require the definition of a damage criterion which could be very simple as truss elements only permit axial stresses. It is clear that there is still a lot to investigate in order to obtain a general usable yarn model. Nevertheless, the model already shows great potential for modelling fibrous materials.

The crushable foam material model of ABAQUS is well suited to model Rohacell polymer foams. However, it would benefit from a damage criterion that physically models the failure of polymer foams.

A realistic needle geometry should be used for further simulations in order to reduce truss element locking.

The stitching process itself was not investigated in depth. Therefore, further research concerning the stitching process is necessary. Nevertheless, the yarn model and the foam model already showed great potential. The simulation of the stitching process was mainly limited by its high computational costs due to the large natural time scale. These costs could be reduced by modelling specific steps in the stitching process with a detailed simulation (submodelling). This reduces the natural time scale, which makes the simulations more computationally feasible.

Appendix A

ABAQUS related terms [1]

A.1 Elements

ABAQUS offers a wide range of elements to model different kinds of geometries and structures. The elements described in this section were used at some moment to model a part of the stitching process. Each element has a unique name, which describes its properties. For example, the solid elements used to model the foam were C3D8R elements, which stands for Continuum 3D 8-node Reduced integration elements. All simulations were performed in 3D, hence, 2D or axisymmetric elements are not discussed here. An illustration of the different elements is shown in Figure A.1.

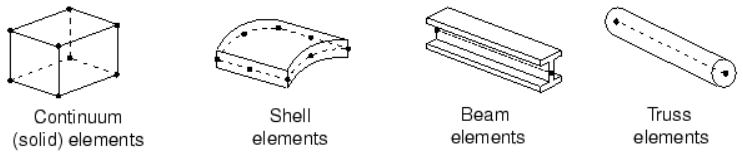

Figure A.1: Illustration of the different element families.[1]

A.1.1 Solid elements (C3D8, C3D20)

Solid or continuum elements model small blocks of material. They can be used to model the widest variety of components. Mainly solid hexahedral brick elements were used in this work, with both linear (C3D8 elements) and quadratic (C3D20 elements) interpolation. Quadratic elements are more suited for simulations involving bending, because they are less susceptible to shear locking. Solid elements have three translational degrees of freedom at each node.

A.1.2 Shell elements (S4R)

Shell elements are used to approximate a 3D continuum material with the 2D theory of shells, which is possible because shells have a thickness that is significantly smaller than the other dimensions. They have three translational and three rotational degrees of freedom at each node.

A.1.3 Beam elements (B31, B32)

Beam theory can be used to approximate 3D continuum slender structures with a 1D theory. Here, the dimensions of the cross-section have to be small compared to the beam's length. Beam elements are line elements that have an axial, torsional and bending stiffness. If it is appropriate to use them in a model, they have the advantage of being geometrically simple. Beam elements have six degrees of freedom at each node (three translational, three rotational), but only two (B31) or three (B32) nodes per element. Hence, a model with beam elements has only a few degrees of freedom.

A.1.4 Truss elements (T3D2, T3D3)

Truss elements are line elements, similar to beam elements. However, they only have an axial stiffness. Hence, trusses can only carry tensile or compressive loads. They are used to model very slender beams (no resistance to bending) or pin-jointed networks, and only have three degrees of freedom at each node (translational). A truss element is composed of two (T3D2) or three (T3D3) nodes, hence, it has very few degrees of freedom, which makes it computationally very inexpensive.

A.2 Terminology

A.2.1 Shear locking

The reason that linear (fully integrated) solid elements are less suited for simulations involving bending is that they are susceptible to shear locking, which causes them to be too stiff in bending. Shear locking can be explained by considering the pure bending of a small piece of material. The material will deform as illustrated in Figure A.2 (a). Lines initially parallel to the horizontal axis are curved, while the vertical lines remain straight and perpendicular to the curved lines. However, the edges of linear elements cannot curve and remain straight after deformation. Figure A.2 (b) shows the deformation due to bending of a single linear element. The dotted lines represent

lines that pass through the integration points of the element. The upper integration line is stretched, which indicates tension, while the bottom line is compressed, which indicates compression. The vertical integration lines are not changed in length for small deformations. These stresses are similar to those of a small piece of material subjected to pure bending. However, the vertical and horizontal lines do not remain perpendicular. This indicates that there is a shear stress acting on the element, which is not consistent with the expected stress state. The shear stress arises because the element edges are unable to curve in linear elements. Hence, the straining of the element causes shearing, rather than the intended bending. Shear locking does not form a problem in quadratic elements, as the edges of these elements are able to curve.

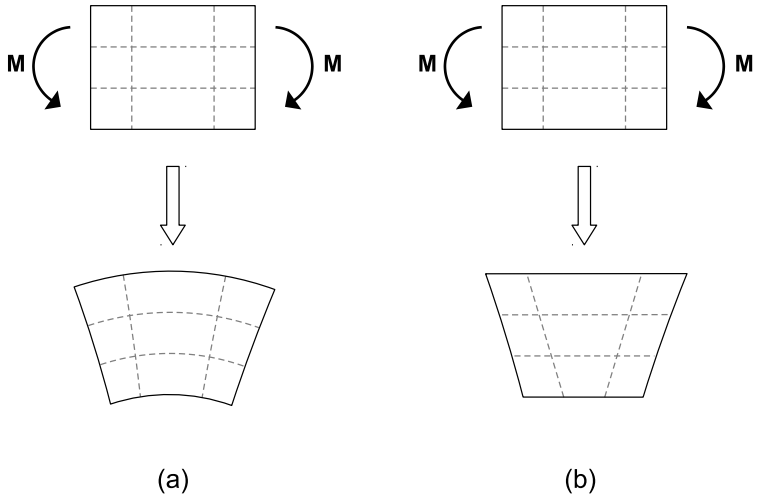

Figure A.2: Illustration of the pure bending of a small piece of material (a) and shear locking in a (fully integrated) linear solid element (b).

A.2.2 Reduced-integration elements

Reduced-integration elements are primarily used in ABAQUS/Explicit because they are computationally inexpensive. The term *reduced-integration* indicates that the elements have less integration points per element. For example, a linear fully integrated solid element (C3D8) has 8 integration points, two in each direction, while a linear reduced-integration solid brick element only has one integration point, which is located in its center. This minimises the computational expense, but can lead to numerical problems, such as hourglassing.

A.2.3 Hourglassing

Linear reduced-integration solid elements are often susceptible to hourglassing, which causes them to be too flexible in bending. Hourglassing can be explained by considering the pure bending of a small piece of material once again, see Figure A.3 (a). Since these element only have one integration point in their center, and their edges are unable to curve, the lines through the integration point stay unchanged, see Figure A.3 (b). Hence, there is no strain energy related to this deformation mode and the elements cannot resist this type of deformation.

ABAQUS introduces a small amount of artificial stiffness to the linear reduced-integration elements to limit hourglassing. Other methods of hourglass control are also available, such as the enhanced hourglass control, which is recommended for low-density foam materials.

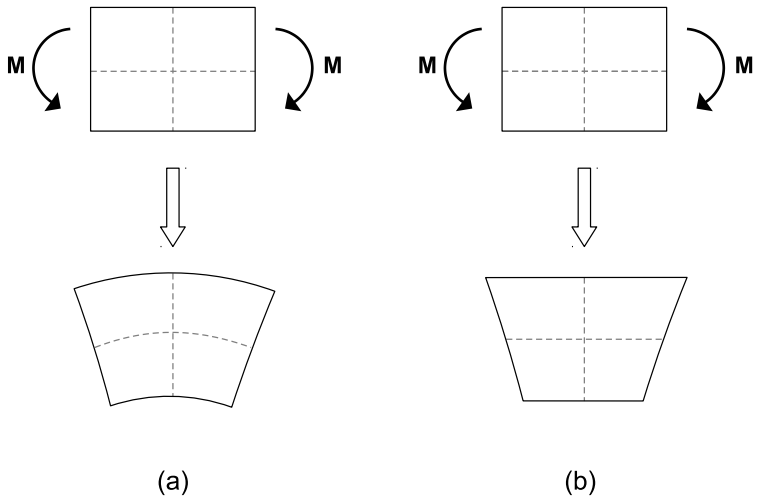

Figure A.3: Illustration of the pure bending of piece of material (a) and hourglassing in a reduced-integration linear solid element (b).

Bibliography

[1] Dassault Systèmes. *Abaqus 6.12 User's Manual*. Dassault Systèmes, 2012.

[2] GC Papanicolaou and D Bakos. Interlaminar fracture behaviour of sandwich structures. *Composites Part A: Applied Science and Manufacturing*, 27(3):165–173, 1996.

[3] Pål G Bergan, Leif Buene, Andreas T Echtermeyer, and Brian Hayman. Assessment of frp sandwich structures for marine applications. *Marine structures*, 7(2):457–473, 1994.

[4] P Potluri, E Kusak, and T.Y Reddy. Novel stitch-bonded sandwich composite structures. *Composite Structures*, 59(2):251 – 259, 2003.

[5] Richard Stewart. Sandwich composites excel at cost-effective, lightweight structures. *Reinforced Plastics*, 55(4):27–31, 2011.

[6] Gefu Ji, Zhenyu Ouyang, and Guoqiang Li. Debonding and impact tolerant sandwich panel with hybrid foam core. *Composite Structures*, 2013.

[7] Jan Verhaeghe. Introducing an affordable composite trailer to a conservative market. *Reinforced Plastics*, 50(5):34–37, 2006.

[8] Anamaría Henao, Marco Carrera, Antonio Miravete, and Luis Castejón. Mechanical performance of through-thickness tufted sandwich structures. *Composite Structures*, 92(9):2052–2059, 2010.

[9] Jae Hoon Kim, Young Shin Lee, Byoung Jun Park, and Duck Hoi Kim. Evaluation of durability and strength of stitched foam-cored sandwich structures. *Composite structures*, 47(1):543–550, 1999.

[10] C Sickinger and A Herrmann. Structural stitching as a method to design high-performance composites in future. In *Proceedings TechTextil Symposium*, 2001.

[11] Giuseppe DellAnno, Denis D Cartié, Ivana K Partridge, and Amir Rezai. Exploring mechanical property balance in tufted carbon fab-

ric/epoxy composites. *Composites Part A: Applied Science and Manufacturing*, 38(11):2366–2373, 2007.

[12] B. Lascoup, Z. Aboura, K. Khellil, and M. Benzeggagh. On the mechanical effect of stitch addition in sandwich panel. *Composites Science and Technology*, 66(10):1385 – 1398, 2006.

[13] B. Lascoup, Z. Aboura, K. Khellil, and M. Benzeggagh. Prediction of out-of-plane behavior of stitched sandwich structure. *Composites Part B: Engineering*, 43(8):2915 – 2920, 2012.

[14] Bing Wang, Linzhi Wu, Xin Jin, Shanyi Du, Yuguo Sun, and Li Ma. Experimental investigation of 3d sandwich structure with core reinforced by composite columns. *Materials & Design*, 31(1):158 – 165, 2010.

[15] Kimberley Dransfield, Caroline Baillie, and Yiu-Wing Mai. Improving the delamination resistance of cfrp by stitchinga review. *Composites Science and Technology*, 50(3):305 – 317, 1994.

[16] Denis D. Cartié and Norman A. Fleck. The effect of pin reinforcement upon the through-thickness compressive strength of foam-cored sandwich panels. *Composites Science and Technology*, 63(16):2401 – 2409, 2003. Porous Materials.

[17] U. K. Vaidya, A. N. Palazotto, and L. N. B. Gummadi. Low velocity impact and compression-after-impact response of z-pin reinforced core sandwich composites. *Journal of Engineering Materials and Technology*, 122(4):434–442, April 2000.

[18] A.N. Palazotto, L.N.B. Gummadi, U.K. Vaidya, and E.J. Herup. Low velocity impact damage characteristics of z-fiber reinforced sandwich panels an experimental study. *Composite Structures*, 43(4):275 – 288, 1998.

[19] Acrosoma. Acrosoma structural composite technology.

[20] M.V. Hosur, M.R. Karim, and S. Jeelani. Experimental investigations on the response of stitched/unstitched woven s2-glass/sc15 epoxy composites under single and repeated low velocity impact loading. *Composite Structures*, 61(12):89 – 102, 2003. ¡ce:title¿Impact on Composites 2002¡/ce:title¿.

[21] K.T. Tan, N. Watanabe, and Y. Iwahori. Effect of stitch density and stitch thread thickness on low-velocity impact damage of stitched composites. *Composites Part A: Applied Science and Manufacturing*, 41(12):1857 – 1868, 2010.

[22] A.P. Mouritz, K.H. Leong, and I. Herszberg. A review of the effect of stitching on the in-plane mechanical properties of fibre-reinforced polymer composites. *Composites Part A: Applied Science and Manufacturing*, 28(12):979 – 991, 1997.

[23] A.P. Mouritz and B.N. Cox. A mechanistic approach to the properties of stitched laminates. *Composites Part A: Applied Science and Manufacturing*, 31(1):1 – 27, 2000.

[24] A.P. Mouritz and B.N. Cox. A mechanistic interpretation of the comparative in-plane mechanical properties of 3d woven, stitched and pinned composites. *Composites Part A: Applied Science and Manufacturing*, 41(6):709 – 728, 2010.

[25] P. Chang, A.P. Mouritz, and B.N. Cox. Properties and failure mechanisms of z-pinned laminates in monotonic and cyclic tension. *Composites Part A: Applied Science and Manufacturing*, 37(10):1501 – 1513, 2006.

[26] Xiaogang Chen. *Modelling and Predicting Textile Behaviour*. Woodhead Publishing, 2010.

[27] Teik-Cheng Lim. A three-level hierarchical approach in modeling sheet thermoforming of knitted-fabric composites. *International journal of mechanical sciences*, 45(6):1097–1117, 2003.

[28] Philippe Boisse, Nahiene Hamila, Fabrice Helenon, B Hagege, and J Cao. Different approaches for woven composite reinforcement forming simulation. *International Journal of Material Forming*, 1(1):21–29, 2008.

[29] Elena Syerko, Sbastien Comas-Cardona, and Christophe Binetruy. Models of mechanical properties/behavior of dry fibrous materials at various scales in bending and tension: A review. *Composites Part A: Applied Science and Manufacturing*, 43(8):1365 – 1388, 2012.

[30] Philippe Boisse, Yamina Aimène, Abdelwaheb Dogui, Samia Dridi, Sébastien Gatouillat, Nahiene Hamila, Muhammad Aurangzeb Khan, Tarek Mabrouki, Fabrice Morestin, and Emmanuelle Vidal-Sallé. Hypoelastic, hyperelastic, discrete and semi-discrete approaches for textile composite reinforcement forming. *International journal of material forming*, 3(2):1229–1240, 2010.

[31] TK Ghosh, SK Batra, and RL Barker. the bending behaviour of plain-woven fabrics part i: A critical review. *Journal of the Textile Institute*, 81(3):245–254, 1990.

[32] Ben Nadler, Panayiotis Papadopoulos, and David J Steigmann. Multiscale constitutive modeling and numerical simulation of fabric ma-

terial. *International journal of solids and structures*, 43(2):206–221, 2006.

[33] CT Lim, VPW Shim, and YH Ng. Finite-element modeling of the ballistic impact of fabric armor. *International Journal of Impact Engineering*, 28(1):13–31, 2003.

[34] Philippe Boisse, Bassem Zouari, and Jean-Luc Daniel. Importance of in-plane shear rigidity in finite element analyses of woven fabric composite preforming. *Composites Part A: Applied Science and Manufacturing*, 37(12):2201–2212, 2006.

[35] F. Trochu, A. Hammami, and Y. Benoit. Prediction of fibre orientation and net shape definition of complex composite parts. *Composites Part A: Applied Science and Manufacturing*, 27(4):319 – 328, 1996. 4th International Conference on Automated Composites.

[36] A.C. Long, C.D. Rudd, M. Blagdon, and P. Smith. Characterizing the processing and performance of aligned reinforcements during preform manufacture. *Composites Part A: Applied Science and Manufacturing*, 27(4):247 – 253, 1996. 4th International Conference on Automated Composites.

[37] David Roylance, Paula Hammas, Joe Ting, Hank Chi, and Brian Scott. Numerical modeling of fabric impact. *ASME-PUBLICATIONS-AD*, 48:155–160, 1995.

[38] V.P.W. Shim, V.B.C. Tan, and T.E. Tay. Modelling deformation and damage characteristics of woven fabric under small projectile impact. *International Journal of Impact Engineering*, 16(4):585 – 605, 1995.

[39] V.B.C. Tan, V.P.W. Shim, and T.E. Tay. Experimental and numerical study of the response of flexible laminates to impact loading. *International Journal of Solids and Structures*, 40(23):6245 – 6266, 2003.

[40] V.B.C. Tan, V.P.W. Shim, and X. Zeng. Modelling crimp in woven fabrics subjected to ballistic impact. *International Journal of Impact Engineering*, 32(14):561 – 574, 2005. 5th International Symposium on Impact Engineering.

[41] S Kawabata, Masako Niwa, and H Kawai. The finite-deformation theory of plain-weave fabrics. part i: The biaxial-deformation theory. *Journal of the Textile Institute*, 64(1):21–46, 1973.

[42] S Kawabata, Masako Niwa, and H Kawai. The finite-deformation theory of plain-weave fabrics. part ii: The uniaxial-deformation theory. *Journal of the Textile Institute*, 64(2):47–61, 1973.

[43] S Kawabata, Masako Niwa, and H Kawai. The finite-deformation theory of plain-weave fabrics. part iii: The shear-deformation theory. *Journal of the Textile Institute*, 64(2):62–85, 1973.

[44] B Ben Boubaker, B Haussy, and JF Ganghoffer. Discrete models of woven structures. macroscopic approach. *Composites Part B: Engineering*, 38(4):498–505, 2007.

[45] Abdelhakim Cherouat and Jean Louis Billoët. Mechanical and numerical modelling of composite manufacturing processes deep-drawing and laying-up of thin pre-impregnated woven fabrics. *Journal of materials processing technology*, 118(1):460–471, 2001.

[46] MJ King, P Jearanaisilawong, and S Socrate. A continuum constitutive model for the mechanical behavior of woven fabrics. *International Journal of Solids and Structures*, 42(13):3867–3896, 2005.

[47] A Gasser, P Boisse, and S Hanklar. Mechanical behaviour of dry fabric reinforcements. 3d simulations versus biaxial tests. *Computational Materials Science*, 17(1):7–20, 2000.

[48] P Boisse, K Buet, A Gasser, and J Launay. Meso/macro-mechanical behaviour of textile reinforcements for thin composites. *Composites Science and Technology*, 61(3):395–401, 2001.

[49] P Boisse, A Gasser, and G Hivet. Analyses of fabric tensile behaviour: determination of the biaxial tension–strain surfaces and their use in forming simulations. *Composites Part A: Applied Science and Manufacturing*, 32(10):1395–1414, 2001.

[50] Philippe Boisse, Alain Gasser, Benjamin Hagege, and Jean-Louis Billoet. Analysis of the mechanical behavior of woven fibrous material using virtual tests at the unit cell level. *Journal of materials science*, 40(22):5955–5962, 2005.

[51] Pierre Badel, Emmanuelle Vidal-Sallé, and Philippe Boisse. Computational determination of in-plane shear mechanical behaviour of textile composite reinforcements. *Computational Materials Science*, 40(4):439–448, 2007.

[52] Pierre Badel, Emmanuelle Vidal-Sallé, and Philippe Boisse. Large deformation analysis of fibrous materials using rate constitutive equations. *Computers & Structures*, 86(11):1164–1175, 2008.

[53] QT Nguyen, Emmanuelle Vidal-Sallé, Philippe Boisse, CH Park, Abdelghani Saouab, Joël Bréard, and Gilles Hivet. Mesoscopic scale analyses of textile composite reinforcement compaction. *Composites Part B: Engineering*, 2012.

[54] P. Potluri and T.V. Sagar. Compaction modelling of textile preforms for composite structures. *Composite Structures*, 86(13):177 – 185, 2008. 14th International Conference on Composite Structures.

[55] J. Page and J. Wang. Prediction of shear force using 3d non-linear fem analyses for a plain weave carbon fabric in a bias extension state. *Finite Elements in Analysis and Design*, 38(8):755 – 764, 2002.

[56] Hua Lin, Martin Sherburn, Jonathan Crookston, Andrew C Long, Mike J Clifford, and I Arthur Jones. Finite element modelling of fabric compression. *Modelling and Simulation in Materials Science and Engineering*, 16(3):035010, 2008.

[57] Rimantas Barauskas and Aušra Abraitienė. Computational analysis of impact of a bullet against the multilayer fabrics in ls-dyna. *International Journal of Impact Engineering*, 34(7):1286–1305, 2007.

[58] Cuong Ha-Minh, Toufik Kanit, François Boussu, and Abdellatif Imad. Numerical multi-scale modeling for textile woven fabric against ballistic impact. *Computational Materials Science*, 50(7):2172–2184, 2011.

[59] Y Duan, M Keefe, TA Bogetti, and BA Cheeseman. Modeling friction effects on the ballistic impact behavior of a single-ply high-strength fabric. *International Journal of Impact Engineering*, 31(8):996–1012, 2005.

[60] Y Duan, M Keefe, TA Bogetti, and B Powers. Finite element modeling of transverse impact on a ballistic fabric. *International Journal of Mechanical Sciences*, 48(1):33–43, 2006.

[61] Y Duan, M Keefe, TA Bogetti, BA Cheeseman, and B Powers. A numerical investigation of the influence of friction on energy absorption by a high-strength fabric subjected to ballistic impact. *International Journal of Impact Engineering*, 32(8):1299–1312, 2006.

[62] MP Rao, Y Duan, M Keefe, BM Powers, and TA Bogetti. Modeling the effects of yarn material properties and friction on the ballistic impact of a plain-weave fabric. *Composite Structures*, 89(4):556–566, 2009.

[63] Gaurav Nilakantan, Michael Keefe, Travis A. Bogetti, Rob Adkinson, and John W. Gillespie Jr. On the finite element analysis of woven fabric impact using multiscale modeling techniques. *International Journal of Solids and Structures*, 47(17):2300 – 2315, 2010.

[64] Gaurav Nilakantan, Michael Keefe, Travis A Bogetti, and John W Gillespie Jr. Multiscale modeling of the impact of textile fabrics based on hybrid element analysis. *International Journal of Impact Engineering*, 37(10):1056–1071, 2010.

[65] Gilles Hivet and Philippe Boisse. Consistent mesoscopic mechanical behaviour model for woven composite reinforcements in biaxial tension. *Composites Part B: Engineering*, 39(2):345–361, 2008.

[66] Pierre Badel, Emmanuelle Vidal-Sallé, Eric Maire, and Philippe Boisse. Simulation and tomography analysis of textile composite reinforcement deformation at the mesoscopic scale. *Composites Science and Technology*, 68(12):2433–2440, 2008.

[67] Ignaas Verpoest and Stepan V Lomov. Virtual textile composites software wisetex: Integration with micro-mechanical, permeability and structural analysis. *Composites Science and Technology*, 65(15):2563–2574, 2005.

[68] F. Robitaille, A.C. Long, I.A. Jones, and C.D. Rudd. Automatically generated geometric descriptions of textile and composite unit cells. *Composites Part A: Applied Science and Manufacturing*, 34(4):303 – 312, 2003.

[69] Simon De Meulemeester, John Githaiga, Lieva Van Langenhove, DV Hung, and Patrick Puissant. Simulation of the dynamic yarn behavior on airjet looms. *Textile research journal*, 75(10):724–730, 2005.

[70] Simon De Meulemeester, Patrick Puissant, and Lieva Van Langenhove. Three-dimensional simulation of the dynamic yarn behavior on air-jet looms. *Textile Research Journal*, 79(18):1706–1714, 2009.

[71] Simon De Meulemeester, Patrick Puissant, and Lieva Van Langenhove. Yarn simulations with sharp edges. *Textile Research Journal*, 81(7):714–729, 2011.

[72] Youqi Wang and Xuekun Sun. Digital-element simulation of textile processes. *Composites Science and Technology*, 61(2):311 – 319, 2001.

[73] Guangming Zhou, Xuekun Sun, and Youqi Wang. Multi-chain digital element analysis in textile mechanics. *Composites Science and Technology*, 64(2):239 – 244, 2004.

[74] Yuyang Miao, Eric Zhou, Youqi Wang, and Bryan A. Cheeseman. Mechanics of textile composites: Micro-geometry. *Composites Science and Technology*, 68(78):1671 – 1678, 2008.

[75] Youqi Wang, Yuyang Miao, Daniel Swenson, Bryan A. Cheeseman, Chian-Feng Yen, and Bruce LaMattina. Digital element approach for simulating impact and penetration of textiles. *International Journal of Impact Engineering*, 37(5):552 – 560, 2010.

[76] Xuekun Sun and Changjie Sun. Mechanical properties of three-dimensional braided composites. *Composite Structures*, 65(34):485 – 492, 2004.

[77] Igor Tsukrov, Harun Bayraktar, Michael Giovinazzo, Jon Goering, Todd Gross, Monica Fruscello, and Lars Martinsson. Finite element modeling to predict cure-induced microcracking in three-dimensional woven composites. *International journal of fracture*, 172(2):209–216, 2011.

[78] Damien Durville. Modelling of contact-friction interactions in entangled fibrous materials. In *Computational Mechanics Proceedings of the Sixth World Wide Congress on Computational Mechanics*, 2004.

[79] Damien Durville. Numerical simulation of entangled materials mechanical properties. *Journal of Materials Science*, 40(22):5941–5948, 2005.

[80] Damien Durville. Finite element simulation of textile materials at mesoscopic scale. *Finite element modelling of textiles and textile composites*, 2007.

[81] Damien Durville. A finite element approach of the behaviour of woven materials at microscopic scale. In *Mechanics of Microstructured Solids*, pages 39–46. Springer, 2009.

[82] Damien Durville. Simulation of the mechanical behaviour of woven fabrics at the scale of fibers. *International journal of material forming*, 3(2):1241–1251, 2010.

[83] Naima Moustaghfir, Selsabil El-Ghezal Jeguirim, Damien Durville, Stéphane Fontaine, and Christiane Wagner-Kocher. Transverse compression behavior of textile rovings: finite element simulation and experimental study. *Journal of Materials Science*, 48(1):462–472, 2013.

[84] Damien Durville. Contact-friction modeling within elastic beam assemblies: an application to knot tightening. *Computational Mechanics*, 49(6):687–707, 2012.

[85] Cédric P Laurent, Damien Durville, Didier Mainard, Jean-François Ganghoffer, and Rachid Rahouadj. A multilayer braided scaffold for anterior cruciate ligament: mechanical modeling at the fiber scale. *Journal of the mechanical behavior of biomedical materials*, 2012.

[86] Hugues Bajas, Damien Durville, Daniel Ciazynski, and Arnaud Devred. Numerical simulation of the mechanical behavior of iter cable-in-conduit conductors. *Applied Superconductivity, IEEE Transactions on*, 20(3):1467–1470, 2010.

[87] Alexandre Torre, Hugues Bajas, D Ciazynski, Damien Durville, and K Weiss. Mechanical-electrical modeling of stretching experiment on 45 nb3sn strands ciccs. *Applied Superconductivity, IEEE Transactions on*, 21(3):2042–2045, 2011.

[88] Y Mahadik and SR Hallett. Finite element modelling of tow geometry in 3d woven fabrics. *Composites Part A: Applied Science and Manufacturing*, 41(9):1192–1200, 2010.

[89] Steve Green, Andrew Long, and Stephen Hallet. Numerical modelling of 3d woven composite preform deformations. Presented at the ACCIS annual conference in 2012, Bristol, United Kingdom, 2012.

[90] M Duhovic and D Bhattacharyya. Simulating the deformation mechanisms of knitted fabric composites. *Composites Part A: Applied Science and Manufacturing*, 37(11):1897–1915, 2006.

[91] Lieva Van Langenhove. Simulating the mechanical properties of a yarn based on the properties and arrangement of its fibers part i: The finite element model. *Textile research journal*, 67(4):263–268, 1997.

[92] Lieva Van Langenhove. Simulating the mechanical properties of a yarn based on the properties and arrangement of its fibers part ii: Results of simulations. *Textile research journal*, 67(5):342–347, 1997.

[93] Lieva Van Langenhove. Simulating the mechanical properties of a yarn based on the properties and arrangement of its fibers part iii: Practical measurements. *Textile research journal*, 67(6):406–412, 1997.

[94] David Rodney, Marc Fivel, and Rémy Dendievel. Discrete modeling of the mechanics of entangled materials. *Physical review letters*, 95(10):108004, 2005.

[95] C Barbier, R Dendievel, and D Rodney. Numerical study of 3d-compressions of entangled materials. *Computational Materials Science*, 45(3):593–596, 2009.

[96] J.W.S. Hearle, J.J. Thwaites, and J. Amirbayat. *Mechanics of flexible fibre assemblies*. NATO advanced study institutes series: Applied sciences. Sijthoff & Noordhoff, 1980.

[97] TV Sagar, P Potluri, and JWS Hearle. Mesoscale modelling of interlaced fibre assemblies using energy method. *Computational materials science*, 28(1):49–62, 2003.

[98] Norman Jones. Elastic-plastic and viscoelastic behavior of a continuous filament yarn. *International Journal of Mechanical Sciences*, 16(9):679 – 687, 1974.

[99] TK Ghosh, SK Batra, and RL Barker. the bending behaviour of plain-woven fabrics part ii: the case of linear thread-bending behaviour. *Journal of the Textile Institute*, 81(3):255–271, 1990.

[100] TK Ghosh, SK Batra, and RL Barker. the bending behaviour of plain-woven fabrics part iii: the case of bilinear thread-bending behaviour and the effect of fabric set. *Journal of the Textile Institute*, 81(3):272–287, 1990.

[101] Y Luo and Ignace Verpoest. Biaxial tension and ultimate deformation of knitted fabric reinforcements. *Composites Part A: applied science and manufacturing*, 33(2):197–203, 2002.

[102] JFA Kessels and R Akkerman. Prediction of the yarn trajectories on complex braided preforms. *Composites Part A: Applied Science and Manufacturing*, 33(8):1073–1081, 2002.

[103] RG Livesey and JD Owen. 47cloth stiffness and hysteresis in bending. *Journal of the Textile Institute Transactions*, 55(10):T516–T530, 1964.

[104] Takashi Komori. A generalized micromechanics of continuous-filament yarns. part i: Underlying formalism. *Textile Research Journal*, 71(10):898–904, 2001.

[105] Xiaoping Gao, Yize Sun, Zhuo Meng, and Zhijun Sun. Analytical approach of mechanical behavior of carpet yarn by mechanical models. *Materials Letters*, 65(14):2228–2230, 2011.

[106] Dan Zenkert and Magnus Burman. Tension, compression and shear fatigue of a closed cell polymer foam. *Composites Science and Technology*, 69(6):785 – 792, 2009. ONR - Dynamic Failure and Durability.

[107] Lorna J. Gibson. Biomechanics of cellular solids. *Journal of Biomechanics*, 38(3):377 – 399, 2005.

[108] QM Li, RAW Mines, and RS Birch. The crush behaviour of rohacell-51wf structural foam. *International Journal of Solids and Structures*, 37(43):6321–6341, 2000.

[109] Lorna J Gibson and Michael F Ashby. *Cellular solids: structure and properties*. Cambridge university press, 1999.

[110] Souhail Youssef, Eric Maire, and Roger Gaertner. Finite element modelling of the actual structure of cellular materials determined by x-ray tomography. *Acta Materialia*, 53(3):719–730, 2005.

[111] S Arezoo, VL Tagarielli, CR Siviour, and N Petrinic. Compressive deformation of rohacell foams: effects of strain rate and temperature. *International Journal of Impact Engineering*, 2012.

[112] E.A. Flores-Johnson and Q.M. Li. Indentation into polymeric foams. *International Journal of Solids and Structures*, 47(16):1987 – 1995, 2010.

[113] VS Deshpande and NA Fleck. Isotropic constitutive models for metallic foams. *Journal of the Mechanics and Physics of Solids*, 48(6):1253–1283, 2000.

[114] VS Deshpande and NA Fleck. Multi-axial yield behaviour of polymer foams. *Acta materialia*, 49(10):1859–1866, 2001.